Chapter 15

The SEA-CALIPSO volcano imaging experiment at Montserrat: plans, campaigns at sea and on land, scientific results, and lessons learned

Q1

B. VOIGHT[1]*, R. S. J. SPARKS[2], E. SHALEV[3,4], T. MINSHULL[5], M. PAULATTO[5], C. ANNEN[1], C. KENEDI[3,4], J. HAMMOND[2], T. J. HENSTOCK[5], L. BROWN[6], E. KIDDLE[2], P. MALIN[3,4], G. MATTIOLI[7], C. AMMON[1], E. ARIAS-DOTSON[8], A. BELOUSOV[1], K. BYERLY[6], L. CAROTHERS[8], A. CLARKE[9], S. DEAN[5], L. ELLETT[10], D. ELSWORTH[1], D. HIDAYAT[1], R. A. HERD[11], M. JOHNSON[8], A. LEE[3], V. MILLER[1], B. MURPHY[10], C. PEIRCE[12], G. RYAN[13], S. SALDANA[14], C. SNELSON[14], R. STEWART[13], R. SYERS[13], J. TARON[1], J. TROFIMOVS[5], C. WIDIWIJAYANTI[1], S. R. YOUNG[1] & W. ZAMORA[8]

[1]*College of Earth and Mineral Sciences, Penn State University, University Park, PA 16802, USA*

[2]*Department of Earth Sciences, University of Bristol, Bristol BS8 1RJ, UK*

[3]*Earth & Ocean Sciences, Duke University, Durham, NC 27708-0227, USA*

[4]*Institute Earth Science & Engineering, University of Auckland, Private Bag 92019, Auckland, New Zealand*

[5]*National Oceanography Centre, University of Southampton, Southampton SO14 3ZH, UK*

[6]*Department of Geosciences, Cornell University, Ithaca, NY 14853, USA*

[7]*Department of Geosciences, University of Arkansas, Fayetteville, AR 72701, USA*

[8]*PASSCAL Instrument Center, East Road Industrial Park, Socorro, NM 87801, USA*

[9]*Department Geological Sciences, Arizona State University, Tempe, Arizona, USA*

[10]*Scripps Institution of Oceanography, University of San Diego, La Jolla, CA 92093, USA*

[11]*School of Environmental Science, University East Anglia, Norwich NR4 7TJ, UK*

[12]*Department of Geological Sciences, University of Durham, Durham DH1 3LE, UK*

[13]*Montserrat Volcano Observatory, Flemmings, Montserrat, West Indies*

[14]*Department of Earth and Environmental Sciences, New Mexico Institute of Mining and Technology, Socorro, NM 87801, USA*

**Corresponding author (e-mail: voight@ems.psu.edu)*

Abstract: Since 1995 the eruption of the andesitic Soufrière Hills Volcano (SHV), Montserrat, has been studied in substantial detail. As an important contribution to this effort, the SEA-CALIPSO experiment was devised to image the arc crust underlying Montserrat, and, if possible, the magma system at SHV using tomography and reflection seismology. Field operations were carried out in October–December 2007, with deployment of 238 seismometers on land supplementing seven volcano observatory stations, and with an array of 10 ocean-bottom seismometers deployed offshore. The RRS *James Cook* on NERC cruise JC19 towed a tuned airgun array plus a digital 48-channel streamer on encircling and radial tracks for 77 h about Montserrat during December 2007, firing 4414 airgun shots and yielding about 47 Gb of data. The main objecctives of the experiment were achieved. Preliminary analyses of these data published in 2010 generated images of heterogeneous high-velocity bodies representing the cores of volcanoes and subjacent intrusions, and shallow areas of low velocity on the flanks of the island that reflect volcaniclastic deposits and hydrothermal alteration. The resolution of this preliminary work did not extend beyond 5 km depth. An improved three-dimensional (3D) seismic velocity model was then obtained by inversion of 181 665 first-arrival travel times from a more-complete sampling of the dataset, yielding clear images to 7.5 km depth of a low-velocity volume that was interpreted as the magma chamber which feeds the current eruption, with an estimated volume 13 km^3. Coupled thermal and seismic modelling revealed properties of the partly crystallized magma. Seismic reflection analyses aimed at imaging structures under southern Montserrat had limited success, and suggest subhorizontal layering interpreted as sills at a depth of between 6 and 19 km. Seismic reflection profiles collected offshore reveal deep fans of volcaniclastic debris and fault offsets, leading to new tectonic interpretations. This chapter presents the project goals and planning concepts, describes in detail the campaigns at sea and on land, summarizes the major results, and identifies the key lessons learned.

The ongoing eruption of the andesitic Soufrière Hills Volcano (SHV), Montserrat, has been studied in detail since 1995, and the volcano has become an important natural laboratory for investigations of volcanic processes (Druitt & Kokelaar 2002; Voight & Sparks 2010). About 1 km^3 of lava has been erupted (Wadge *et al.* 2010). Deep processes exert important controls on this eruption, but the structure of the crust, upper mantle and the magmatic system has been inadequately defined. Thus, we designed the SEA-CALIPSO experiment to investigate the physical structure of the arc crust under Montserrat through active source seismic
Q2 tomography and reflection seismology (Voight *et al.* 2010*b*). The SEA-CALIPSO experiment ('Seismic Experiment with Airgun-source') was conducted under the umbrella of the CALIPSO consortium project ('Caribbean Andesitic Lava Island Precision Seismo-geodetic Observatory') (Mattioli *et al.* 2004). SEA-CALIPSO complements a number of ancillary CALIPSO project studies, involving analyses of global positioning system (GPS) and strainmeter data (Elsworth *et al.* 2008; Chardot *et al.* 2010; Foroozan *et al.* 2010, 2011; Linde *et al.* 2010; Mattioli *et al.* 2010; Voight *et al.* 2010*a*, *c*), receiver function investiga- Q3
tions (Sevilla *et al.* 2010), and petrological studies (Kiddle *et al.* 2010).

From: WADGE, G., ROBERTSON, R. E. A. & VOIGHT, B. (eds) 2014. *The Eruption of Soufrière Hills Volcano, Montserrat from 2000 to 2010*. Geological Society, London, Memoirs, **39**, 251–287. http://dx.doi.org/10.1144/M39.15

The outcomes of this project contribute to an improved understanding of volcanic processes, island arc volcanism and tectonics, arc crust evolution, and magma genesis. The experiment successfully imaged the subsurface under Montserrat and the surrounding offshore region, and detected and characterized the shallow magma chamber.

This paper provides background on the tectonic and magmatic setting, describes the SEA-CALIPSO aims, plans, support and funding, outlines details of the active seismic source, the seismometer arrays and other equipment, delineates the land and shipborne operations, and summarizes important research outcomes. The chapter concludes with a discussion of critical issues affecting

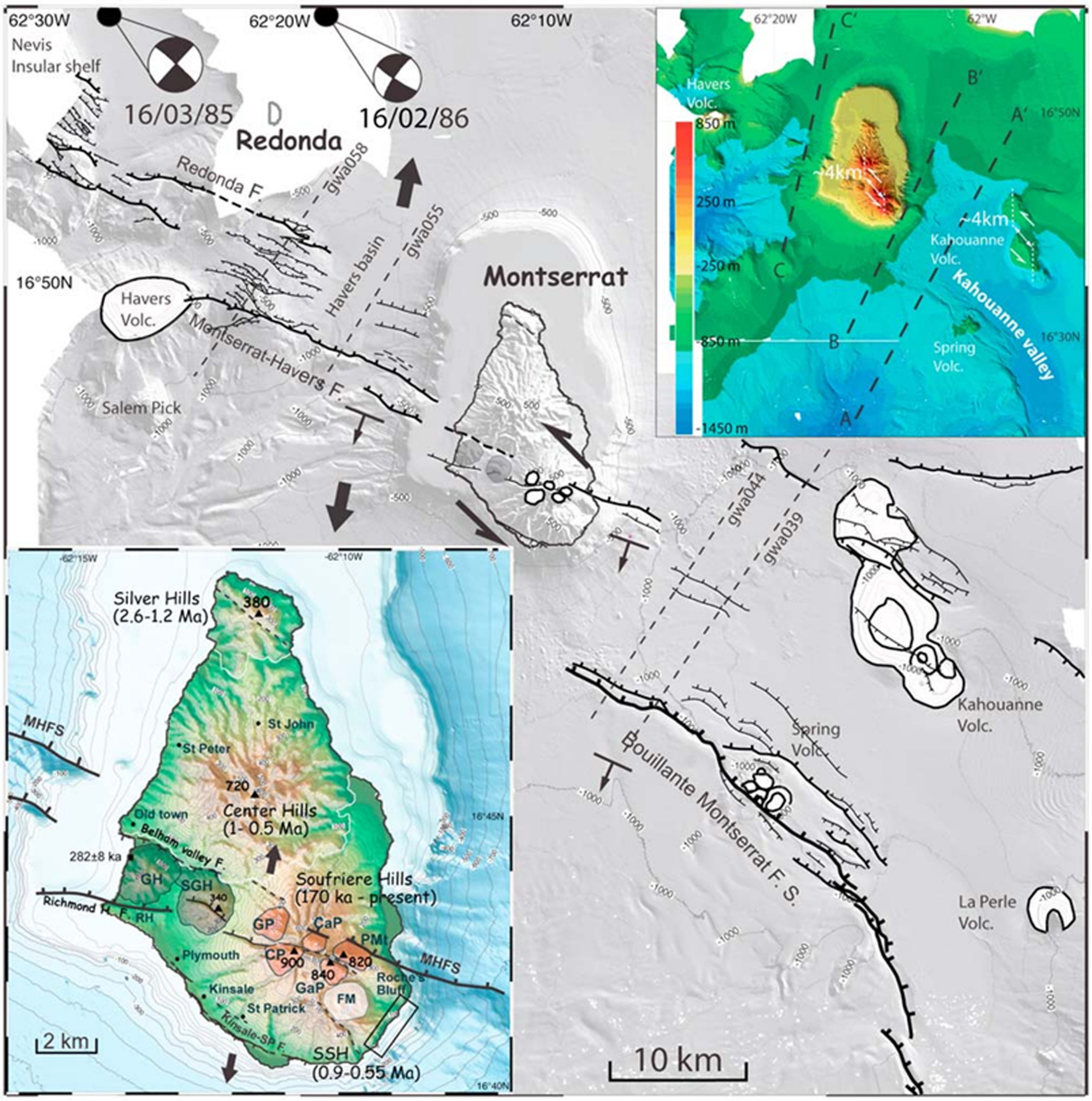

Colour online/colour hardcopy

Fig. 15.1. Seafloor bathymetry and tectonic setting for Montserrat and SEA-CALIPSO experiment (after Feuillet *et al.* 2010). Topography and insular shelf bathymetry from Le Friant *et al.* (2004). Bathymetry from AGUADOMAR and GWADASEIS cruises. Contours at 100 m interval. Active faults, black lines with ticks. Seismicity from PDE USGS. Double black arrows, local direction of extension. Large-scale sinistral shear direction is indicated. Half black arrow with bars, regional-scale tilt of the MHFS footwall. Dashed lines with names, location of seismic profiles in Feuillet *et al.* (2010). In white, submarine volcanoes. Top right inset: N225°E illuminated bathymetry and topography. Sinistral offsets of volcanic complexes are indicated by white dashed lines with a double arrow. The numbers in kilometres indicate the offsets. Dashed black lines, location of bathymetric profiles in Feuillet *et al.* (2010, fig. S2). Bottom left inset: volcano tectonic map of Montserrat. Volcanic complex ages from Harford *et al.* (2002). In orange, Soufrière Hills domes: CaP, Castle Peak; CP, Chances Peak; GaP, Galways Peak; GP, Gages Peak; PMt, Perches Mountain. In white, South Soufrière Hills dome: FM, Fergus Mountain. In grey: GH, Garibaldi Hill; SGH, St George's Hill; Kinsale-SP F., Kinsale–St Patrick Fault; MHFS, Montserrat Havers Fault System; RH, Richmond Hill; SSH, South Soufrière Hills. Inferred or less active faults are indicated by dashed lines.

the success of the venture, and offers some key lessons learned that could be of value to researchers involved in future volcano imaging projects.

Background

The island of Montserrat in the volcanic arc of the Lesser Antilles was clearly an ideal target for a seismic tomography experiment, partly because of its small size and relatively simple volcanic history, and especially because of the need to better understand the current dangerous eruption (Voight *et al.* 2010*b*). The tectonic setting and bathymetry about Montserrat is shown in Figure 15.1. Montserrat is composed of the lava domes and associated pyroclastic deposits of three andesite volcanoes, Silver Hills (2600–1200 ka), Centre Hills (*c.* 950–550 ka) and the Soufrière Hills Volcano (170 ka – present) (Fig. 15.1, inset). The three volcanoes have very similar petrology and a clear age progression from north to south (Harford *et al.* 2002), making comparisons between the volcanic centres straightforward and valuable. Volcanic activity at SHV started in 1995 after over three centuries of quiescence and was preceded by a series of periods of increased seismic activity spaced approximately at three-decade intervals (Powell 1938; Perret 1939; Shepherd *et al.* 1971; Aspinall *et al.* 1998). The activity is characterized by the growth of an andesite lava dome, and associated dome collapses, explosions and pyroclastic flows. The eruption is still ongoing in 2013 and has so far consisted of five eruptive phases of continuous lava extrusion interrupted by periods of quiescence (Wadge *et al.* 2010).

The magmatic system of SHV is thought to be composed of four main elements: a primary source of mafic magma in the mantle wedge with storage in the deep crust at about 30 km depth (Zellmer *et al.* 2003*a*, *b*; Sevilla *et al.* 2010); a mid-crustal magma storage region where andesite is generated by fractionation of basalt (Sparks & Young 2002; Elsworth *et al.* 2008); a shallow magma reservoir, where andesite resides prior to eruption and undergoes further transformation (Murphy *et al.* 2000); and a strato-volcano, consisting of a core of lava domes and a soft apron of volcaniclastic deposits (Harford *et al.* 2002; Paulatto *et al.* 2010*a*, *b*; Shalev *et al.* 2010). Some characteristics of the shallow magma reservoir have been constrained with petrological and geodetic data. Analysis of SHV andesites and modelling of ground deformation and magma efflux suggest that the shallow magma chamber lies below a depth of approximately 5 km, but details on its geometry are debated (Murphy *et al.* 2000; Voight *et al.* 2006, 2010*c*; Elsworth *et al.* 2008; Hautmann *et al.* 2009, 2010; Foroozan *et al.* 2010; Mattioli *et al.* 2010). The dynamics of magma flow are influenced by geometric considerations (Voight *et al.* 1999, 2006, 2010*c*; Melnik & Sparks 2002, 2005; Widiwijayanti *et al.* 2005; Costa *et al.* 2007; Foroozan *et al.* 2011; Melnik & Costa 2014). Geothermometry indicates that the magma is relatively cool (*c.* 850 °C) and highly crystalline (60–65 vol%) (Murphy *et al.* 2000; Rutherford & Devine 2003). Several independent observations support the hypothesis of continued input of mafic magma at depth during the course of the SHV eruption (Humphreys *et al.* 2009; Barclay *et al.* 2010; Christopher *et al.* 2010; Voight *et al.* 2010*c*; Edmonds *et al.* 2011).

Our tomographical studies were aimed at improving the understanding of the magmatic system (e.g. Lees 2007). Analyses of our data proceeded in several steps. Our preliminary results generated useful images of the subsurface at Montserrat (Kenedi *et al.* 2010; Paulatto *et al.* 2010*a*; Shalev *et al.* 2010), but lacked the resolution beyond 5 km depth to constrain the shallow crustal magma chamber. An improved three-dimensional (3D) seismic velocity model for Montserrat was then obtained by regularized inversion of first-arrival travel times from a more complete subset of wide-angle seismic data recorded on our array of land and ocean-bottom seismometers (Paulatto *et al.* 2012). Some key results from these various researches are summarized below, following discussion of the planning and execution of the experiment.

Planning and funding

Plans and preparations

Our project plans evolved between 2004 and 2007. Our initial concept was to record signals from a 3 day active source experiment using an airgun array towed by a research vessel around Montserrat (Fig. 15.2a) taking opportunistic advantage of the NERC RRS *James Clark Ross* operation scheduled for May 2005. In this original plan we expected about 10 Gb of data to be collected from around 100 seismometers on land, and, after stacking, about 1000 shot points and up to 100 000 separate ray paths. The loan of seismometers was approved by IRIS-PASSCAL (Incorporated Research Institutions for Seismology (IRIS)-Program for Array Seismic Studies of the Continental Lithosphere (PASSCAL)). However, owing to cruise schedule delays, our cruise availability was withdrawn for 2005, and was rescheduled to 2007. Although not welcomed at the time, this delay proved useful in providing opportunities for development of more thorough planning, more ship time, the addition of important equipment and augmented financial support, all factors that facilitated a vastly improved experiment. In retrospect, we were quite fortunate that the delay occurred because the full success of the experiment hinged critically on several of these factors.

Once funds were largely in place and following a planning workshop in Washington, DC in November 2006, final-stage logistical plans were worked out in May 2007 with a meeting involving the participating institutions. A cruise planning meeting was held at Southampton on 5 May 2007, with formal minutes circulated by Colin Day (UKORS) to note recent pertinent developments, and to highlight points that needed to be circulated to participants of the project and required some action. It was noted, for instance, that B. Voight was looking into streamer acquisition and support, and that the principal investigator (PI) of the previous JC18 cruise agreed to allow GeoPro staff and airgun kit to be loaded onto the vessel at the beginning of his cruise, after re-assurance that the kit and activity would not affect his JC18 work. The RRS *James Cook* was scheduled to be in Antigua port call between 30 November and 3 December. The mobilization logistics were planned, with loading and stowing of GeoPro airgun equipment to be carried out on 5 November, with GeoPro to mobilize kit at Antigua port call. Two GeoPro technicians would board the JC18 cruise to test equipment, and it was noted that if a streamer is deployed then this must be loaded onto the *James Cook* in this same period.

Our Duke University colleagues (subsequently associated with University of Auckland) led the land seismometer operations, and sent teams to Montserrat for scouting and deployment in August, October, November and December 2007. These trips included participants from Penn State University, a representative from the Seismic Research Centre of the University of West Indies, and several from IRIS-PASSCAL. The final deployment in December 2007 required numerous personnel and involved assistance from the main collaborating institutions, as well as the University of East Anglia, UK, New Mexico Institute of Mining and Technology and the University of Auckland, together with local cooperation and assistance, especially from the Montserrat Volcano Observatory (MVO). Sea operations were led by colleagues from the University of Bristol and the University of Southampton, and mainly involved use of the RRS *James Cook* (NERC).

The active-source imaging experiment had two components: a seismic reflection component, aimed at imaging the top of the magma body using wide-angle seismic reflections;, and a seismic tomographical component, in which any velocity anomaly associated with the magma body, as well as the larger-scale

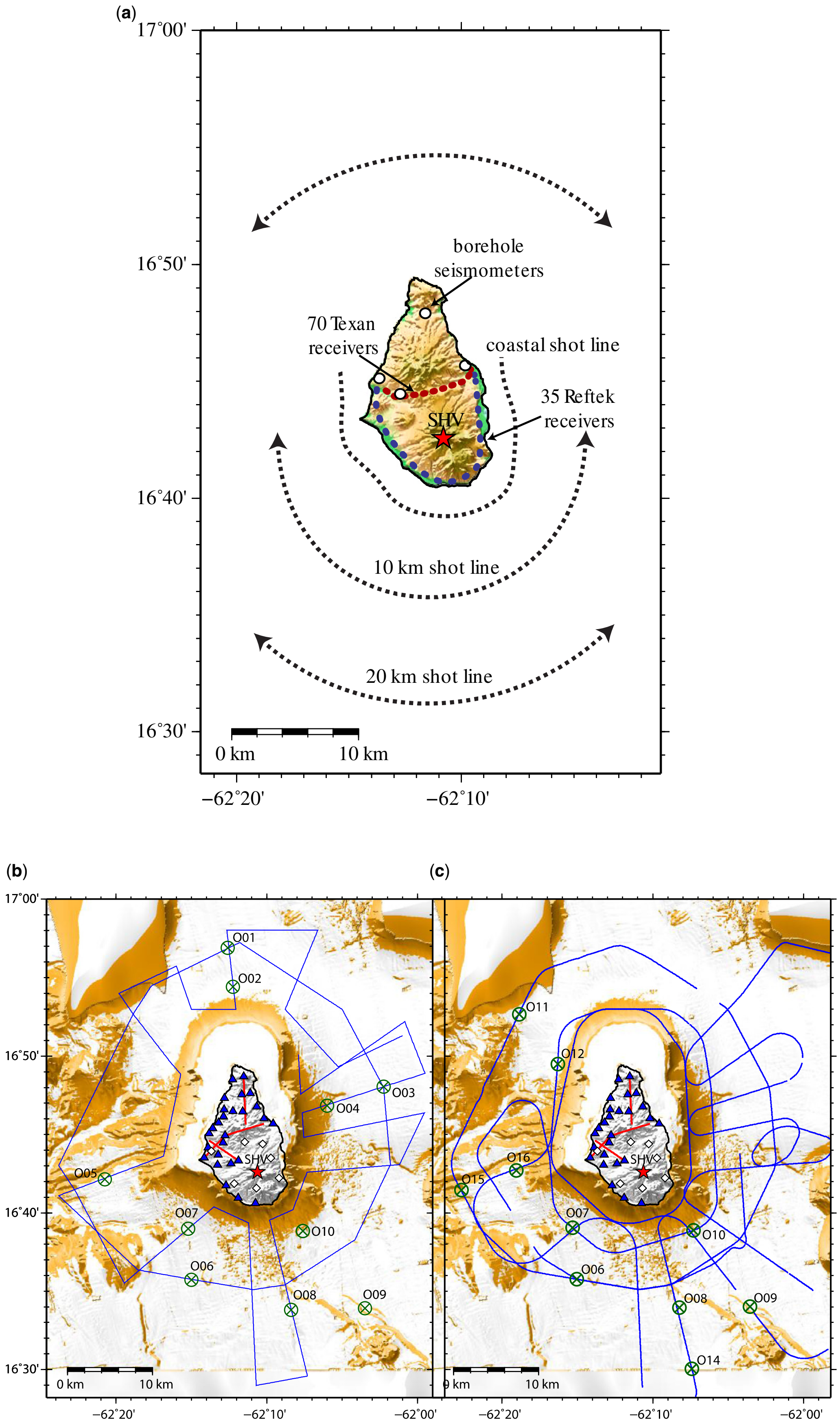

Colour online/ colour hardcopy

Fig. 15.2. Evolution of shiptrack plans. (**a**) Sketch from 2004 showing the original concept of shiptracks (shotlines), with a Texan array onshore. (**b**) Bathymetric map showing the OBS deployment sites planned for 2007 and the actual shiptrack. Anticipated OBS sites are shown offshore as crossed-circles. Land stations include Refteks (blue triangles) and Texan arrays (red lines). DEM from Le Friant *et al.* (2004). (**c**) Similar figure showing the final OBS station array and shiptrack positions. Note the substantially changed OBS site locations. The orange areas have a seafloor slope gradient above 10°, which we tried to avoid when deploying OBSs.

crustal structure, could be determined. The planned experiment geometry was based on principles set out by Okaya *et al.* (2002) and on previous experience at volcanic ocean islands (Evangelidis *et al.* 2004; Minshull *et al.* 2005; cf. Zandomeneghi *et al.* 2009).

Ray-trace modelling to assist planning used an estimated velocity structure based on models that evolved at the MVO, derived by trial-and-error modification of a seismic model previously developed at Guadeloupe, the volcanic island immediately to the south of Montserrat (Power *et al.* 1998). This modelling showed that for a geometry involving onshore receivers only, the refracted rays might not reach a magma body at approximately 5 km, the position that had been inferred from earlier petrological and seismic arguments (Aspinall *et al.* 1998; Barclay *et al.* 1998). Thus, we aimed to improve ray penetration by deploying ocean-bottom seismometers (OBSs) up to 20 km from the Montserrat coast, expanding the source–receiver offsets.

The planned shooting tracks comprised a series of subcircular tracks at 2–10 km from the coast, supplemented by radial tracks extending up to 30 km from the coast to determine deeper velocity structure (Fig. 15.2b). A streamer was added to our plans in order to map the sediment thickness, and thus to account for corresponding travel-time delays in signals from the airgun shots.

Funding and support

A proposal was submitted to NERC for the survey and associated science in July 2005 and received an Alpha 3 grade, making the project eligible for free access to NERC ships. NERC permitted our use of the ship on the condition that external financial support could be secured for add-on ship costs such as airguns, and we managed to cobble together the necessary funds from several sources. Funding overall was provided by the NSF, NERC, Discovery Channel TV, the British Geological Survey (BGS) and the Foreign and Commonwealth Office (FCO) of the UK. In several grants, the NSF covered the IRIS-PASSCAL operations, streamer costs, and field costs and analyses by US-based university research groups. The NSF had approved funding in 2004 for the originally planned 2005 deployment, and generously allowed us to carry over these funds for the rescheduled cruise. Likewise, PASSCAL arranged to reschedule provision of seismic equipment for 2007, and increased the number of loaned instruments. Funding for UK university research was provided by NERC. Funding from Discovery Channel TV proved essential in supporting costs for an augmented airgun array and technical support, and BGS supported the important OBS operations. The FCO supported costs for required environmental impact reporting.

Seismic source

The seismic source, provided on commercial contract by GeoPro, consisted of eight Bolt 'Long Life' units assembled on two rigid frames connected to the ship by electric cables and high-pressure tubes, towed side by side with a separation of 9 m (e.g. Bailey & Garces 1988). The total volume of the array was 2600 cu. in. (42.61 l), subdivided into 1430 cu. in. on the port-side frame and 970 on the starboard-side frame (Figs 15.3 & 15.4). The airgun source comprised 2×500, 1×340, 3×290 and 2×195 cu. in. (2×8.2, 1×5.6, 3×4.8 and 2×3.2 l) guns in clustered pairs. The source design was a compromise that maximized low-frequency energy and tuning to attenuate the bubble pulse, had modelled 6 dB points of approximately 5 and 50 Hz, and a primary-to-bubble ratio of about 3.5 to 1 (Strandenes *et al.* 1991).

Synchronization of the guns was obtained by GPS using a 'Long-Shot' gun controller, and time-triggering was given by a quartz clock driven by GPS timing. The source fired at a constant shot interval of 60 s at a pressure of 2000 psi (1.382×10^7 Pa). This shot interval was used in order to avoid contamination of records by previous-shot noise (Nakamura *et al.* 1987; Christeson *et al.* 1996). The array was towed at a depth of 10 m and at an average speed of 4.5 knots (2.3 m s^{-1}), giving a mean shot spacing of 139 m. Shot coordinates were calculated by interpolating the ship's navigation using a gun setback of 91 m (Fig. 15.5). Altogether 4414 shots were fired over a period of 77 h, with a few interruptions due to gun maintenance or the presence of marine mammals or other vessels in proximity of the guns.

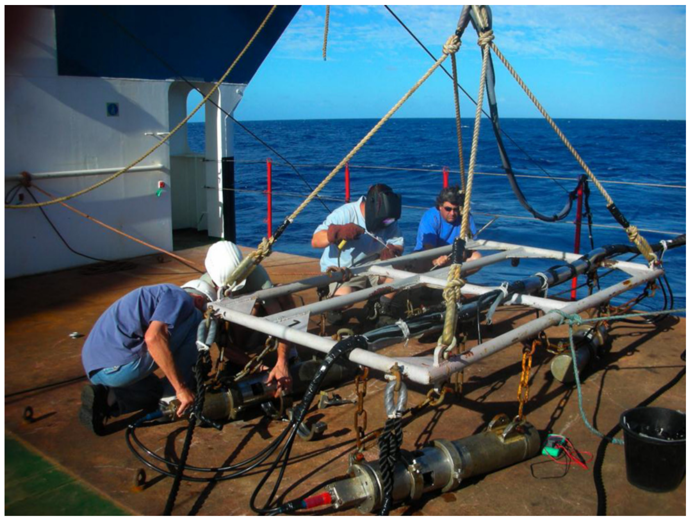

Colour online/mono hardcopy

Fig. 15.3. Bolt 'Long Life' airgun units assembled on a rigid frame and connected to the ship by electric cables and high-pressure tubes. Two frames were used, towed side-by-side with a separation of 9 m. Photograph courtesy of S. Sparks.

Seismometers and other equipment

Ocean-bottom seismometers

The OBSs were supplied by OBIC, the Ocean Bottom Instrument Consortium (Minshull *et al.* 2005), comprising the University of Southampton, Durham University and Imperial College. The instruments deployed were three LC2000 two-component OBSs and seven LC2000 four-component OBSs designed by Scripps Institution of Oceanography (Fig. 15.6). The four-channel OBSs were equipped with a hydrophone and a three-component 4.5 Hz geophone package, and the two-channel OBSs were equipped with a hydrophone and a 2 Hz vertical geophone. The sample rate for the experiment was set at 250 Hz.

OBS sites were chosen to avoid potentially hazardous areas such as submarine canyons, steep slopes and areas covered by recent debris flows, and to be outside the 'Maritime Exclusion Zone' set for volcanic hazards around the south of Montserrat. Sites to the west, on the lee of the island with respect to the predominant trade winds, were preferred to facilitate deployment and recovery of the instruments.

OBS coordinates were determined after the cruise by minimizing residuals between observed and calculated first arrivals of seismic waves through the water from GPS-located shots near each OBS, leading to OBS position uncertainties of 20–50 m, from shot location uncertainties of 5–20 m (Paulatto *et al.* 2012). The JC19 Cruise Report (NOC 2008) lists the distances

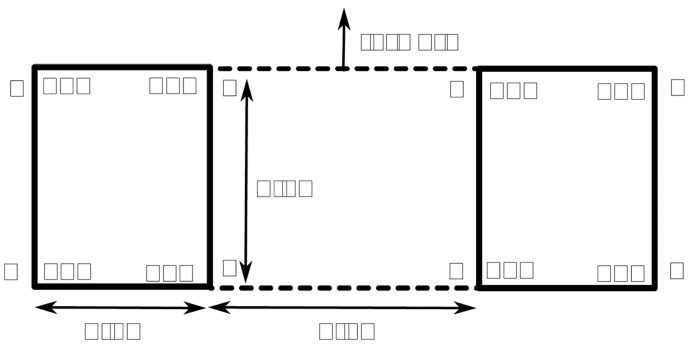

Q14

Fig. 15.4. Schematics of the gun array. Gun numbers and volumes in cu. in. are shown. The total volume is 2600 cu. in.

Colour online/colour hardcopy

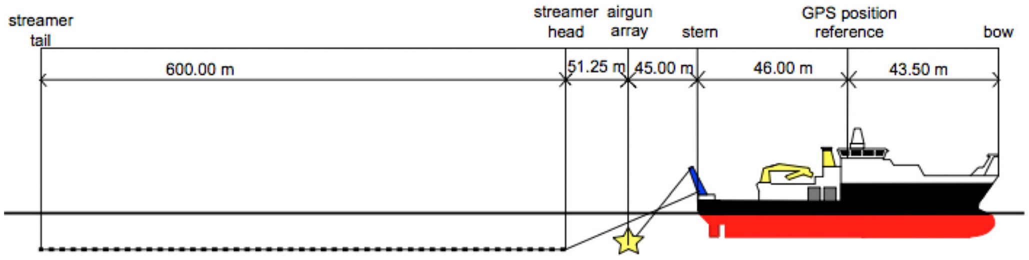

Fig. 15.5. Schematics of the ship, airgun array position and streamer geometry used in SEA-CALIPSO experiment (after NOC 2008).

between deployment position and relocated position, the direction of drift from the north, and serial number and number of channels for all instruments, plus instrument deployment and recovery times, sync time, end of record periods, and time drift of the instrument clock during recording period.

All instruments deployed were recovered after recording continuously the 4414 shots fired from the RRS *James Cook*. Most instruments recorded successfully on all channels. The only exceptions were the instruments on sites O09 and O14 (Fig. 15.2). The instrument on Site O09, 15 km SSE of the Montserrat coast, was a four- component OBS but recorded only on two channels, the hydrophone and the vertical geophone, because of a weak connection in the datalogger. The instrument on Site O14, 19 km south of the coast, was a four-component type, but the geophone mounted in the vertical position was a horizontal-type phone and this resulted in unusable data on the vertical component.

Land array

Two types of land-based seismographs were provided by IRIS-PASSCAL, the RefTek RT130 recorder with three-component Mark Products L22 2.0 Hz geophones (hereafter called the RefTek) (Fig. 15.7), and the compact RefTek RT125A, a single vertical-component Mark Products L40 (or L28) 4.5 Hz sensor and single-channel datalogger with self-contained battery supply (hereafter referred to as the Texan) (Fig. 15.8). A total of 29

Colour online/colour hardcopy

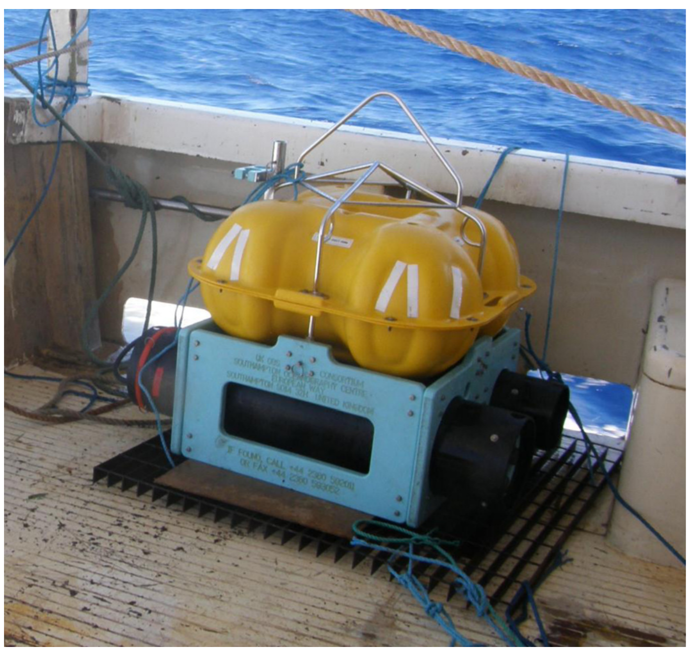

Fig. 15.6. An LC2000 four-component Ocean-Bottom Seismometer (OBS). Instrument was designed by Scripps Institution of Oceanography. Photograph courtesy of M. Paulatto.

RefTeks were deployed from October through to December, powered by deep-cycle 12 V batteries with solar panel recharging. PASSCAL technicians accompanied the two deployment trips to maintain the instruments and to instruct other participants on installation. A total of 204 Texans were deployed, only during the December experiment. The distribution of all seismometers is shown in Figures 15.9 and 15.10, and coordinates of all stations are given in Appendix 1. Q4

RefTeks were intended primarily for 3D tomography analysis, while the Texans were intended for two purposes, for reflection seismology and to fill-in gaps in the tomographical grid. The design for the 3D tomography required that the three-component RefTeks be arrayed as closely as possible in a more or less evenly spaced regular grid (Fig. 15.9). In the planned tomographical analysis, the subsurface is described by velocity nodes at *X*, *Y* and *Z* coordinates (Shalev *et al.* 2010), with node density (adjusted based on the number of rays passing in the vicinity of the node) higher in the centre of the array. A higher node density and higher resolution is possible where there are more data, and this is influenced by station density. The number of RefTek stations was limited by availability from IRIS-PASSCAL. Sites were primary chosen to be easily accessible by car, but many instruments had to be deployed on foot or with access by boat from the sea, especially in the south of the island. The final RefTek grid developed did not include the higher parts of the Centre Hills and Soufrière Hills due to forbidding terrain and difficulty or hazards of installation. The final array consisted of stations about every 1–2 km and produced a final resolution of approximately 500 m (Fig. 15.9) (Shalev *et al.* 2010). Limited access within the exclusion zone resulted in poorer coverage in the south than in the north.

The permanent MVO seismic network, then comprising nine broadband seismographs (Guralp CMG-40 T) and two short-period vertical-component seismographs (Mark Products L4) more or less evenly spaced around Soufrière Hills (Fig. 15.9), also recorded the shots. Seven of these stations were used.

The design for the reflection survey included three quasi-linear Texan arrays on the island, integrated with the ship track. Two of these arrays radiated outwards from SHV, and the ship track followed the continuation of the alignment offshore on the opposite side of the volcano (cf. Figs 15.2b, c & 15.9). The radial lines were designed to 'undershoot' SHV and, with increasing distance between shots and receivers, the seismic waves could, in principle, reach deeper reflectors under the volcano.

Another array was designed to receive reflections for detailed, horizontal 'fan' style recording of the marine source as it traversed an offshore arc about the volcano. The array approximated a NE-orientated arc of the SHV circumference, located about 6 km north and NW of the SHV summit (Figs 15.9 & 15.10), that mirrored an offshore arc, about 6 km south and SE of the SHV (Fig. 15.2b). To record the greatest number of rays through the volcano subsurface, the circumferential array was designed to cover the longest feasible NE–SW path across Montserrat. While the ship made rings at increased radius from the volcano, Montserrat's narrowing northern tip and increasing number of deep, incised valleys in the north discouraged deployment of a second arc of instruments.

Colour online/colour hardcopy

Fig. 15.7. The RefTek RT130 seismometer recorder, with three-component Mark Products model L22, 2.0 Hz geophone. Photograph courtesy of B. Voight.

While in advanced stages of planning in July 2007 we received disturbing news from B. Beaudoin at PASSCAL:

> I regret to inform you that our entire Texan pool was in a serious truck accident in China . . . it appears that many, if not most, of the Texan's oscillators have been damaged. We will be receiving half of the equipment at PASSCAL by mid-August and will begin testing dataloggers. The remaining equipment will return to PASSCAL early-September and will also need testing. Depending on the severity and magnitude of damage the dataloggers may need to be returned to RefTek . . . At this time we are unable to guarantee that we will have Texans available for shipping to SEA-CALIPSO. I am sorry that we cannot promise Texans at this time, however we will do everything possible to meet our commitment.

This circumstance caused us to promptly seek Texans from other sources in contingency, and we had limited success in securing a promise from New Mexico Institute of Mining and Technology of about 35 instruments, as a fall-back solution. Fortunately, by mid-September, PASSCAL had done sufficient testing of the equipment involved in the accident to firmly commit 140 units of 256 MB Texans for SEA-CALIPSO, and by December we had obtained the full number (205) of Texans originally planned. Of these, 204 were deployed.

Colour online/colour hardcopy

Fig. 15.8. The RefTek RT125A seismometer ('Texan'), with cable to a single vertical component Mark Products L40 (or L28) 4.5 Hz sensor. Photograph courtesy of B. Voight.

Figure 15.2c displays the distribution of installed seismic stations and the ship tracks, which broadly match the original plans with the exception of some OBS sites (cf. Fig. 15.2b). Some modifications are apparent due to logistic issues, especially at sea and as described below.

Seismic lines, sonobuoys and XBT probes

A 600 m 48-channel streamer provided by Scripps Oceanographic Institution and operated by their technical staff recorded 26 seismic lines during shooting. The geometry of the streamer is shown in Figure 15.5. The sample frequency used was 500 Hz. The streamer was used to map the sediment thickness, in order to account for travel-time delays in signals from the airgun shots, and to provide reflection profiles indicating sediment type and structure.

Deployment of 48 sonobuoys donated by Lamont-Doherty Oceanographic Institution was accomplished during the cruise, with the intent of providing better ray coverage offshore. The sonobuoys were stripped from the parachute and deployed by hand from the stern of the ship (NOC 2008). A shipboard radio receiver was set up to record the signals transmitted by the sonobuoys. The sonobuoy data were then digitized and recorded on two additional channels on the MCS datalogger. However, due to the poor state of preservation of the instruments, most failed immediately and sank, and only a few recorded more than a few shots.

Expendable bathythermograph (XBT) probes were deployed and measured the vertical temperature distribution in the water column (NOC 2008). The maximum depth reached was 875 m. In most cases, the copper wire snapped when the probe reached a depth of about 200 m.

Land operations

The on-land phase lasted between October and December 2007 with the initial deployment of Refteks mostly completed in October, and the deployment of the Texans conducted from 17 to 21 December 2007 prior to and during the active-source seismic experiment.

Montserrat has a very short runway in the north on which only small planes can land. There were a limited number of passenger flights scheduled from Antigua, and no air shipments for cargo. Shipping cargo by freighter from the United States required a substantial margin between shipping and expected arrival times due to unpredictable freight schedules. A local customs agent on Montserrat kept track of SEA-CALIPSO shipments and the receiving of the equipment, and provided useful advice on negotiating local bureaucracy.

The operational base of the experiment was a large rented villa (west of the MVO, near OLVN in Fig. 15.9) that from October to December 2007 housed scouting and deployment teams, and provided secure instrument storage. PASSCAL technicians used an apartment in the villa to test and work on instruments. In December, with the arrival of 35 land-based participants, the villa served as operational headquarters (HQ) for radio and telephone communications with hiking teams and the ship, providing for changes in timing of hiking routes, and discussions of adjustments in shiptracks.

RefTek sites were accessible by vehicle or foot in the northern third of Montserrat, outside of the volcanic exclusion zone, and including both Centre and Silver Hills (Fig. 15.11). Instrument locations were isolated as much as possible from vehicle traffic, electric wires, cliffs or water waves that might interfere with seismic signals. Sites had to be reasonably secure from theft of the battery and solar panels. Final locations included the gardens and yards of private homes, local businesses, a Water Authority water storage tank, the MVO and the airport. Teams visited each

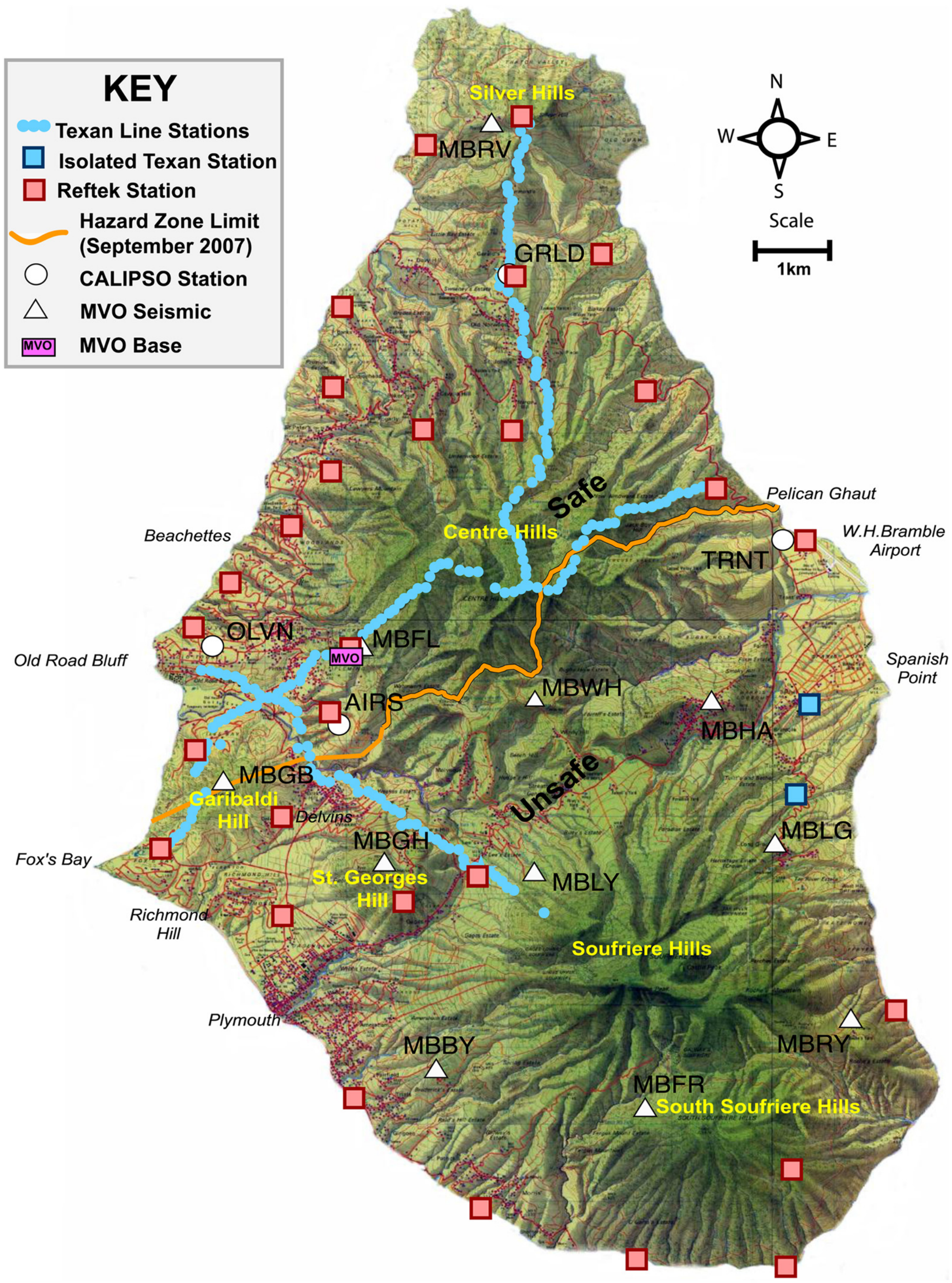

Colour online/colour hardcopy

Fig. 15.9. Deployed instruments, on topographical base map of Montserrat. Inset table provides key. Refteks, orange squares; Texans, strings of blue dots, and blue squares near Spanish Point; MVO seismograph sites, white triangles; CALIPSO strainmeter sites, white dots; hazard zone safe–unsafe boundary, orange line; MVO, purple rectangle.

site in advance and received permission from the resident or official in charge. Land station coordinates were determined by direct GPS measurement, leading to uncertainties of about 5 m in horizontal position and 50 m in station altitude.

In the southern two-thirds of Montserrat, within the volcanic exclusion zone and including South Soufrière Hills and SHV, most of the RefTek locations were accessible only by small boat transport of people and instruments (Fig. 15.12). The limited access resulted in poorer coverage in the south than in the north (Fig. 15.9). Deployments required permissions on a given day from the MVO, and radio or mobile phone contact with the MVO. Landing sites included the beaches south of Plymouth and along the Tar River Delta, and, with more difficulty, shoreline rocks near the southern point of Montserrat. Sites were accessible with relative ease in October but with great difficulty in December owing to strong winds and wave action.

The primary challenge in deploying the Texans during the experiment was that the 204 dataloggers had very limited battery capacity and had to be deployed in conjunction with the anticipated hours of airgun shooting, which could not be known with certainty beforehand. Within a few hours on either side of the experiment, five teams hiked over 5–10 km of steep, rough terrain, installing and/or collecting an instrument every 100 m. The duration of these treks ranged from several to as much as 9 h. The design of the Texan is such that if battery power is lost, the timing fails and renders the data unusable. Thus, it was of crucial importance that the instruments be collected and data uploaded promptly, before the batteries died. Because the airgun shooting duration was expected to be similar to the Texan battery life, the hiking deployment was planned closely around the hours of the shooting. We had requested, from PASSCAL, tests of instruments adjusted for longer-life lithium batteries;

Colour online/colour hardcopy

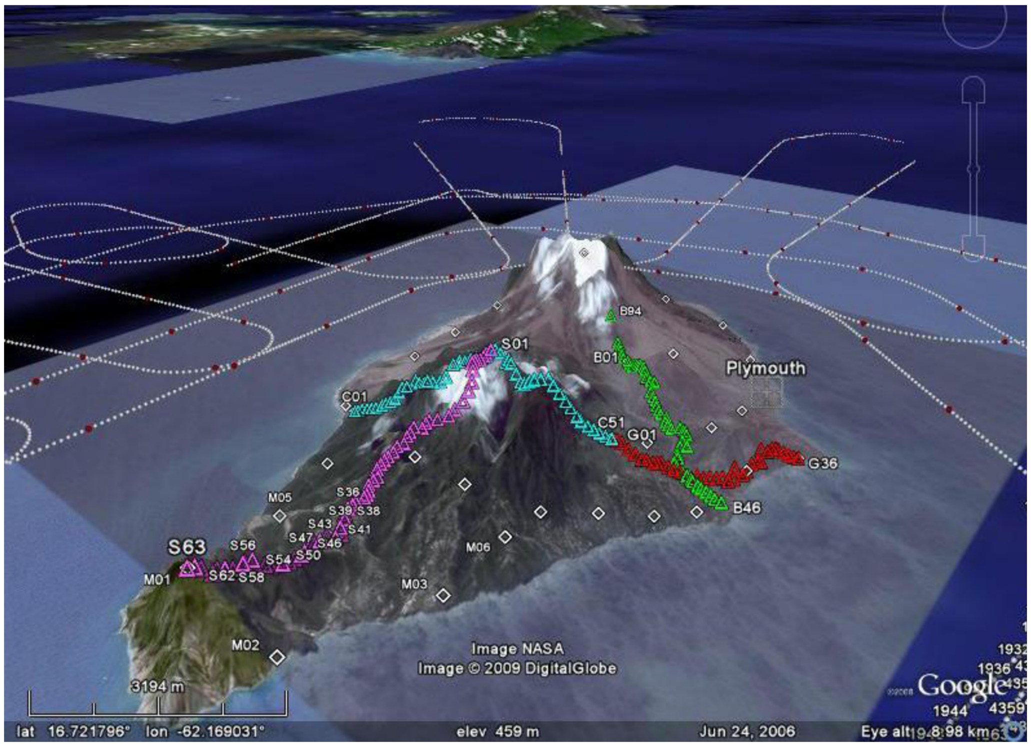

Q13

Fig. 15.10. Oblique view of Montserrat island towards the SE. The volcanic centres of Silver Hills, Centre Hills and Soufrière Hills run from north to south (left to right). Texan array lines are shown by coloured triangles, with two arrays intersecting across the top of the Centre Hills (cf. Fig. 15.9). The array in green is radial to the Soufrière Hills Volcano, and roughly follows the Belham River Valley. Refteks are shown by white diamonds. Shiptracks are shown offshore, and the island of Guadeloupe, to the south, is at the top of the image. Image courtesy of NASA 2009.

however these modications affected the electronics systems and the reliability of performance was reduced, so this approach was abandoned. Contingency plans were devised to accommodate staggered start/stop times for the standard instruments for several hours at the beginning and end of the shooting. These contingency plans were not used in the experiment because of the shortened shooting time. Frequent communications between HQ and the ship were vital in adjusting to maritime developments that could influence land operations.

Texans were placed every 100 m over a total of approximately 20 km; for installation, each team was assigned one line accessible by road and one hiking line. Texans were in place for approximately 90 h, accommodating both the 77 h of actual shooting and the approximate 100 h battery life. Although the 77 h of shooting time was less than that anticipated (approximately 100 h), the reduction of shooting time 'resolved' our battery life problem. One line of easily accessible Texans was retrieved, the data uploaded and instruments reinstalled mid-experiment for a quality check in order to confirm that signals were being received, and to look at preliminary results. The road-based Texans were installed at the side of roadways, on public land where possible, thereby requiring the fewest possible number of permissions. Two lines required the exclusion zone to be entered and, therefore, access permission was needed from the MVO. Two Texans were installed by B. Voight and R. Herd on the NE side of the volcano, at Whites Yard and inland from Spanish Point.

Colour online/colour hardcopy

Fig. 15.11. Installation of RefTek seismometer stations. (**a**) The RefTeks were deployed from October through to December 2007, powered by deep cycle batteries with solar panel recharging. Typical site, at M10 Royal Palm, in partly foliated terrain with buried seismometer and plastic container for the datalogger and battery. Frame with a solar panel in the rear. Photograph courtesy of V. Miller. (**b**) Site installation at M15 Air Studios. Photograph courtesy of B. Voight.

Colour online/ colour hardcopy

Fig. 15.12. Loading RefTek equipment aboard the vessel *Daily Bread* at Little Bay in north Montserrat, for deployment along the south coast in October 2007.

For the Centre Hills hiking lines, the difficulty of parts of this terrain would be hard to overstate (Figs 15.10 & 15.13). The Centre Hills are characterized by mountainous rainforest with steep ridges and valleys. Hikers were on precipitous, wet and slippery soil-veneered slopes, using trails made almost invisible in places by dense vegetation. Local guides (and one from East Anglia, UK) cleared paths with machetes prior and during the experiment, and were vital in getting the groups up into the mountains. Safety considerations included carrying First Aid kits and radios for communication with HQ and the MVO. All groups carried portable GPS units suited to forest cover, for navigation and to mark the instrument locations.

Ship-board operations

The offshore field campaign consisted of the 5 day seismic cruise JC19 on the RRS *James Cook* plus the OBS deployment from the vessel *Beryx*. The JC19 cruise lasted from 16 to 21 December, and, as has been stated, comprised 77 h of continuous shooting with an artificial seismic source and collection of MCS seismic data around the island of Montserrat. The cruise started and finished in St John's, Antigua, 30 nautical miles east of Montserrat. The shooting took place between 17 and 20 December.

The OBS deployment was accomplished from the 12 m vessel *Beryx* (Fig. 15.14) by a team hosted by the Institut Regional de Peche et Mer (IRPM) in Gourbeyre, Basse Terre, Guadeloupe, where it was given access to dry working space for the set-up of the instruments. Guadeloupe is approximately 50 nautical miles south of Montserrat. The OBS deployment was scheduled to take place on 9, 10, 11 and 12 December 2007, but was delayed due to the late delivery of the equipment. The equipment was delivered on 12 December, and the instruments were deployed on 13, 15 and 16 December. The OBS deployment locations had to be changed from the previously planned locations mainly due to concerns about the safety of the team and the equipment because of rough seas caused by the presence of a tropical storm over Haiti that sent reinforced trade winds over the Lesser Antilles. The deployment challenged the skills of the skipper and dedicated OBIC staff. The OBS instrument recovery was accomplished on 21 and 22 December.

The RRS *James Cook* docked in Antigua on schedule, from 30 November to 3 December, where early preparations for the SEA-CALIPSO cruise were undertaken (Fig. 15.15). Major items of equipment loaded on board were: (1) the eight-airgun array; (2) 12 XBTs to measure the water-column temperature; (3) the 600 m 48-channel digital streamer; (4) 48 sonobuoys donated by Lamont-Doherty Earth Observatory; (5) cetacean monitoring equipment supplied by Seiche Measurements Ltd for purposes of marine mammal environmental control; and (6) two PASSCAL Refteks for shot-time recording. The deck plan is shown in Figure 15.16. The airgun and streamer engineers set up and tested their equipment at the port. This included synchronizing the streamer and airgun clocks, and supplying the streamer datalogger with an electronic pulse from the airgun trigger mechanism ('Long-Shot' airgun controller). Much of the loading and testing of the equipment had to be carried out before the preceding JC18 cruise, also supported at Antigua port call. The turn-around time between cruises JC18 and JC19 was limited to a half day on 16 December, requiring efficiency in equipment off-loading and loading, and testing.

On 16 December, the airguns were installed and tested. The streamer winch had been damaged badly during transit, but a spare winch was found and made suitable for the cruise (Fig. 15.17). The cetacean monitoring equipment (Passive Acoustic Monitoring, PAM) was set up. A radio mast was erected on the ship to receive transmission from the sonobuoys, and the computers were set up in the ship's laboratory. In addition, a RefTek (the land station seismometer type) datalogger and an OBS datalogger were set up in the ship laboratory. All datalogging systems (streamer, sonobuoy, RefTek, OBS) recorded an electronic pulse from the airgun trigger mechanism for accurate timing. The depth indicators used to monitor the airgun depth were delayed at customs and, consequently, the ship was late leaving Antigua, so shooting began on the morning of 17 December.

As previously mentioned, extremely rough sea conditions made OBS deployments east of Montserrat untenable, and sites to the the lee of the island were chosen to facilitate deployment and recovery of the instruments. This circumstance required modification of shiptracks, with consultations carried out between the offshore and onshore leadership groups. Both radial and quasi-circular tracks needed to be realigned with respect to the existing OBS positions.

When at sea shooting around Montserrat on 17–21 December, all equipment was monitored 24 h each day. The airguns were deployed by hoist from the rear deck of the RRS *James Cook* (Fig. 15.18a, b). One team of watchkeepers monitored airgun depths and misfires, streamer depth and quality, and ship navigation and speed, and deployed sonobuoys. Specialist engineers were on call for the streamer or airguns. A second team of watchkeepers monitored for cetaceans. During daylight hours, this team both kept watch from the bridge and monitored the PAM (Passive Acoustic Monitoring) microphone array. At night, just the PAM was monitored. In the case of a cetacean sighting, shooting was halted, a 20 min clearance period was enforced and then the airguns were switched on using a 'soft start' (turning on each gun 3 min apart).

The deployment involved 77 h of active shooting (Fig. 15.18c, d), with several short (31–37 min) interruptions, once to deviate ship-path for a yacht on a collision course, once to repair a gun logger and three times due to sea mammals in the vicinity. The possibility of serious interference of the shooting schedule by marine mammal detection was a worrisome concern because frequent sightings would have had major impacts on both sea and land operations, and the success of the experiment. The period of active shooting was also affected by several longer pauses required by ship command at the beginning and end of the 5 days of ship operations, to a degree not anticipated beforehand, and these pauses required adjustments to both land and sea operations. The cumulative effect of these pauses reduced the shooting time available and required modifications of the ship track, particularly for the final day. The decisions were developed by consultation between the offshore and onshore leadership groups.

Colour online/colour hardcopy

Fig. 15.13. Installation of Texan seismometer stations. Texans were installed in December 2007 just before the airgun shooting. (**a**) Hikers carried Texans across rugged terrain of the Centre Hills, mountainous rainforest with steep ridges and valleys. Trails on precipitous wet slopes could be almost invisible because of dense vegetation, and were cleared with machetes shortly before the experiment. Photograph courtesy of B. Voight. (**b**) Installation on the north–south Texan array line on top of Katy Hill (near the words 'Centre Hills' in Fig. 15.9), in elfin cloud-forest vegetation with thick undergrowth. Photograph courtesy of A. Belousov. (**c**)–(**e**) Sequence showing the Texan installation. Pit with a seismometer and bubble level; seismometer plus datalogger in a protective bag prior to burial; view after the burial with a location flag. Photograph courtesy of G. Mattioli.

As noted above, many shipboard problems of varied complexity were encountered and efficiently resolved. These were critical to the success of the operation, to the credit of the dedicated and skilled National Marine Services technical staff, the professionalism of the officers and crew of the RRS *James Cook*, and the efficient work of the GeoPro airgun team.

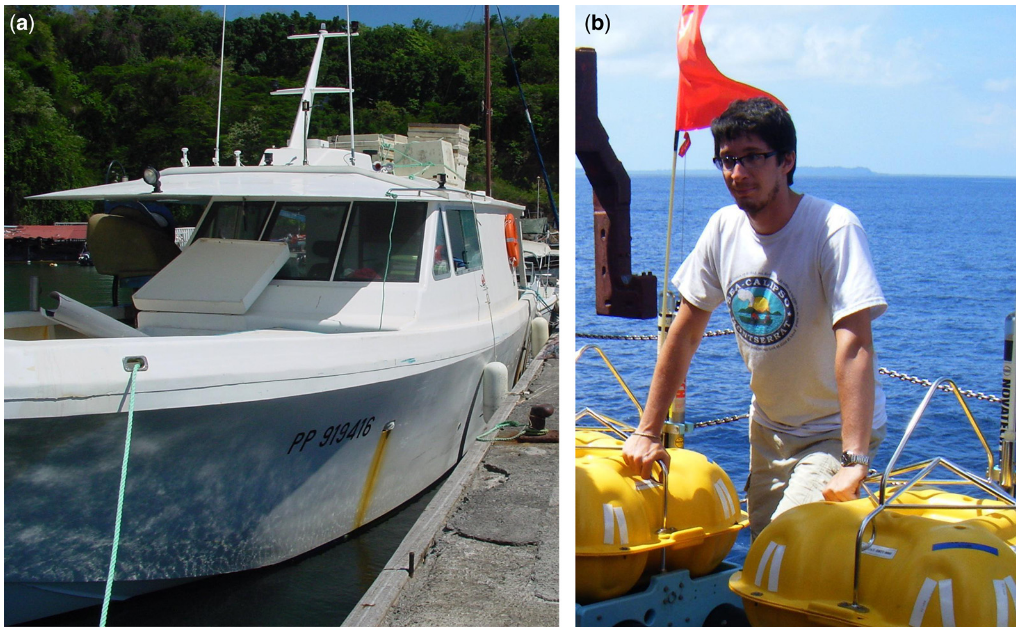

Colour online/colour hardcopy

Fig. 15.14. Installation of ocean-bottom seismometer stations. (**a**) The 34 m vessel *Beryx*, based in Gourbeyre, Basse Terre, Guadeloupe, was used for OBS deployments in rough seas. (**b**) Onboard the *Beryx*, with two LC2000 OBS units being readied for deployment. Photograph courtesy of M. Paulatto.

Scientific results

This section focuses on five main topics: data and 2D modelling; the preliminary 3D analyses of tomography; the 3D velocity model generated with further analysis; reflection imaging of deep structures; and offshore reflection profiling.

Data and 2D modelling

The data quality is generally high, with first arrivals recognized at up to 50 km offset for the OBSs on both hydrophone and vertical geophone (Paulatto *et al.* 2010*a*). The horizontal components are also of high quality, suggesting that the instrument–seabed

Colour online/colour hardcopy

Fig. 15.15. RRS *James Cook* (**a**) at sea and (**b**) at anchorage in St Johns, Antigua. (**c**) Loading equipment and supplies for cruise JC19 at Antigua port call.

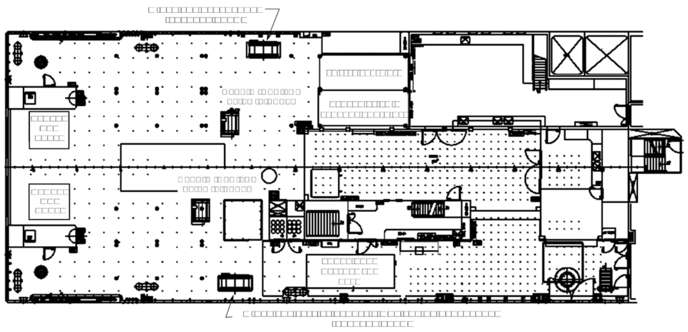

Fig. 15.16. Ship deck plan for the JC19 cruise.

coupling was good. For the land stations, data quality depends strongly on the local noise conditions and host materials. Example data sections are shown in Figure 15.19. Identified phases include crustal refracted P-wave arrivals and their multiples, refractions turning in the sediments, and wide-angle basement reflections. In the OBS data (Fig. 15.19a, b), two distinct P-wave refractors can be distinguished, with apparent velocities of 2.3 km s^{-1} (layer 1) and 4.0–6.0 km s^{-1} (layer 2), respectively, giving a first indication of the offshore velocity structure. Phases have been manually picked, from the vertical geophone or hydrophone data, depending on which one presented the best data. Picking uncertainties were estimated visually. For first arrivals at short offset, uncertainties are between 20 and 40 ms, and at longer offsets between 20 and 100 ms. Reflected phases that are masked by the first-arrivals coda have uncertainties of 40 ms. Some gaps are present in the dataset owing to short interruptions in shooting caused by sea mammals or other vessels in the vicinity and airgun maintenance.

A subset of the data was selected for the modelling presented in Paulatto *et al.* (2010*a*), consisting of four OBSs and four land stations, approximately aligned on a SE–NW line crossing Soufrière Hills and Centre Hills (black dashed line in Fig. 15.20; cf. Fig. 15.9). Records of the shots on the radial line to the SE of the island, and other isolated shots on the crossings between the selected profile and the shooting track in the NW, were analysed and travel times were inverted to obtain a provisional 2D seismic velocity profile through the island, with the further aim to guide the inversion of the full 3D dataset.

The regularized inversion approach developed by Hobro *et al.* (2003) has been used. This method allows the data misfit and

Colour online/colour hardcopy

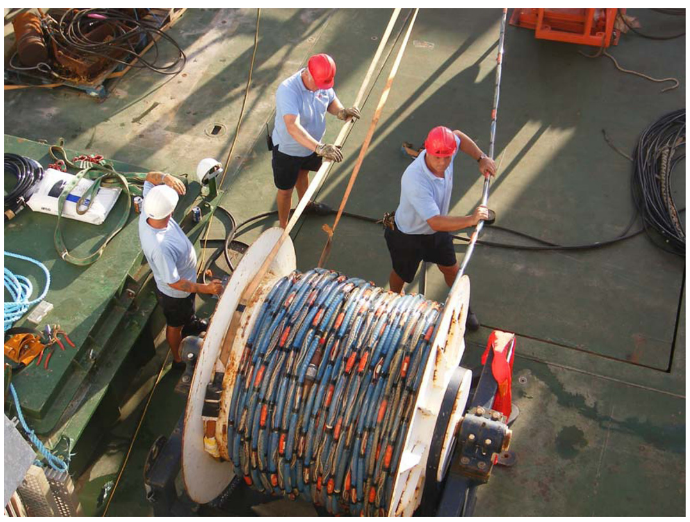

Fig. 15.17. Deck winch in streamer operations during JC19 on RRS *James Cook*. Photograph courtesy of J. Hammond.

model roughness to be minimized at the same time to give a minimum-structure model, and it allows the simultaneous inversion of refractions, wide-angle reflections and multichannel seismic data.

The final 2D velocity model (Fig. 15.21b) extends 54 km in the horizontal direction, and from the top of Soufrière Hills at almost 1000 m elevation to a depth of 10 km below sea level (bsl). The ray coverage reaches 10 km depth and is denser on the SE of the island where shots were fired along a radial line coincident with the segment chosen for the 2D model (Fig. 15.21c). Layer 1 comprises the sediment layer offshore and volcanic edifice on land, and is characterized by a strong lateral velocity gradient in proximity of the coast. Velocities vary from 1.5 to 3.0 km s^{-1} offshore and from 2.5 to 5.5 km s^{-1} onshore. A high-velocity core is imaged under the island, with the two highest velocity regions located under the volcanic edifices of Soufrière Hills and Centre Hills, and also extending into layer 2. Offshore velocities in layer 2 vary from 4.0 km s^{-1} at the top to approximately 6.5 km s^{-1} at a depth of 10 km. Onshore velocities vary from 5.0 to 6.5 km s^{-1}. The interface between layer 1 and 2 is located at a depth of between 2.0 and 2.8 km. The thickness of layer 1 ranges from 1 km, far from the island, to a maximum value of 3.6 km under the Soufrière and Centre Hills, both of which have maximum elevations of about 1 km above sea level.

This velocity model reveals the presence of large lateral velocity variations beneath the volcanic edifice, extending over the entire depth range of the model. Layer 1 is interpreted as a sedimentary layer ($V_p = 1.5–3.0$ km s^{-1}) plus extrusive and intrusive volcanic material forming the island of Montserrat ($V_p =$ 3.0–5.5 km s^{-1}). Since resolution below about 5.0 km is poor, interpretation of the velocity structure in layer 2 has to be cautious. Paulatto *et al.* (2010*a*) distinguished two different regions within layer 2: a well-constrained upper sublayer extending down to 5.0–7.0 km bsl, with velocities of between 3.5 and 6.0 km s^{-1}, and characterized by a strong vertical and lateral velocity gradient, and a lower sublayer with velocities over 6.0 km s^{-1}, a lower-velocity gradient, and extending to the bottom of the model, which is at a depth of 10 km. Layer 1 plus the upper sublayer of layer 2 correspond to the upper layer defined by Boynton *et al.* (1979), while the lower sublayer corresponds to the top of the middle layer.

In layer 1 the predominant feature of the velocity field is the presence of high P-wave velocities beneath the island contrasting with the lower-velocity sediments on the flanks and beneath the ocean floor. The velocity contours mirror the topography and suggest that the high-velocity region has two cores, below Soufrière Hills and Centre Hills, respectively.

Paulatto *et al.* (2010*a*) distinguished three regions within layer 1: a core, an apron and the normal sedimentary cover, each characterized by different seismic velocities. The core has velocities similar to those found in the upper crust ($V_p = 4.0–5.5$ km s^{-1}) and broadly compatible with an andesitic composition (Christensen & Mooney 1995), as suggested by the surface geology (Harford *et al.* 2002). The interpretation of the high-velocity core of layer 1 is based on the exposed geology of the SHV, on the identification of numerous noritic xenoliths with hypabyssal textures in the lavas (Kiddle *et al.* 2010) and on geophysical evidence that indicates that the current eruption is fed from a shallow dyke (e.g. Mattioli *et al.* 1998; Hautmann *et al.* 2009). The exposed geology consists of andesite domes, breccias formed by rockfalls and mass wasting, and hydrothermally altered equivalents (e.g. Harford *et al.* 2002). These observations indicate that the core includes a pile of andesitic domes, and a system of a dykes and sills that represent the feeders for several dome eruptions over the last 170 ka. Eruptions, flank collapses, rockfalls and erosion displace material from the top of the volcanoes and deposit it on the flanks and on the seabed, and this material, intermixed with pelagic sediments, makes up the lower-velocity apron around the cores (Le Friant *et al.* 2004, 2009). This

Colour online/colour hardcopy

Fig. 15.18. Airgun operations during JC19 on the RRS *James Cook*. (**a**) Hoist operations on stern rear deck. Photograph courtesy of J. Hammond. (**b**) Airgun cluster being prepared for deployment off the stern. Photograph courtesy of J. Hammond. (**c**) Shooting on a radial track offshore eastern Montserrat. Airgun explosion bubbles are visible behind the hoist. The Tar River Valley leading up to the Soufrière Hills Volcano is in the distance with the volcano summit covered by cloud cap. Photograph courtesy of S. Sparks. (**d**) Synchronized explosions from the dual airgun clusters, offshore Montserrat. Photograph courtesy of S. Sparks.

region exhibits a strong lateral velocity gradient, and has velocities that are intermediate between the solid andesite and the submarine sediments ($V_p = 2.5–4.0\ \mathrm{km\ s^{-1}}$). Different degrees of compaction, clast vesicularity, grain size, water content and percentage of pelagic sediments could account for the range in seismic velocities observed. This kind of structure is not limited to the subaerial part of the island but continues downwards to the bottom of layer 1, suggesting that the main eruption style for the island's entire history was similar to that exhibited by the current eruption.

Velocities in the sediment layer in the offshore region are those of normal oceanic sediments ($V_p = 1.5-3.0\ \mathrm{km\ s^{-1}}$) (cf. Hamilton 1980). The range of velocities observed is consistent with data from sediment cores collected in the region (Reid *et al.* 1996; Le Friant *et al.* 2008) that suggest that the main sediment components are hemipelagic calcareous and volcaniclastic

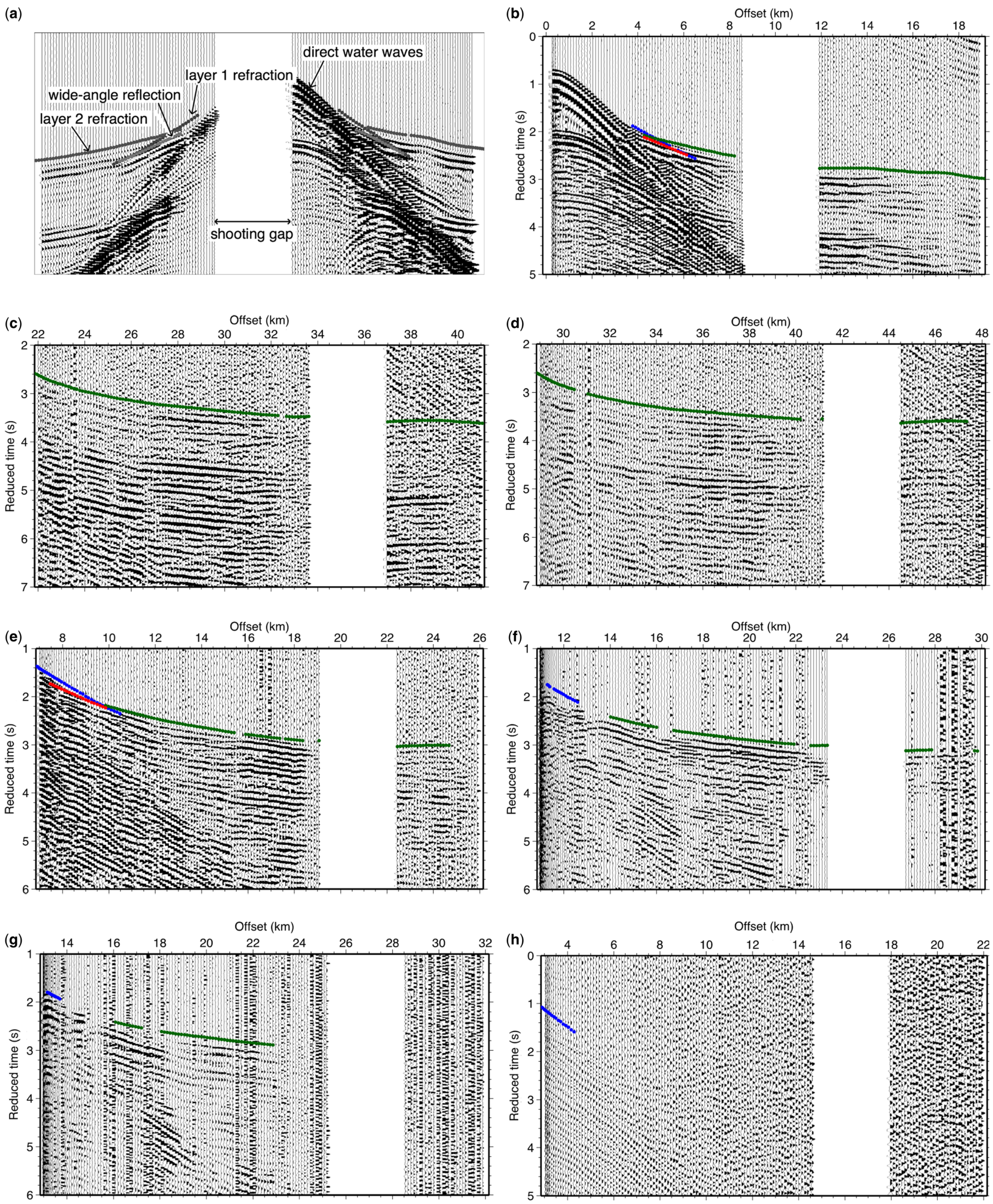

Colour online/colour hardcopy

Fig. 15.19. Examples of seismic data plotted as common receiver gathers (after Paulatto *et al.* 2010*a*). Panels correspond to the radial shooting line from point A (right end of the panels) to site O10 (left end), shown in Figure 15.20, recorded on the eight instruments used in the 2D inversion. (**a**)–(**d**) Hydrophone channel recordings of OBS stations O09, O10, O12 and O11. (**e**, **f**) Vertical geophone recordings of Texan stations B94 and C46. (**g**, **h**) Vertical component recording of Reftek 130 stations M11 and M30. Synthetic travel times calculated through the final velocity model are superimposed on the data (blue, layer 1 refractions; green, layer 2 refractions; red, basement reflections). The white gap present in all panels corresponds to an interruption in shooting due to marine mammals in the vicinity of the guns. A minimum-phase filter with corner frequencies 3–5–20–25 Hz was applied to the data. Amplitudes are normalized with a factor inversely proportional to offset.

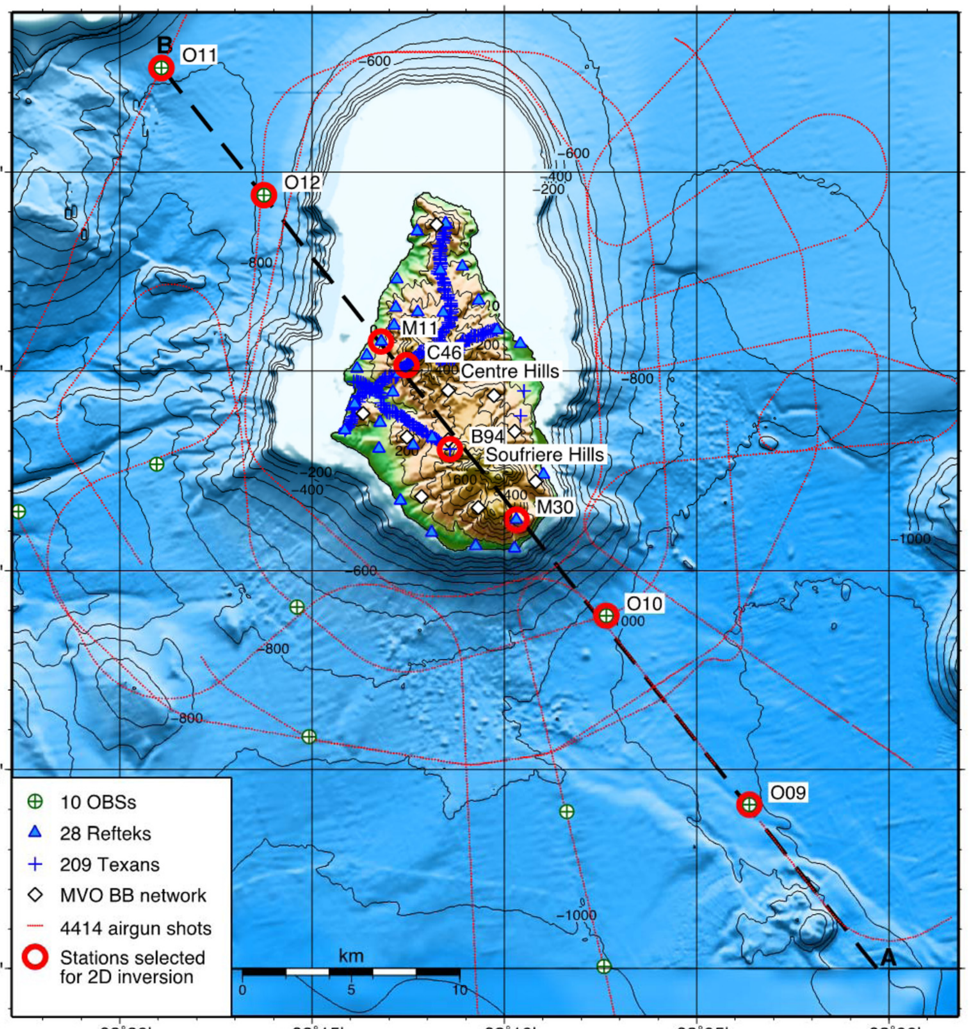

Colour online/colour hardcopy

Fig. 15.20. Bathymetric map of Montserrat with SEA-CALIPSO station array and shot positions. The black dashed line marks the position of the 2D tomographical section presented in the Paulatto *et al.* (2010*a*) study. The digital elevation model (DEM) was obtained by merging the GEBCO 08 Grid (http://www.gebco.net) with a detailed elevation model of Montserrat and the surrounding seafloor from Le Friant *et al.* (2004).

sediments, interspersed with turbidites. The gradual decrease in velocity with increasing distance from the coast (Fig. 15.21b) is attributed to a variation in the volcaniclastic content, and to different volcaniclastic sedimentary facies having different physical characteristics. Coarse-grained sediments are expected to be more abundant close to the shelf slope, while fine-grained sediments are deposited further away (e.g. Trofimovs *et al.* 2006).

The interface that separates layer 1 and 2 is interpreted as the palaeo-seabed at the time when volcanic activity shifted from the outer to the inner Lesser Antilles Arc (*c.* 22 ka). Far from the

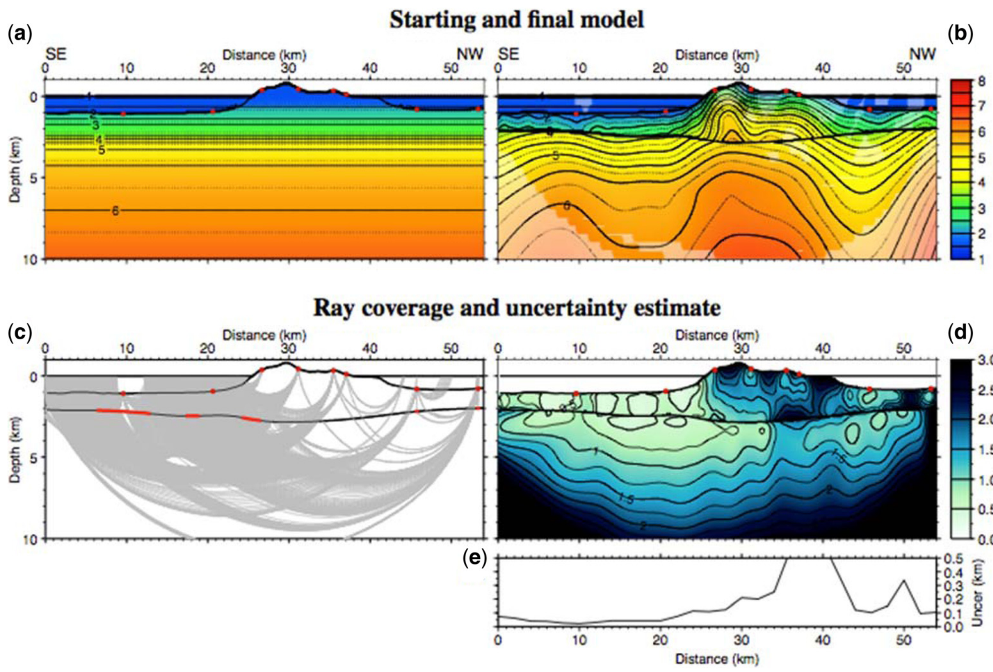

Colour online/colour hardcopy

Fig. 15.21. (**a**) Starting model for 2D inversion process. (**b**) Final two-layer model, paler areas are not sampled by rays inverted in the final step. (**c**) Ray coverage of final model. Segments of the basement interface that are sampled by wide-angle reflections are highlighted in red. (**d**) Velocity uncertainty estimate. (**e**) Depth uncertainty estimate for basement interface. Station positions are marked by red dots. Vertical exaggeration is 2:1. After Paulatto *et al.* (2010*a*).

island, where layer 1 thickness is about 1200 m, this interpretation gives a mean sedimentation rate of 5.4 cm ka^{-1}. This result is in agreement with sedimentation rate estimates from sediment cores in the Lesser Antilles (Reid *et al.* 1996; Le Friant *et al.* 2008). The interface is depressed under the island, suggesting that the load of the volcanic edifice may be causing flexure of the underlying lithosphere. There is also evidence in the coincident seismic reflection data collected (Kenedi *et al.* 2010) that a major extensional fault is crossed by this section, and could play a role in depressing the basement under the island. The interface is well constrained in the offshore region SE of the island, where it clearly corresponds to a discontinuity in physical characteristics, but is only loosely constrained beneath the island where there is no velocity contrast. It is not yet clear whether the reflector imaged beneath South Soufrière Hills (at $x = 26$ km in Fig. 15.21c) corresponds to the same feature as the reflector imaged offshore, separating the sediments from the igneous crust, or whether it is a distinct feature, possibly corresponding to a sill.

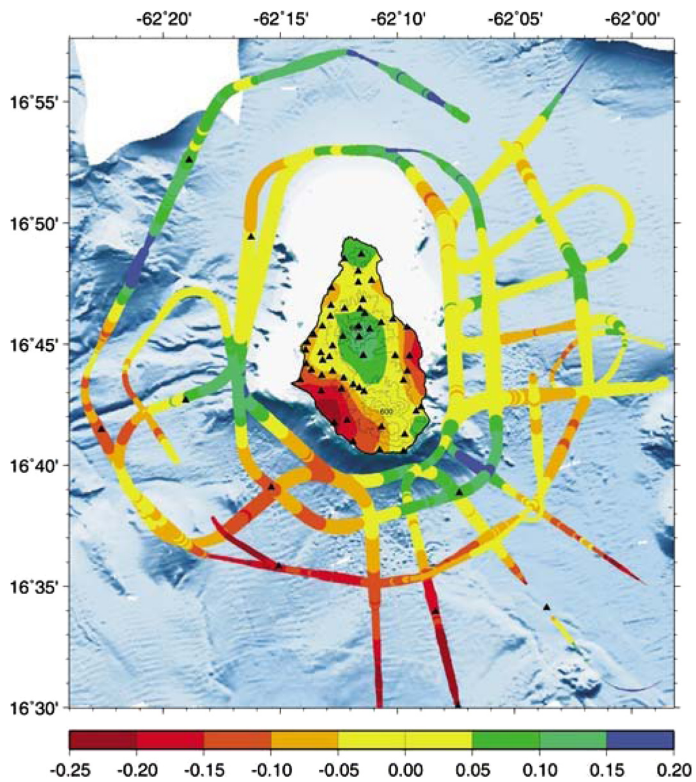

Fig. 15.22. Map of 3D tomography area showing bathymetry, topography contours, ship track and station locations used in the Shalev *et al.* (2010) study, and average time residuals for shots and land-based recorders. Black triangles mark the seismic stations included in the tomographical inversion. The stations offshore are ocean-bottom seismometers. Colours indicate the average residuals (time computed minus time observed) in seconds (see the bar scale), where red represents slow and blue represents fast. On land, the colours contour the average residuals; on water, colours represent the average residual for each shot. The width of the ship track line is proportional to the number of seismic stations that recorded an airgun blast from a particular point on the track.

Colour online/colour hardcopy

Preliminary 3D seismic velocity model

In another preliminary study developed in early 2008 (Shalev *et al.* 2010), the first-arrival time data were inverted using the tomography code from Shalev & Lees (1998). The method develops a cubic *b*-spline description of the 3D volume, and applies an LSQR algorithm to invert the data. The study used 115 158 ray paths derived from 58 stations, including 25 Refteks, 19 Texans, seven OBSs and seven MVO broadband stations in the exclusion zone (Fig. 15.22).

Starting conditions were two 1D velocity models (Shalev *et al.* 2010, fig. 2), one each for land and for ocean, with the boundary between them defined as the bathymetric line at 200 m water depth. The target cube for the 3D inversion comprised $50 \times 45 \times 8$ km, with a horizontal velocity grid spacing of 0.5 km in the land area, 1 km for the ocean near the land and 5 km near the outer boundaries (Shalev *et al.* 2010, auxiliary material). Vertical grid spacing was 0.5 km to a depth of 5 km, and 1 km below 5 km. A smaller grid spacing of 0.25 km was tested for the centre of the land area but showed no improvement.

To check for resolution of the 3D inversion, Shalev *et al.* (2010) ran chequerboard tests based on the starting 1D velocity models. A consistent recovery of the pattern was observed to a depth of over 4 km in the area of good ray coverage under the island, but below 5 km depth the resolution was unreliable (Shalev *et al.* 2010, auxiliary material). Although the acquisition geometry of the experiment was designed to target magma storage zones at >5 km depth under SHV, the actual seismic velocities beneath and surrounding Montserrat turned out to be faster than expected, thus turning back most of the refracting seismic energy at depths <5 km. The result for the dataset used in this preliminary study was that the first-arrival P-wave tomography produced a reliable image of the velocity structure only between 1 and 5 km in depth, and extending approximately to the shelf break.

Results of the tomographical inversion are shown in Figure 15.23. Notable features in the P-wave velocity structure are high-velocity anomalies below all three volcanic centres, at about 2–3 km depth. The most prominent of these is the anomaly below Centre Hills, with a similar but less intense anomaly under SHV (Figs 15.23a & 15.24).

Other large and consistent anomalies are the low-velocity volumes on the flanks of the volcanic centres. There are three such anomalies, to the NE, NW and SW of Centre Hills. These anomalies are stable regardless of inversion parameters. The east–west cross-section (Fig. 15.23d) shows both a high-velocity body under SHV and a low-velocity anomaly west of SHV. The suggestion from the image that the two anomalies are elongated downwards and away from the centre of the island could be an artefact of ray paths coming from the perimeter toward the centre, but the geometric positions of the main high-amplitude anomalies are stable.

The fast anomalies beneath the three volcanic centres are interpreted to correspond mainly to dense crystallized andesite comprising dome cores, sills, dykes or irregular shaped intrusions, and adjacent altered zones with silica precipitation, that are seismically faster than the surrounding material. The latter materials comprise lavas and volcaniclastic deposits, including talus, block-and-ash flow deposits and lahars. The interpretation of crystalline cores are consistent with the work of Harford & Sparks (2001), who suggested that recurring intrusions solidify at depths up to 3 km under SHV, and by other evidence that suggests that dykes may rise to shallow depths under SHV (Mattioli *et al.* 1998; Costa *et al.* 2007; Hautmann *et al.* 2009; Chardot *et al.* 2010; Linde *et al.* 2010; Voight *et al.* 2010*a*). The high velocities observed are also consistent with nodules in eruption products (Kiddle *et al.* 2010).

The locations of the low-velocity anomalies NE of Centre Hills and west of SHV suggest a relationship with the volcanic centres (Fig. 15.24), and the features probably represent synvolcanic apron deposits. An extension of such low-velocity features to 3–4 km depth could be problematic. There is good evidence from offshore seismic reflection profiles for buried volcaniclastic deposits to a depth of 2 km off the east coast of Montserrat (Kenedi *et al.* 2010). These low-velocity features could also result from hydrothermal alteration, which has been shown to reduce seismic velocities in oceanic rocks (Carlson 2001). Evidence for hydrothermal circulation beneath

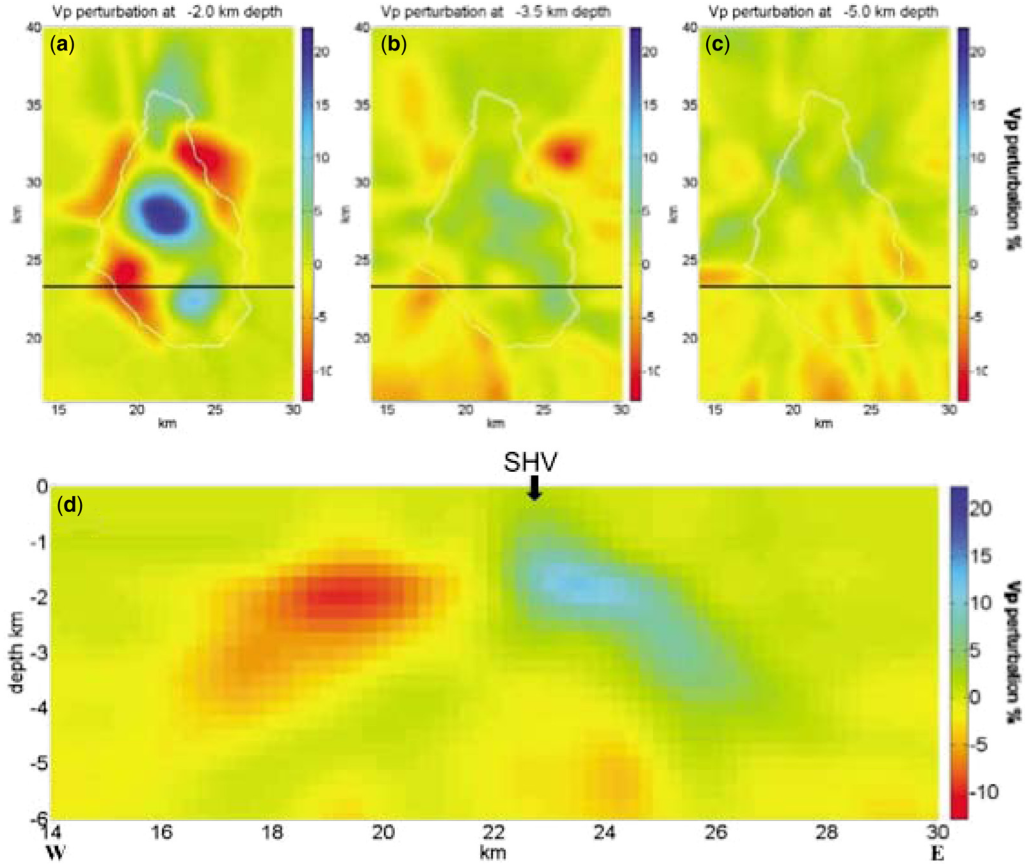

Colour online/ colour hardcopy

Q13

Fig. 15.23. P-wave tomography results displayed as perturbation from the average velocity at each depth. Blue represents faster velocities and red represents slower velocities. Map view slices through the target volume at depths of (**a**) 2.0, (**b**) 3.5 and (**c**) 5.0 km. The black line marks the location of (**d**) the cross-section across the SHV. The outline of Montserrat is a white line on all map view slices. After Shalev *et al.* (2010).

the Garibaldi–Richmond–St George's hills region includes anomalous seismic activity (Rowe *et al.* 2004), surface hot springs and ponds, and hot water in boreholes (Chiodini *et al.* 1996). A recent magnetotelluric (MT) study on Montserrat shows good correlation between these low-velocity zones and low resistivity at a depth of 1–4 km (G. Ryan & P. Malin unpublished data 2009).

Enhanced 3D seismic velocity model

In further analyses reported by Paulatto *et al.* (2012), first-arrival travel times were inverted to generate a 3D seismic velocity model using a tomography code based on the regularized least-squares approach (Hobro *et al.* 2003). The algorithm allows a realistic multi-layer model parameterization. The vertical components of 61 land stations were used in this study, selected to provide a regular coverage of the island and yielding 181 665 first-arrival recordings (Fig. 15.25). This dataset is more comprehensive than that used in the preliminary work and was developed during a thorough PhD dissertation study by Paulatto in Q5 which special attention was given to data from all 10 OBS stations, in addition to land stations.

Some characteristics of the upper crustal structure are evident in the raw data. Field recordings at OBS stations show delayed first arrivals and decreased signal-to-noise ratios for seismic waves undershooting SHV (Fig. 15.26), a signature often associated with the presence of magma bodies. The delay is matched closely by synthetic first arrivals for the final model, but not by

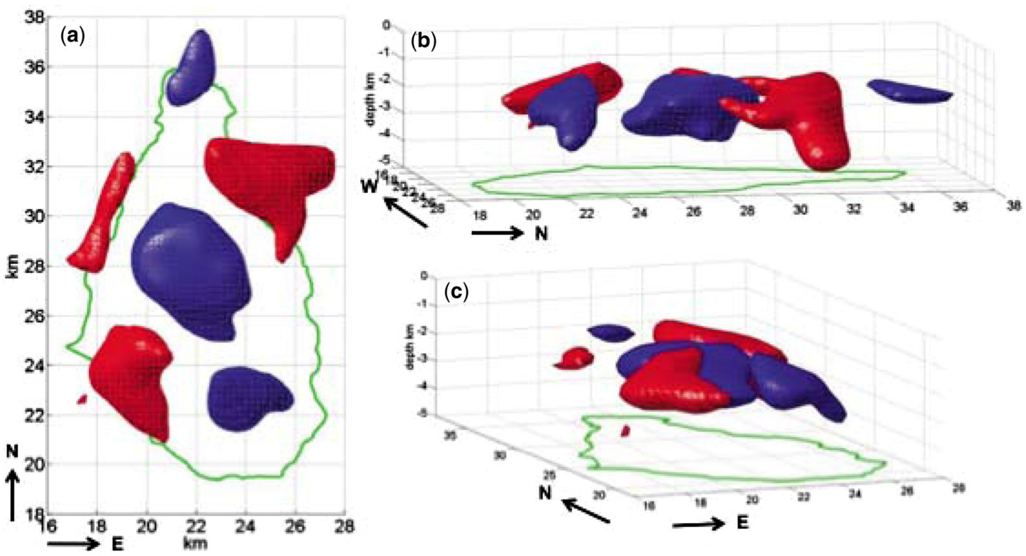

Colour online/ colour hardcopy

Fig. 15.24. Three-dimensional iso-surfaces of velocity anomalies, after Shalev *et al.* (2010). The blue surfaces define anomalies that are >6% faster than average. The red surfaces represent anomalies that are >6% slower than average. (**a**) Map view. (**b**) View from the ESE. (**c**) View from the SSW.

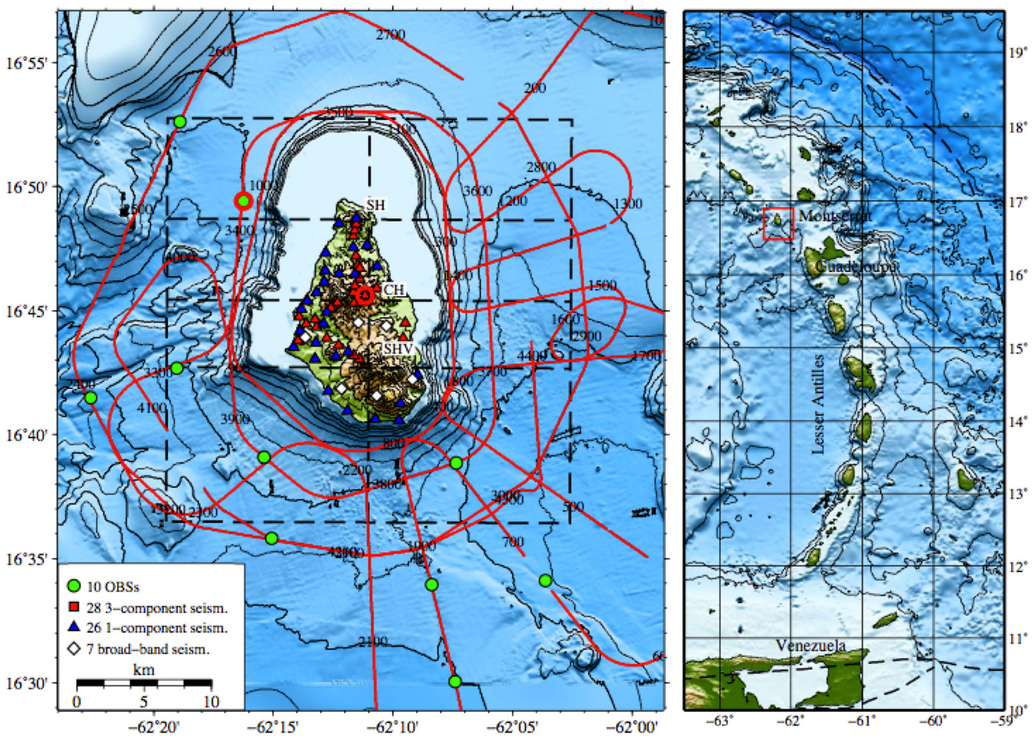

Fig. 15.25. Topographical map of survey area with recording array and shot positions. Contour interval is 200 m. Shiptrack shown by the red line with shot numbers labelled every 100 shots. Locations of the sections shown in Figure 15.28 are marked with black dashed lines. SH, Silver Hills; CH, Centre Hills; SHV, Soufrière Hills Volcano. Reftek stations in blue, Texans in red and MVO stations in white. The stations corresponding to the example data in Paulatto *et al.* (2012, figs 2 & 3) are highlighted in red. The panel on the right shows the location of Montserrat in the Lesser Antilles. Plate boundaries from Coffin *et al.* (1998). Digital elevation model from Le Friant *et al.* (2004) and the GEBCO 08 Grid (http://www.gebco.net).

Colour online/ colour hardcopy

first arrivals from an earlier smoother model, suggesting that the source of the delay is captured in the final model. The delay is larger for offsets of 30–40 km, corresponding to rays turning at depths of 6–7 km, and has a maximum of about 0.2 s. The reduced signal-to-noise ratio is probably due to the shadow zone of a low-seismic velocity body.

Seismic velocities were defined by interpolating a quadratic *b*-spline polynomial over a regular rectangular grid. The grid spacing was set to 1 km in all directions in the early inversion iterations, and the vertical grid spacing was reduced to 0.5 km after iteration 36 to allow stronger vertical velocity gradients. The starting model was based on OBS data alone and was, therefore, representative of the offshore structure but not the island structure. It was composed of three laterally homogeneous layers, separated by interfaces representing the seabed and the sea surface. The top or first layer is an air layer with constant $V_p = 0.34$ km s^{-1}. The second layer is a water layer, with V_p decreasing from 1.53 km s^{-1} at the surface to 1.49 km s^{-1} at a depth of 1 km. The third layer is a solid layer with initial laterally homogeneous velocity structure determined from a 2D inversion of a subset of the data (Paulatto *et al.* 2010*a*).

A first estimate of the model resolution was obtained by calculating the ray density in each model cell. The deepest rays turn at about 12 km depth and the shallowest at a few hundred metres beneath the seabed (Fig. 15.27). The ray coverage is densest at a depth of about 3 km beneath the island and decreases beneath 5 km depth where most land-station rays reach their deepest point. Beneath this depth the model is constrained predominantly by rays undershooting the island, recorded at seafloor instruments.

Chequerboard tests (Zelt 1998; Seher *et al.* 2010) were carried out with patterns of varying lateral and vertical dimension. Each test consisted of inverting a synthetic dataset obtained by ray tracing in a perturbed model built by superimposing an 8% 3D sinusoidal seismic velocity perturbation onto the final model. The resolution is limited in the top 2 km by the irregular sampling and by the fact that most rays are subparallel, and is best between 2 and 6 km where the ray coverage is higher and rays cover a large range of azimuths. Between 6 and 7.5 km, the resolution is still acceptable, but it degrades rapidly below a depth of 7.5 km (Paulatto *et al.* 2012).

The final seismic velocity model (Fig. 15.28) shows that the three volcanic centres on Montserrat share a similar shallow structure, characterized by a prominent high-seismic-velocity core, probably comprising lava domes and intrusions, surrounded by a lower-seismic-velocity apron of volcaniclastic and pelagic sediments, in agreement with previous tomographical models (Paulatto *et al.* 2010*a*; Shalev *et al.* 2010). But at depths greater than 4 km, the new results show that the three volcanoes are strikingly different: beneath Centre Hills and Silver Hills, the core seismic velocities remain higher than their surroundings; however, beneath SHV, we observe a low-velocity volume, or LVV. Calculation of the seismic velocity anomaly with respect to the structure of the older volcanic centres shows that the LVV is 6–8 km wide and at least 4 km high, with a volume of over 100 km^3. The top is at a depth of about 5 km but the base is not resolved, as the resolution analysis shows that objects of the size of the LVV can be resolved at depths of up to 7.5 km but not much greater. The volume of the LVV shallower than 7.5 km, with seismic velocity reduced by more than 0.5 km s^{-1}, is about 20 km^3.

An LVV could be caused by variations in lithology, by elevated temperatures (Carlson 2001) and/or by the presence of partial melt. Significant variations in lithology are unlikely as the three volcanoes have quite similar compositions (Harford *et al.* 2002). To understand the effect of smoothing introduced by seismic tomography, and to test compatibility of our model with previous geological and geodetic constraints on the magma chamber properties, we integrated our tomographical results with numerical models of magma chamber growth (Paulatto *et al.* 2012). We modelled the 3D temperature and melt distribution in the upper crust from incremental growth of a magma chamber by repeated injection of sills at specified depths (Annen *et al.* 2008). This conceptual model of magma emplacement is supported by observations of intrusive bodies elsewhere (Searle *et al.* 2003; de Saint-Blanquat *et al.* 2006; Michel *et al.* 2008) and by SEA-CALIPSO seismic imaging of horizontal reflectors beneath southern Montserrat that are interpreted as sills (Byerly *et al.* 2010).

To simulate the emplacement of a sill, the cells corresponding to the location and dimensions of the sill, and the cells corresponding to a central conduit extending between the lower boundary of the domain and the depth of the sill, are set to a temperature of 850 °C and to a melt fraction of 0.35, which are the estimated

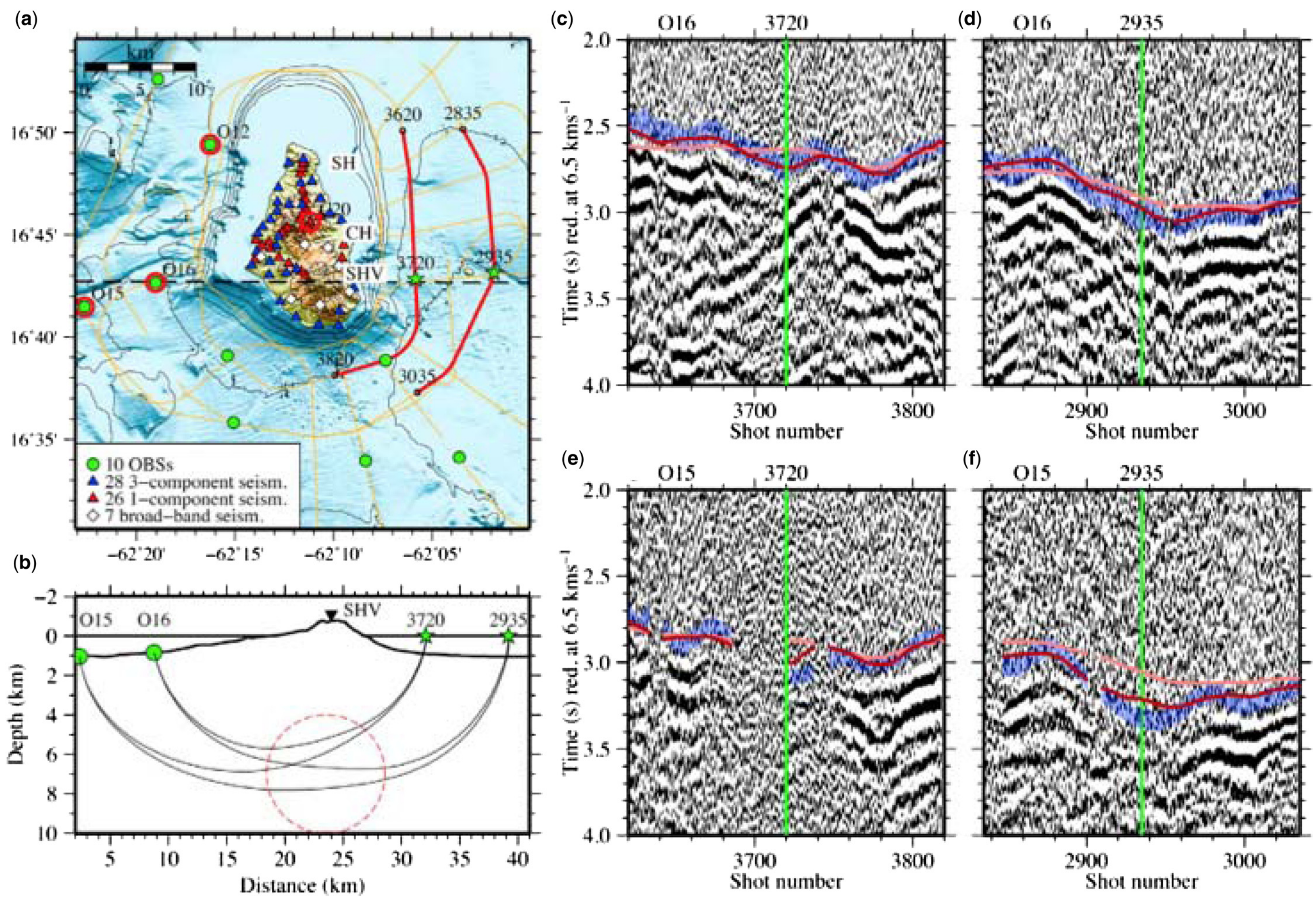

Colour online/ colour hardcopy

Q13

Fig. 15.26. Field recordings showing delayed first arrivals and reduced signal-to-noise ratio beneath SHV, after Paulatto *et al.* (2012). (**a**) Map with the location of instruments and data sections. The ship track is in orange, shots corresponding to the sections shown in (b) & (f) are highlighted in red. (**b**) Section through Soufrière Hills Volcano, corresponding to the dashed line in (a), showing the topography and ray trajectories. The approximate extent of the low-velocity volume (LVV) is marked with a dashed red circle. (**c**)–(**f**) Data corresponding to shots highlighted in (a). First arrivals with error bars are shown in blue. Travel-times for the final model are shown in red. Travel times for the preliminary smoothed model are in pink (Paulatto *et al.* 2012, fig. 5, iteration 36). The traces highlighted in green correspond to shots noted by the green stars in (a).

characteristics of SHV magma from petrology (Murphy *et al.* 2000). The cells beneath the intruded sill are shifted downwards to accommodate the new intrusion. This mechanism of floor depression is based on the assumption of mass exchange between a deeper reservoir and the shallow magma chamber that we are modelling, and is observed in plutons (Cruden 1998). Two models that reflect best the understanding of the recent volcanic history and productivity are shown in Paulatto *et al.* (2012, fig. 15.11). The temperature and melt distributions predicted by these models were used to estimate seismic velocity anomalies, using the same methods as employed in the inverse estimation of temperature and melt.

The resulting model anomalies (Fig. 15.29c, g) have much sharper edges and a larger magnitude than the observed seismic velocity anomaly. Several factors can contribute to smoothing in seismic tomography, but, at the depth of the LVV, the main cause of smoothing is the limited bandwidth of the seismic signal. This effect was estimated by smoothing the synthetic magma chamber models using a depth-dependent 3D Gaussian filter with width equal to the estimated Fresnel radius for a signal with a dominant frequency of 6–25 Hz (Paulatto *et al.* 2012, appendix). The filter output estimates the sharpest model that can be recovered with travel-time tomography (Fig. 15.29d, h). The filtered synthetic magma chamber models show that only 10–30% of the actual anomaly amplitude is recovered by seismic tomography. The observed LVV is consistent with a magma chamber with size and geometry similar to model A (Fig. 15.29a–d), which has a volume of approximately 13 km^3 with a melt fraction of >0.30 between depths of 5.5 and 7.5 km, and a maximum melt fraction of just below 0.35. The total intruded volume is about twice this amount.

A larger magma chamber (*c.* 20 km^3) could be accommodated if it extended deeper than 7.5 km. The results of model B (Fig. 15.29e–h) show that a magma chamber with radius smaller than 1 km yields too small a seismic velocity anomaly to fit the tomographical results. Paulatto *et al.* (2012) concluded that the magma chamber has a radius of 1–2 km, and extends from a depth of about 5.5 to at least 7.5 km.

Imaging deep reflectors

Subsurface imaging was the motivation for the design of the dense reflection spreads consisting of over 200 Texan recorders equipped with 4.5 Hz geophones. These deployments constituted three lines (Fig. 15.30): two effectively radiating NW and north from SHV, and the third providing fan coverage for sources on and SE of SHV. These arrays were designed in part to 'undershoot' SHV with airgun sources, with the main aim to image reflections from the top of the magma chamber.

Unfortunately, despite careful application of processing and enhancement techniques, this main aim was not realized and

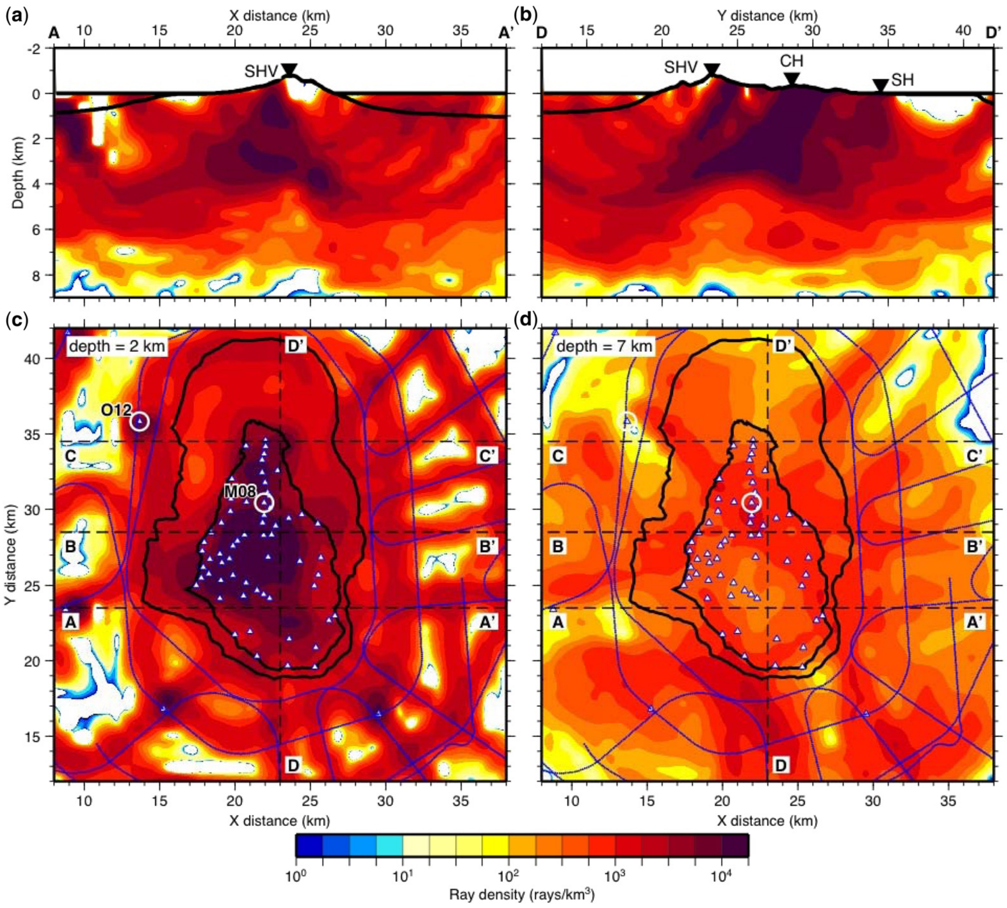

Colour online/ colour hardcopy

Fig. 15.27. Ray density. (**a**) West–east section. (**b**) South–north section. (**c**, **d**) Horizontal sections at depths of 2 and 7 km, respectively. After Paulatto *et al.* (2012).

analysis results were disappointing. Conventional CMP (common mid-point) processing of the airgun shots recorded by the Texan arrays proved relatively ineffective at imaging crustal structure. The minimum source–receiver offsets that were imposed by bathymetric and other limitations on how close the ship could approach the island, and safety and time constraints on how close the receivers could be placed near SHV, left only relatively wide-angle reflections available for imaging. Imaging at such offsets is difficult under even ideal conditions, given the relatively close arrival times of true reflected energy with direct and refracted arrivals. Such discrimination is made even more difficult by interference from water-bottom multiples that are generated by marine artificial sources at these water depths. A more serious problem with the array geometry was that the reflector midpoints corresponding to the actual source track–receiver deployments largely fell offshore, with relatively few actually sampling under either Montserrat in general or SHV in particular. For the ‘best’ stack generated from the Belham Valley array (Fig. 15.30) best aligned to undershoot SHV, only a small fraction of the seismic section falls on the island, and the portion that does lacks upper-crustal coverage due to the large minimum-offsets available. The data hint of some subhorizontal reflectors, but the quality of the data makes such inferences strained.

Although continuous, as opposed to windowed, recording was primarily imposed by the regular nature of the airgun source (one shot every 60 s), such recording also allowed the recording of natural sources and, in particular, a number of microearthquakes that occurred near the summit of SHV. These earthquake recordings, processed using a selected subset of traditional multichannel reflection techniques, provide our most substantive indications of reflecting crustal structures near SHV.

The microearthquakes were recorded from 17 to 20 December 2007. Twenty local events were identified from the continuous data recording and correlated with events from the areal seismic network. Locations made with HypoEllipse (Lahr 1999) indicated that the epicentres were centreed under the summit of SHV at relatively shallow depth, thus providing near-vertical reflection coverage for depth points relatively close to SHV (Fig. 15.30). The data from these microearthquakes were treated in the same manner as borehole shots in a conventional controlled source profile. Attention was focused on the Belham Valley line, which samples most closely to the SHV. Analysis concentrated on seven events that had a horizontal location error of less than 1 km, with the reported location accepted for processing purposes.

The raw earthquake gathers (e.g. Fig. 15.31) show clear indications of organized energy that cannot be attributed to direct P-, S- or surface-wave energy, but rather suggest moveout consistent with reflected arrivals. However, individual reflections are difficult to trace undisrupted across the array, which we suspected was due to relative static shifts associated with the overlying crust. Starting with the raw data, elevation statics were applied to correct for changes in topography along the seismic lines, then the data were bandpass filtered from 1 to 8 Hz. To further improve reflection coherence, we applied a form of refraction statics. First P-wave arrivals were aligned to near-horizontal using linear moveout (LMO) corrections. Deviations of the first arrival time from horizontal were manually picked and used to apply a static shift to force alignment of the first arrival. The LMO correction was subsequently removed, hopefully with increased lateral alignment of reflections as well as first arrivals. A normal moveout correction (NMO) was then applied using an average velocity of 5 km s^{-1} from 0 to 10 s to image reflection geometry at depth. Several additional coherency enhancement techniques, which included FX-deconvolution, trace mixing and FK-filtering, were tested to further increase the visibility of reflected energy.

The processed gathers for all seven events show strong similarities (e.g. subhorizontal reflectivity), despite being recorded for different earthquake sources (Byerly *et al.* 2010). But it is unclear whether one can defend a reflection-for-reflection correlation between the various gathers. We simply assert that the

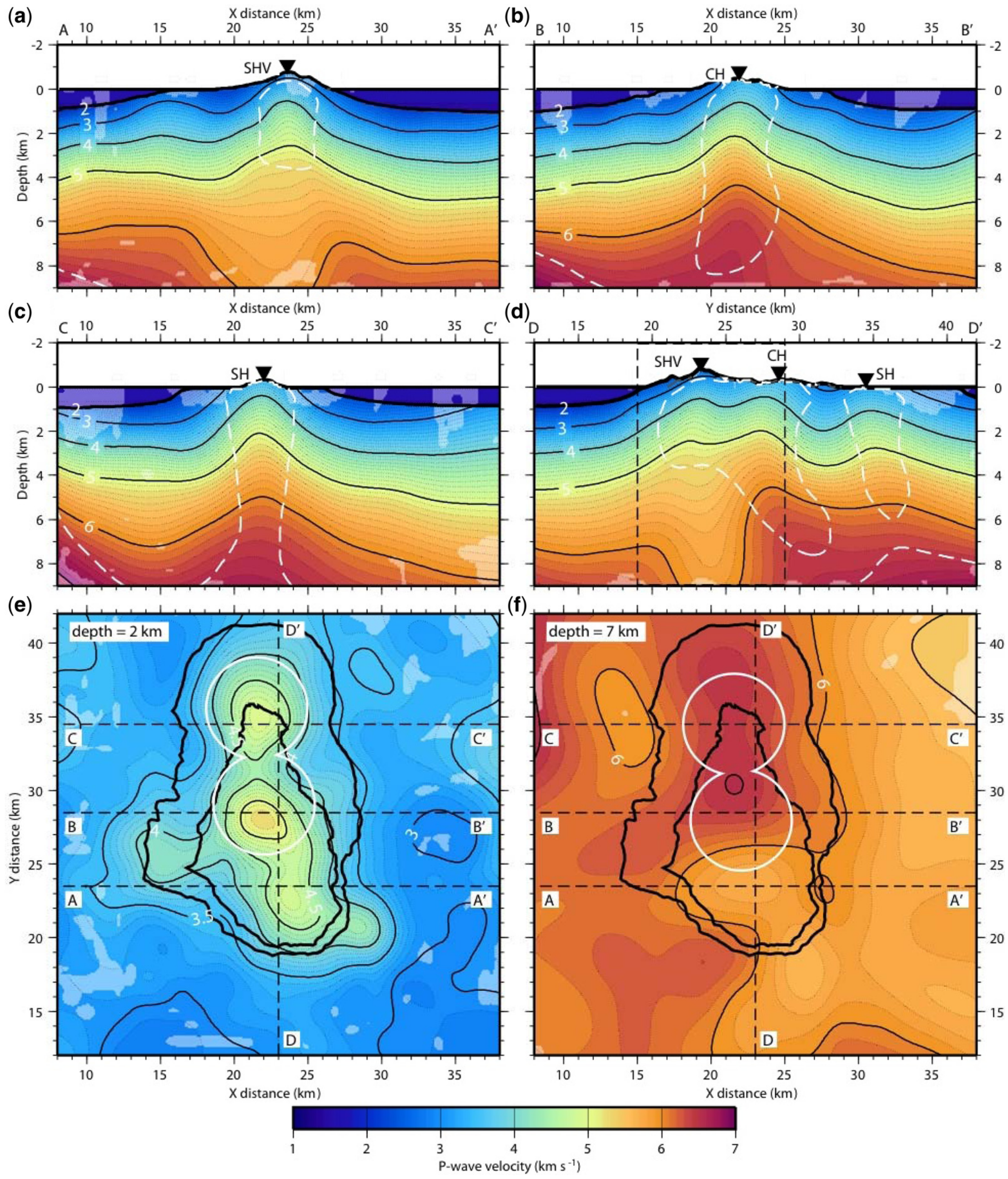

Colour online/colour hardcopy

Fig. 15.28. Final seismic velocity model. (**a**)–(**c**) West–east sections through the three major volcanic centres. The high-seismic-velocity cores of the volcanoes are marked with a white dashed lines representing the 0.25 km s^{-1} seismic velocity anomaly contour with respect to the average seismic velocity of the island. (**d**) South–north section. The dashed frame marks the section of a model shown in Paulatto *et al.* (2012, figs 10–12). (**e**) & (**f**) Horizontal sections at 2 and 7 km depth bsl, respectively. The coastline and the 200 m depth contour are marked with thick black lines. The white circles bound the area over which the reference model for seismic velocity anomalies was calculated. Lighter areas have no ray coverage. After Paulatto *et al.* (2012).

overall similarity in reflectivity argues that geological layering at a common depth, rather than noise, is being imaged. As shown in Byerly *et al.* (2010, auxiliary material), noise gathers do not replicate the key features of the microearthquake gathers, and thus we are confident that the coherent energy evident in our images originated from the microearthquake sources. The resulting individual Q7 earthquake gathers show consistent subhorizontal energy between depths of 6 and 19 km beneath the NW flank of SHV. These amplitudes, which need enhancement just to be visible, provide little support for their interpretation as fluid bodies at depth. Our attempts to identify the polarity of these reflectors were unfruitful, and we are left with the conjecture that these reflectors represent either buried volcanic layering and/or later sills intruded into mid-crustal levels. The sill interpretation seems more consistent with the needed impedance contrasts to generate detectable reflections from depth. The Moho lies near 30 km (Sevilla *et al.* 2010), much deeper than any of the prominent reflections indicated by these images. Finally, the presence of sill-like features in the upper or middle crust beneath an active volcano is not surprising. Similar results were obtained using recorded ambient 'noise' from the Texan recordings (L. Brown, written commun.). The primary value of these studies is their demonstration that relatively high-resolution reflection imaging of crustal structure is feasible using microearthquake or ambient noise sources.

Offshore reflection profiling

The SEA-CALIPSO experiment included a 48-channel 600 m digital streamer used in a seismic reflection survey to explore local submarine deposits and faults, and expand knowledge based on previous seismic and bathymetric studies (e.g. Feuillet *et al.* 2001, 2002). Although a low source frequency and long shot interval were selected to maximize the first-arrival tomography data, and were, thus, less optimal for the reflection study, quite useful results were obtained (Kenedi *et al.* 2010). Here we present some key results from our survey, and discuss their implications on the local tectonic and volcanic interactions.

The region examined and tectonic context are illustrated in Figure 15.32 (cf. Fig. 15.1 for a broader regional setting). The shot lines are numbered and, of these, selected sections are shown in Figures 15.33–15.35 (for the section locations, see the red profile lines in Fig. 15.32). The data were bandpass filtered between 4 and 64 Hz, stacked and migrated using sediment velocities from semblance analysis. Time to depth conversions used an average sediment velocity of 2200 m s^{-1} (Paulatto *et al.* 2010*a*).

On and west of Montserrat, young andesitic domes (<300 ka) and structurally uplifted areas (Harford *et al.* 2002) are aligned due to normal faulting as part of the extensional Montserrat–Havers Fault System (MHFS) (Feuillet *et al.* 2010). The MHFS

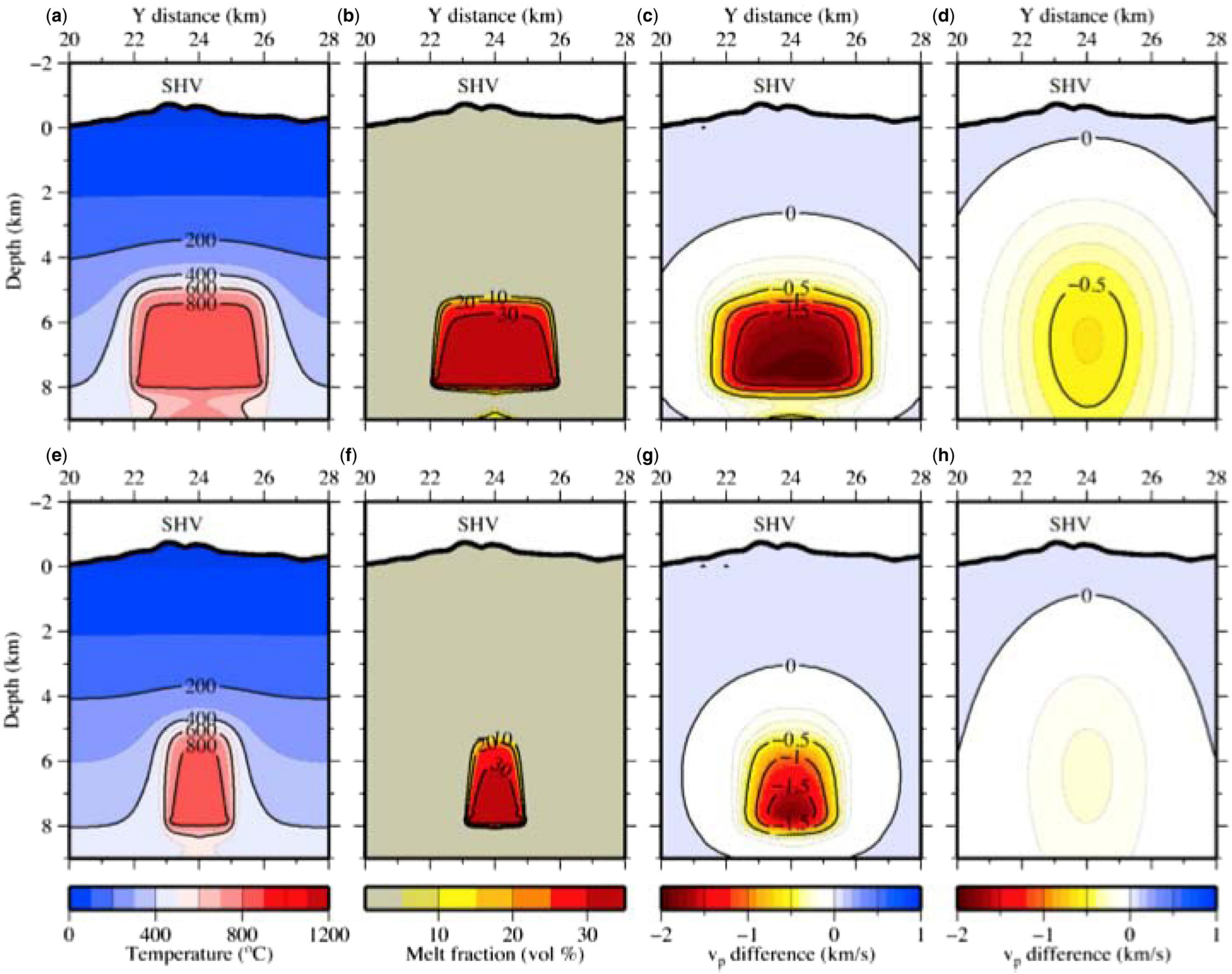

Colour online/ colour hardcopy

Q13

Fig. 15.29. Models of magma chamber accretion and predicted seismic velocity anomaly (after Paulatto *et al.* 2012). Model A (top panels): two successive events of underaccretion of 300 m-thick sills with 2 km radius at 400 year intervals, each starting at 5 km depth and lasting 4000 years, with a 15 000 year repose period. (**a**) Present-day temperature distribution, corresponding to 4000 years after the start of the second intrusion event. (**b**) Melt fraction. (**c**) Calculated P-wave velocity anomaly. (**d**) P-wave velocity anomaly of filtered model. (**e**)–(**h**) Model B: same as (a)–(d) for sills with 1 km radius.

includes an ESE-trending lineament interpreted as the Belham Valley Fault (BVF) (Harford *et al.* 2002) (Fig. 15.32). Normal faulting continues SE of Montserrat with a right step to the Bouillante–Montserrat Fault System (BMF) (Fig. 15.32). Extension with approximately a north–south trend is prevalent in the region, which Feuillet *et al.* (2010) suggested is accommodated as oblique shear along a series of en echelon and mainly NE-dipping normal fault systems, including the BMF, MHFS and the Redonda Fault System (RFS) (Fig. 15.32). Kenedi *et al.* (2010) proposed that these systems also accommodate minor local shear that has resulted in the rotation of older sediments, and deformation of the footwall of the BVF and related faults.

Off the eastern shelf, reflection profiles are dominated by chaotic sediment packages of volcaniclastic debris. Eastwards-tapering sediment lenses extend offshore from Silver Hills and Centre Hills (lines 7 and 9: Figs 15.32 & 15.33). The debris from Silver Hills (Line 7) extends approximately 10 km from the shelf and overlies strata that step down towards Montserrat. From Centre Hills also (Line 9), debris onlaps layered sediments that dip westwards, from 1.5 s two-way travel time (twt) at km 12 to 2.2 s twt at km 5 (Fig. 15.33). The apparent dip (Line 9) and downwards fault-step pattern (Line 7) towards the island are consistent with island subsidence or with rotation on the hanging wall of the MHFS faults (Fig. 15.32).

From Centre Hills, the debris lenses have accumulated in stacks, the largest being about 10 km long (Fig. 15.33). The lenses are onlapped by and alternate with subhorizontal strata. Kenedi *et al.* (2010) interpreted the lenses as submarine fans from emplacements of volcaniclastic flows, caused largely by lava-dome collapses, and deposited over several hundred ka. Coarse submarine fans have formed in this way during the current volcanism and have produced tapering units that extend as far as 8 km offshore (Trofimovs *et al.* 2008, 2011; Le Friant *et al.* 2009, 2010).

Where fans are overlain by flat-lying sediment, sedimentation rates can be estimated. Off Silver Hills, a large fan is covered by about 80 m of flat sediments and, since Silver Hills became extinct at about 1 Ma (Harford *et al.* 2002), the sedimentation rate was approximately 8 cm ka^{-1}. Off Centre Hills, the sediments are 44 m thick and, assuming the Centre Hills became extinct at about 500 ka, the rate was approximately 9 cm ka^{-1}. Le Friant *et al.* (2008) reported hemipelagic sedimentation rates 60 km offshore as 1–3 cm ka^{-1} and, at about 16 km offshore,

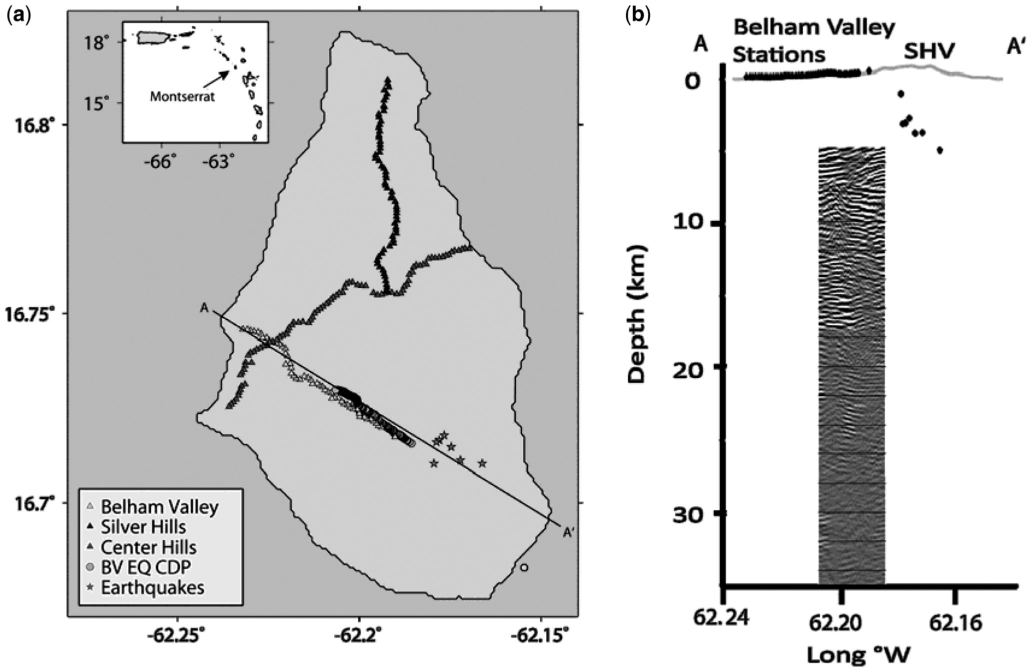

Fig. 15.30. (**a**) Map of Montserrat showing the locations of the Texan seismic arrays (triangles), along with the best-located microearthquakes used in this study (stars). The CDP reflection points corresponding to the Belham Valley recordings of a typical event are shown as circles. (**b**) Schematic cross-section illustrating depths of the sources relative to the recording spread, together with a resulting image (source gather). After Byerly *et al.* (2010).

Trofimovs *et al.* (2010) reported rates of 4–7 cm ka^{-1}. Our higher rates are consistent with a persistent near-shore source.

The north–south reflection profiles off the eastern shelf cut across the debris fans. Approximately 1–2 km offshore (Line 2, Fig. 15.34), a mounded feature is visible just below the seafloor between km 6 and km 11. SHV flow deposits 4–5 km off the shelf are indicated by the mound on Line 23 between km 10 and km 20. A 6 km-wide channel is visible in Line 2 at km 11–km 15, which is interpreted as an embayment associated with a previously described gravity flow (Le Friant *et al.* 2004) (see Fig. 15.32). The southern slope of the embayment is consistent with the fault scarp north of Roche's Bluff (located in Fig. 15.32), subsequently modified by landsliding.

Off the west coast, north-dipping fault scarps offset the ocean floor on profiles approximately 6 and 14 km offshore (lines 21 and 15: Figs 15.32 & 15.35). The western scarp offset at km 10

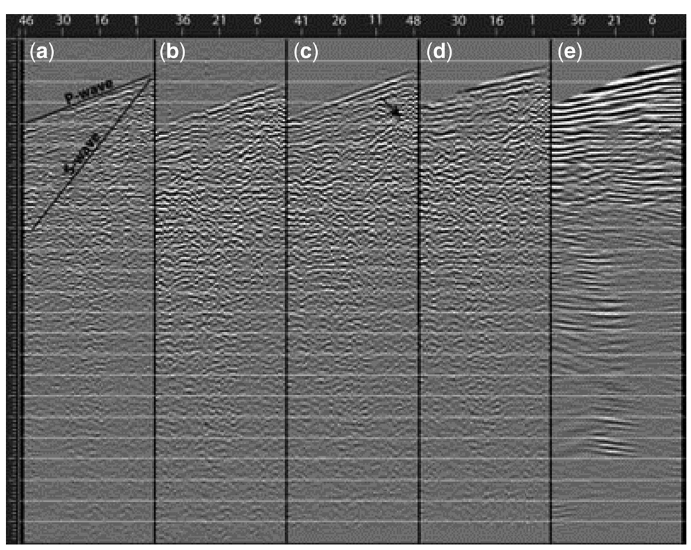

Fig. 15.31. Example microearthquake gather illustrating the processing steps used to enhance possible deep reflections. (**a**) Raw data. (**b**) Data with bandpass filter and elevation statics. (**c**) Alignment using first arrivals and linear moveout. (**d**) Display with NMO. (**e**) NMO, FX-decon and trace mix (applied twice). After Byerly *et al.* (2010).

of Line 15 is at least 40 m. The MHFS fault scarp and south-tilted footwall block are clear features also on the nearby profile gwa 058 of Feuillet *et al.* (2010). To the north, several faults break the ocean floor, indicating recent activity. A normal fault-bounded step in the morphology near km 16 on Line 15 is associated with the RFS (Fig. 15.32). Further north, buried scarps have created basins of folded, syn-rift sediments, and, beyond km 23, faulting is buried by about 100 m of flat basin-filling sediments.

In the south, both profiles reveal complex footwall deformation. At km 4–km 10 of Line 15, a series of small basins have formed on the tilted footwall, which is an ascending slope over about 1300 m of elevation. On the elevated footwall of Line 21 (at km 1), a minor graben is infilled by subhorizontal sediment (Fig. 15.35).

At km 3–km 6 on Line 21, sediments appear to dip to the south and onlap onto a major north-dipping normal fault (Fig. 15.35). This fault is not the same as the principal scarp fault of Line 15, but is en echelon and south of it by about 2 km (Fig. 15.32) (Feuillet *et al.* 2010, fig 2). The fault may coincide with an along-strike projection of the BVF (see Fig. 15.32).

These images have led to some new tectonic interpretations of southern Montserrat, via integration of our new data with older studies and the work of Feuillet *et al.* (2010). Kenedi *et al.* (2010) agreed with the regional model of Feuillet *et al.* (2010) that the major fault systems RFS, MHFS and BMF are mainly normal and arranged in a right-stepping en echelon structure, and also that, on the large scale, this section of the arc accommodates regional left-lateral shear. They disagreed with the interpretations of some onshore features discussed in Feuillet *et al.* (2010), and included a discussion of the SHV feeder dyke in relation to the complexity of local tectonic and magmatic stresses.

Feuillet *et al.* (2010) reintroduced an old idea (e.g. Rea 1974) that Garibaldi and St George's Hills are volcanic cones, and suggested they were fed by vents in a fissure parallel to the BVF. However, the field evidence does not support this hypothesis. St George's, Garibaldi and Richmond hills are composed mainly of distal block-and-ash-flow and pumice-and-ash flow deposits, and epiclastic beds (Harford *et al.* 2002). The 3D tomography (Shalev *et al.* 2010) indicates low P-wave velocity material under St George's and Garibaldi hills quite dissimilar to the high-velocity cores under SHV and Centre hills. Thus, the morphology of these hills is not primary; they are fault-bounded tectonic uplifts that have been deformed by (mostly) normal faults, and deposits have been tilted beyond the sedimentary depositional-slope limits.

Colour online/colour hardcopy

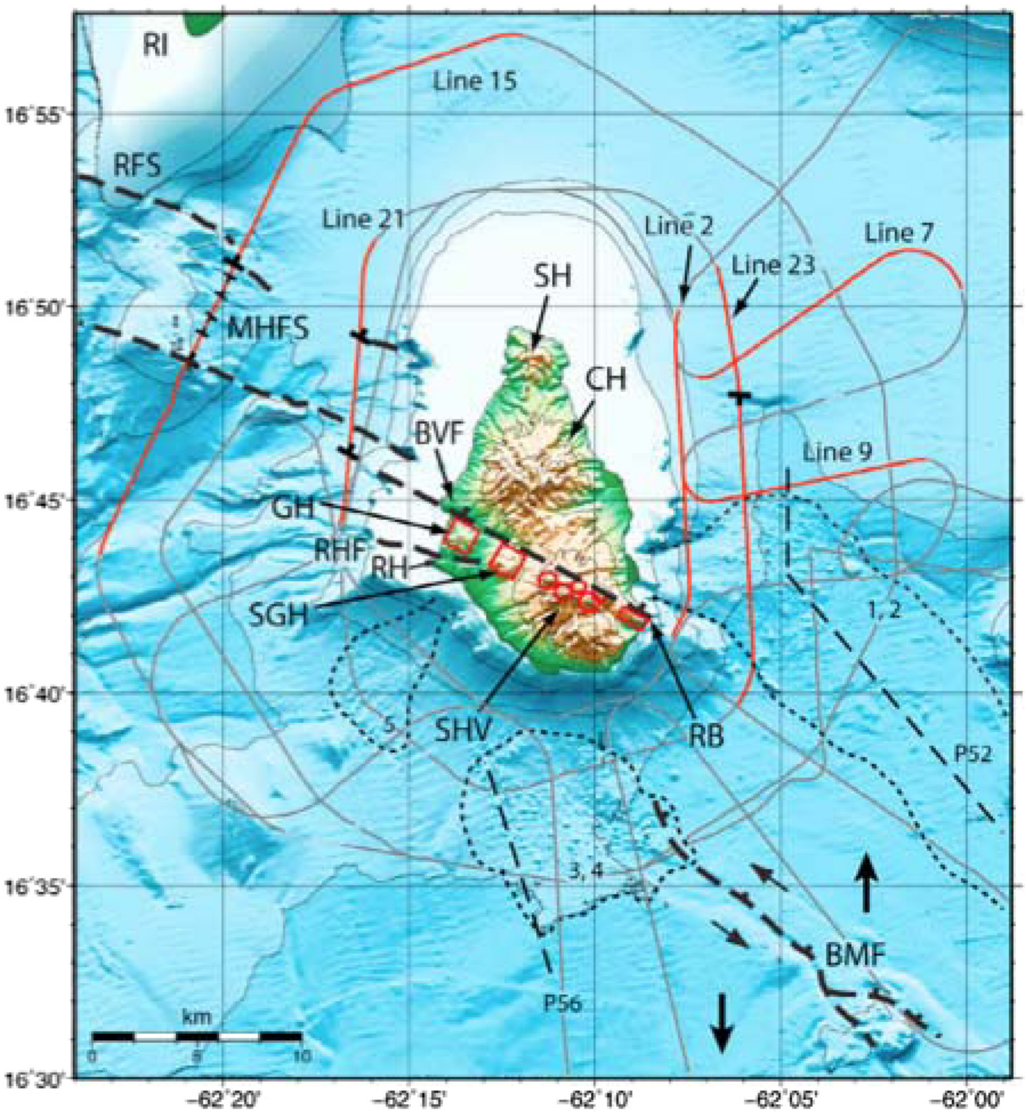

Fig. 15.32. Montserrat bathymetry and tectonic model. Grey curved line: track of the RRS *James Cook*. Lines in red (7, 9, 2, 23, 15 and 21) are discussed in this chapter. Red circles, volcanic centres; black fault symbols, normal faults from profiles, apparent dip as indicated; thick dashed lines, major fault of the fault systems, including BVF and possible extension to RB; large black arrows, extension direction (after Feuillet *et al.* 2001); dotted lines, gravity flow deposits 1–5 of Le Friant *et al.* (2004); red squares, tectonic uplifts; thin dashed lines, cross sections (P52, P56) along deposits from Le Friant *et al.* (2004); orange fault north of the map, inferred from 1985–1986 Redonda earthquake mechanisms (Girardin *et al.* 1991; Feuillet *et al.* 2002). BMF, Bouillante–Montserrat Fault System; BVF, Belham Valley Fault; CH, Centre Hills; GH, Garibaldi Hill; MHFS, Montserrat–Havers Fault System; RB, Roche's Bluff; RFS, Redonda Fault System; RH, Richmond Hill; RHF, Richmond Hill Fault; RI, Redonda Island; SGH, St George's Hill; SH, Silver Hills; SHV, Soufrière Hills Volcano. Bathymetry map from Institut de Physique du Globe de Paris and M. Paulatto, NOCS. After Kenedi *et al.* (2010).

A related issue is the BVF, which, in contrast to Feuillet *et al.* (2010) but following Harford *et al.* (2002), we interpret as a north-dipping normal fault. This is consistent with our interpretation of Garibaldi and St George's hills as tectonic uplifts; in addition, these onshore blocks seem analogous to the prominent elevated footwalls seen offshore on lines 15 and 21 (Fig. 15.35) (cf. Feuillet *et al.* 2010, fig. 3, profiles gwa 055 and 058). The noth-dipping fault in our marine profile Line 21 (Fig. 15.35, *c.* km 3) is aligned with the BVF as an along-strike projection, and the north-dip on the offshore profile supports a similar interpretation for the BVF. Finally, 3D tomography (Shalev *et al.* 2010) suggests that the contact of the P-wave velocity anomaly boundary under St George's Hill dips roughly 50°N.

Regionally, southern Montserrat is part of a transtensional regime with extensional overprinting. Transtensional deformation zones involve rotation, local compression and uplift (Dewey *et al.* 1998), which are consistent with the uplifted blocks and also westwards-dipping sediments off the east coast. Locally, southern Montserrat includes a right-step between the MHFS and the BMF, en echelon normal fault systems in sinistral slip; thus, uplift may have been encouraged by a minor contractional component (Deng *et al.* 1986; Cunningham & Mann 2007). The marine reflection profiles and related onshore data (e.g. Miller *et al.* 2010) indicate that on Montserrat the interplay among local faulting, volcanism and stresses is complex. The regional transtensional system of en echelon faults (cf. Feuillet *et al.* 2010) has influenced volcanism, while the local fault step suggests both a component of compression near SHV, and complicated and evolving stress regimes and fault movements.

Discussion and lessons learned

Scientific issues

The SEA-CALIPSO study is a rare active source tomographical experiment of an active andesitic island strato-volcano, and the first to present a detailed image of an island arc volcano in the Lesser Antilles. The current and future results of this research should help scientists to better understand volcanism at Montserrat, and provide insights on how regions of intermediate composition are developed within primarily basaltic crust at inter-oceanic arcs. This research enables comparisons of the Lesser Antilles arc with other arcs such as the Marianas, Izu-Bonin, Kuriles and Aleutians, and provides constraints for dynamic models of magma flow and explosive volcanism.

Our experiment used as many as 180 000 ray paths in damped smoothed inversions over a 47 × 54-km target area to produce 2D and 3D images of the P-wave seismic velocity (Paulatto *et al.* 2010*a*, *b*; Shalev *et al.* 2010). In the preliminary work, 2D inversions of a subset of data using first arrivals and wide-angle reflections revealed a heterogeneous high-velocity body underneath the island, representing the cores of volcanoes and subjacent intrusions (Fig. 15.29) (Paulatto *et al.* 2010*a*, *b*; Voight *et al.*

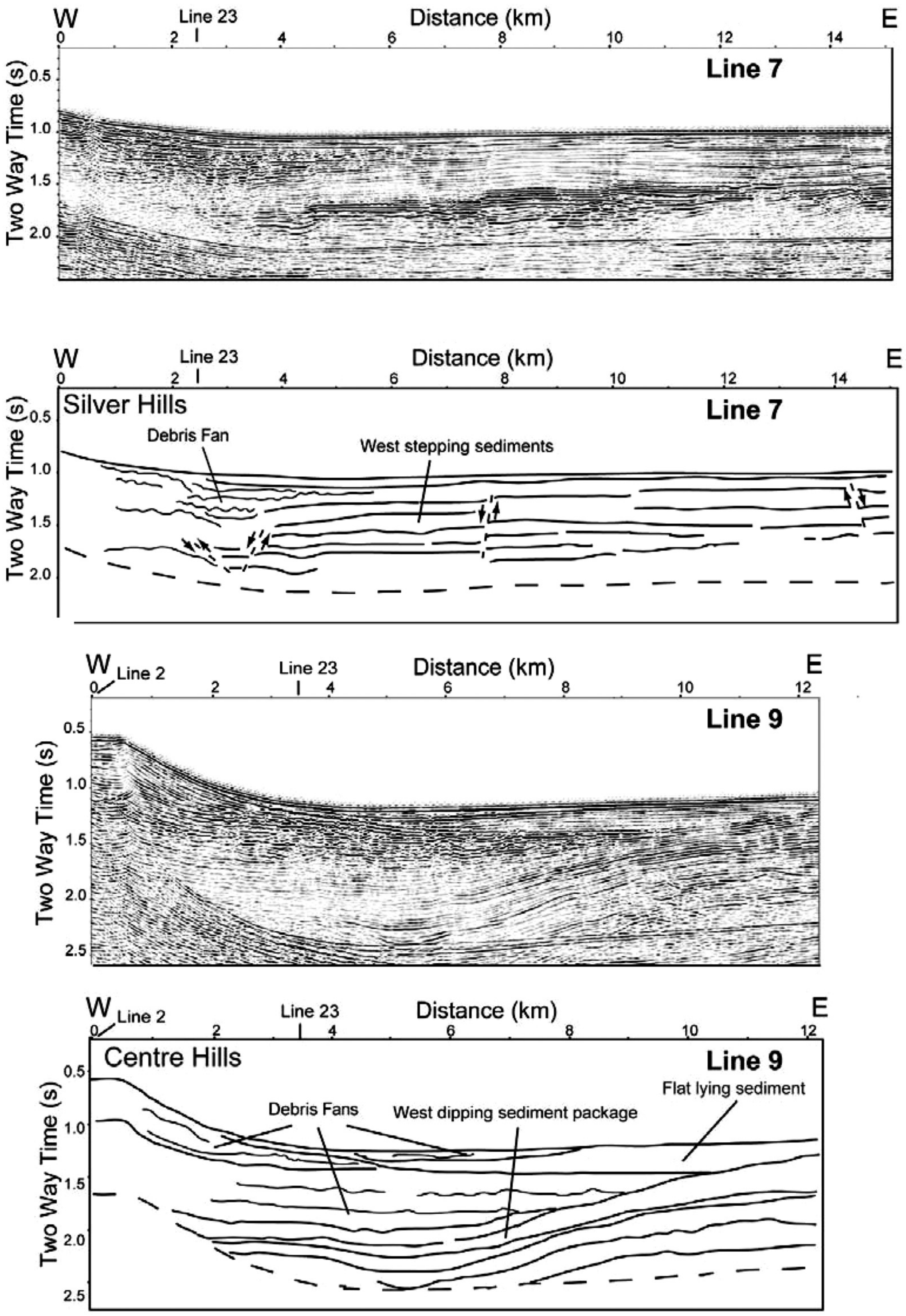

Fig. 15.33. Seismic reflection profiles and annotated interpretations of radial lines 7 and 9. Solid lines, strong reflectors and sediment packages; short dashed lines, faults; thin dashed line, bottom multiple. The intersection with lines 2 and 23 is indicated at the top. After Kenedi *et al.* (2010).

2010*b*). An interface at a depth of about 2 km was identified, and interpreted as the palaeo-seafloor probably depressed under the island from volcanic loading.

The better-constrained 3D inversions described in this chapter show that high-velocity cores, interpreted as crystallized intrusions, underlie each of the volcanic centres (Figs 15.23, 15.24 & 15.28) (Shalev *et al.* 2010; Paulatto *et al.* 2012). Such cores underlie the extinct centres to depths of nearly 8 km but occur only above 5 km under SHV (Fig. 15.28). A LVV underlies SHV at depths of between about 5 and nearly 8 km, and is interpreted as a reservoir of partly crystallized magma that feeds the current eruption (Fig. 15.36). Two shallow areas of low velocity in the NE and SW flanks of the island reflect volcaniclastic deposits and hydrothermal alteration (Fig. 15.24).

Related research using receiver functions define the Mohorovic crust–mantle discontinuity at about 30 km in depth at this location (Sevilla *et al.* 2010). Offshore reflection profile lines reveal deep wedges of volcaniclastic debris, and important tectonic details that illuminate the intimate connection between tectonics, volcanism and sedimentation in volcanic arcs (Figs 15.32–15.35).

Integration of seismic tomography with thermal numerical models allowed us to go beyond simple static constraints on present-day melt distribution (Fig. 15.29) (Paulatto *et al.* 2012). In our models, the magma chamber formed by repeated intrusion of andesite sills over a few thousand years, although our results are non-unique inasmuch as different emplacement histories can produce similar melt and temperature distributions. A single longer series of sill injections with a slower accretion rate

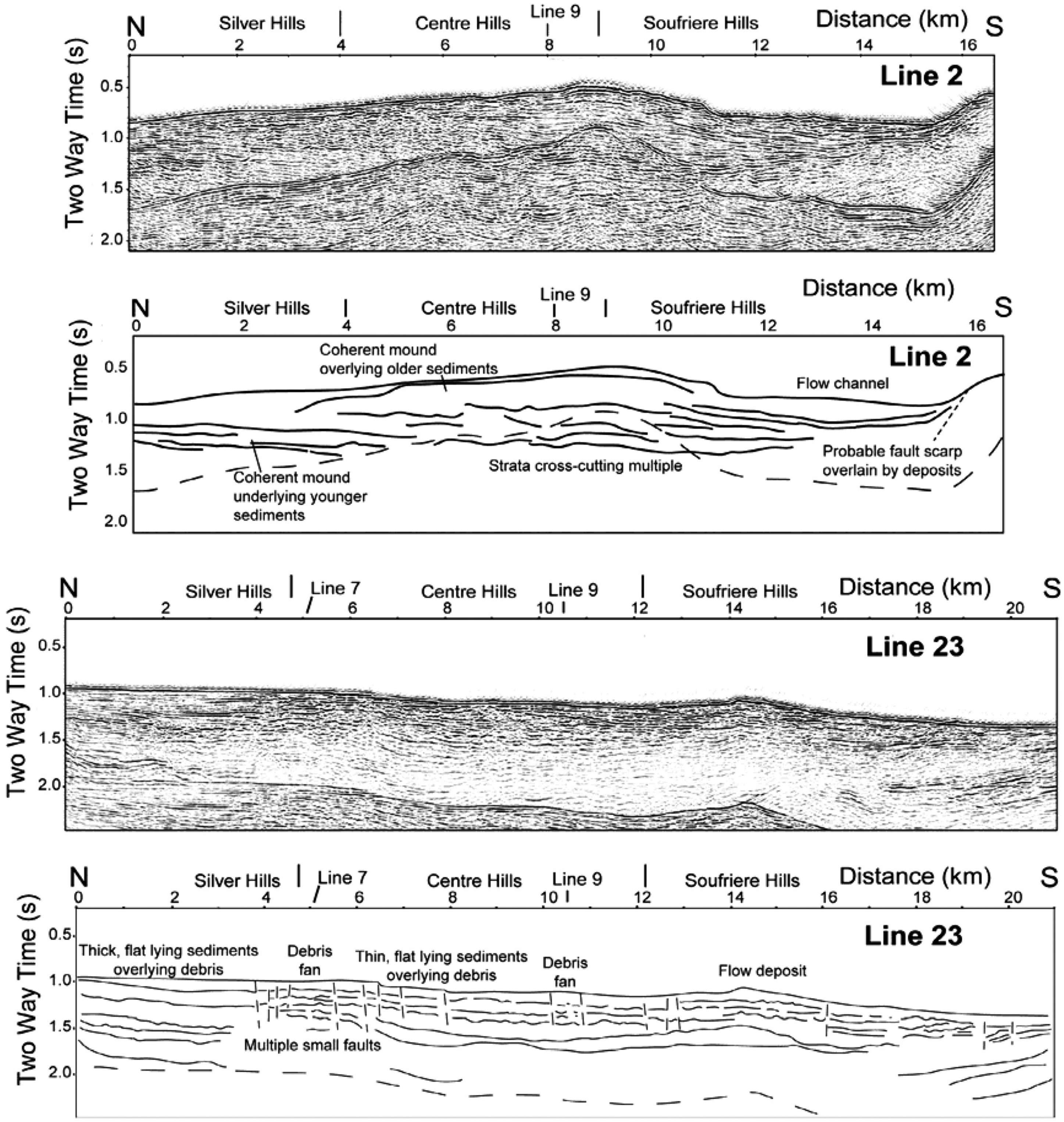

Fig. 15.34. Seismic reflection profiles and annotated interpretations of lines 2 and 23, parallel to the east coast. Description as in Figure 41. The intersection with lines 7 and 9 indicated at the top. Vertical lines at the top, boundaries between the major volcanic centres. After Kenedi *et al.* (2010). Q12

could give a similar present-day seismic anomaly as two shorter series, with a faster accretion rate separated by a repose period. Magma chamber growth over several tens of thousand years or more induces thermal anomalies that are too cool and too broad to fit the tomography data. Overaccretion and underaccretion can give similar results, but the latter seems more consistent with field observations of exhumed granitic plutons (Wiebe & Collins 1998). In rapidly growing magma chambers, the emplacement dynamics are likely to be more complex, so underaccretion represents a simplified model. In our preferred model, the magma chamber would become almost completely solidified 37 000 years after the last emplacement (Paulatto *et al.* 2012, fig. 15.11). Shallow magma chambers of similar volume to our model can become solid over a few thousand to a few tens of thousand years if they are not continuously replenished by new influx (Annen *et al.* 2008; Annen 2009).

These results reinforce the hypothesis that typical arc-volcano magma chambers are transient features, which only exist during active phases. Our experiment highlights the indication that even a shallow magma chamber as large as 13 km^3 is difficult to

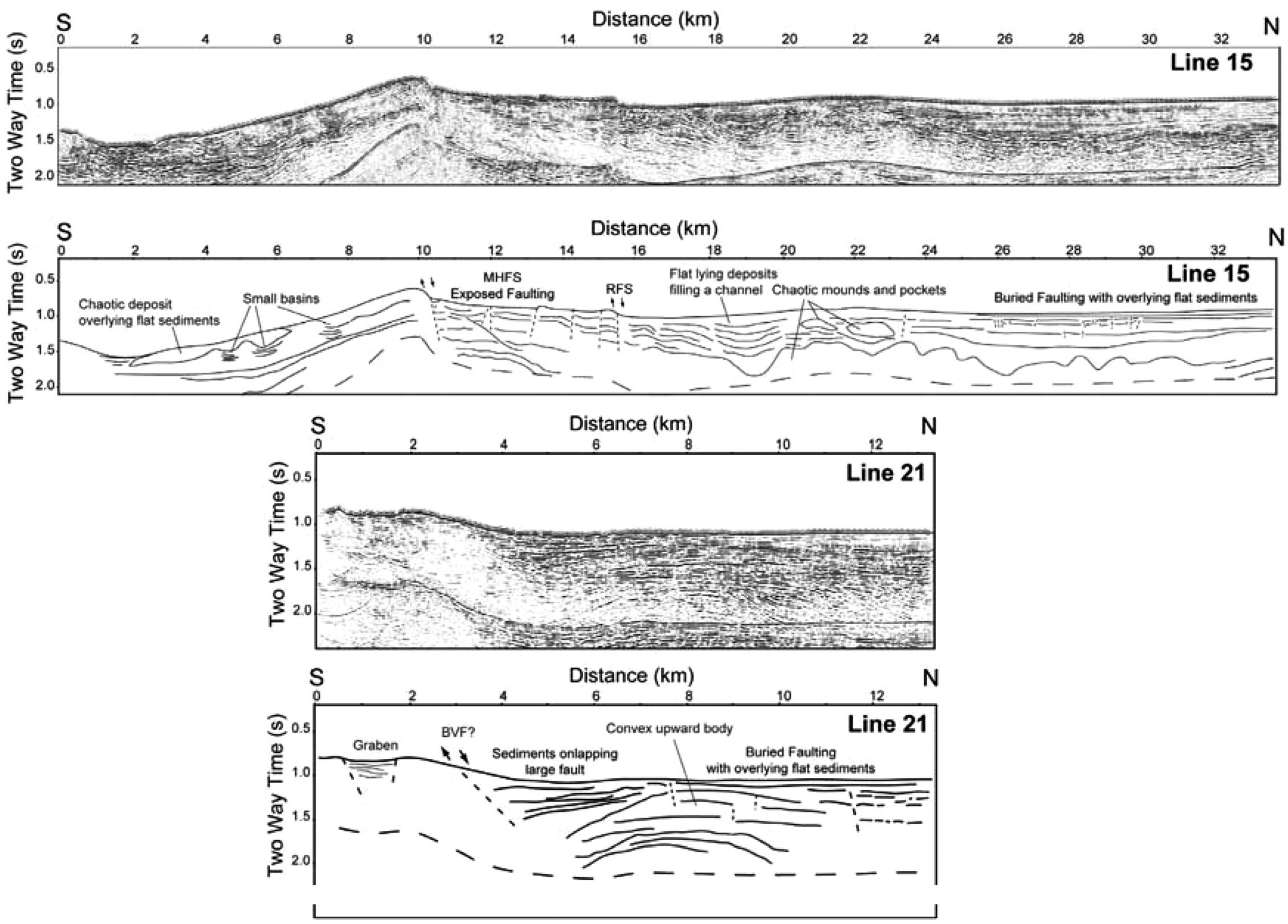

Fig. 15.35. Seismic reflection profiles and annotated interpretations of lines 15 and 21, off the west coast. Description as in Figure 41. After Kenedi *et al.* (2010).

detect and constrain with seismic tomography, and that associated low-seismic-velocity anomalies may be significantly underestimated. Deeper or smaller magma chambers may prove impossible to detect with travel-time seismic tomography.

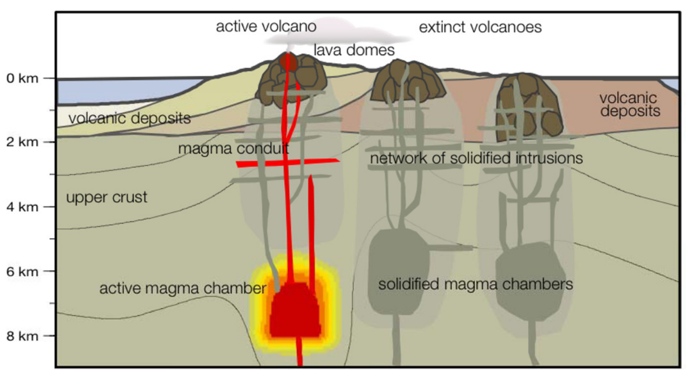

Colour online/ colour hardcopy

Fig. 15.36. Schematic north–south (from right to left) cross-section through Montserrat, illustrating insights from the SEA-CALIPSO experiment. The volcanic centres shown are, right to left, the extinct Silver Hills and Centre Hills complexes, underlain by solidified intrusions and magma chambers, and the Soufrière Hills Volcano, underlain by some solidified intrusions at a shallow level, but with a partly molten magma chamber below a depth of 5 km. Contours of the P-wave velocity are shown schematically and can be compared with Figure 15.28.

Further, where an LVV is detected, melt content is only poorly constrained by seismic data solely, and an adequate interpretation must rely on independent constraints. The melt fraction estimated under SHV from the velocity anomaly alone is only 3–10%, similar to tomography-based estimates at other magmatic systems (Haslinger *et al.* 2001; Menke *et al.* 2002). This estimate is too low. However, we show that with the use of thermal models, and by taking into consideration the smoothing imposed by limited seismic resolution (Fig. 15.29), that the observed LVV under SHV is consistent with the presence of a magma chamber with more than 30% melt as more clearly indicated by the observed petrology. Thus, the approach developed in this research, based on integrating seismic tomography with numerical models of magma chamber formation and incorporating petrological and geodetic constraints, can reveal the characteristics and dynamics of magmatic systems with a level of detail that none of these methods alone has achieved (Paulatto *et al.* 2012).

Finally, we comment here on reflection imaging. This was the main motivation for our deployment of dense reflection spreads in three main lines (Fig. 15.9), designed to 'undershoot' SHV with airgun sources and to image reflections from the top of the magma chamber. Unfortunately, despite careful application of processing and enhancement techniques, this main aim was not realized and analysis results were disappointing. The conventional CMP processing of the airgun shots recorded by the Texan arrays proved relatively ineffective at imaging crustal structure, for the several reasons discussed previously. In retrospect, there seems to be little that could have been done on this small island to improve the reflection geometry, given the resources available and the constraints that existed. Placing receivers closer to SHV, or moving the ship much closer to the island, were not realistic possibilities. More near-vertical reflection geometries were needed. However, the continuous recording employed in this experiment enabled us to test two relatively unconventional, but potentially promising, approaches to reflection imaging near volcanoes, including using natural earthquake sources to produce reflection seismic sections (Byerly *et al.* 2010) and seismic interferometry, extracting surface waves and body waves from cross-correlating seismic noise (L. Brown written comm.).

Operational issues

Here we highlight five topics: (1) inspiration and perspiration; (2) experiment timing and equipment issues; (3) communications; (4) impact of potential volcano activity on the experiment; and (5) our interactions with local residents.

The success of our experiment owed a great deal to a large number of competent and enthusiastic people from diverse institutions who proved they were able to work hard and very well together towards a common goal over a several year period, planning carefully and assisting each other, and responding creatively to a number of difficult technical problems that arose. The team was ably supported by professional technical teams at PASSCAL, Scripps, OBIC and NERC Marine Services, aided by the MVO, and generously assisted with supplemental funding from several sources to meet specific problems. The lesson is to devise promising research and then to populate the research team with the best expertise possible, seeking to include experienced individuals who can set egos aside in favour of benefiting the common effort.

Our initial concept was to record both natural earthquakes and signals from a 3 day active source experiment using an airgun array towed by a research vessel around Montserrat, taking opportunistic advantage of a previously planned NERC ship operation scheduled in May 2005. Owing to ship schedule delays, the cruise availability for us was withdrawn for 2005 and needed to be rescheduled for 2007. Although disappointing for us at the time, in retrospect, this delay proved to be absolutely vital to the success of our experiment. We were able to develop more thorough plans, acquire additional ship time and obtain additional financial support. We were able to double the size of the land seismometer array, leading to improved tomographical resolution. We added a digital streamer, which provided the local sediment thickness data needed to account for travel-time delays in signals from the airgun shots and, in addition, to provide useful reflection profiles indicating sediment type and structure. Also, of critical importance, we were able to include an OBS component in the experiment. The OBS array expanded the source–receiver offsets and this was the most significant factor in our achieving the resolution at depth needed to image the magma chamber. The sum of these components resulted in a vastly improved and successful experiment.

Well-planned and redundant communication systems also were vital to success. The requirement of the successful land operation was to have all seismometers recording data when the airgun shooting took place, whereas the precise timing of ship operations could not be firmly known beforehand. Significant changes in ship activity out of the control of the Chief Scientist occurred near the beginning and end of the experiment, but redundant communications enabled the necessary flexible adjustments to land operations and reprogramming of instruments. Similarly, near the end of the shooting phase of the experiment, some final adjustments needed to be made to the ship track, and good communications facilitated discussion between land and sea teams in prioritizing the options. A clear discussion of all experimental plans in advance, and involving both land-based and ship-based staff and ship's officers, is useful for developing contingency flexibility and in avoiding misunderstandings. **Q8**

Fortunately for us, the activity at the Soufrière Hills Volcano was low during this experiment. The only volcano-related incident was that one scouting mission by boat had to be abandoned due to the observation of rockfalls down the crater valley on the east flank. Nonetheless, the experiment required precautions compatible with the possibility of the volcano erupting. Participants went into the volcanic exclusion zone multiple times by boat, car and foot; each time, HQ and the MVO were involved by radio or mobile phone communication. In some cases, the MVO staff was required as an escort. In the unlikely event of a large-ash producing eruption, HQ and the MVO were kept informed about the Centre Hills hikers' timing and locations.

Finally, as a generalization, many residents of Montserrat have had an uneasy relationship with scientists connected to monitoring and research on the Soufrière Hills Volcano. Volcanologists have been responsible for forecasting what the volcano might do and have provided scientific advice to the authorities since the eruption began in 1995. Both the unpredictable behaviour of the volcano and misunderstandings between the public, authorities

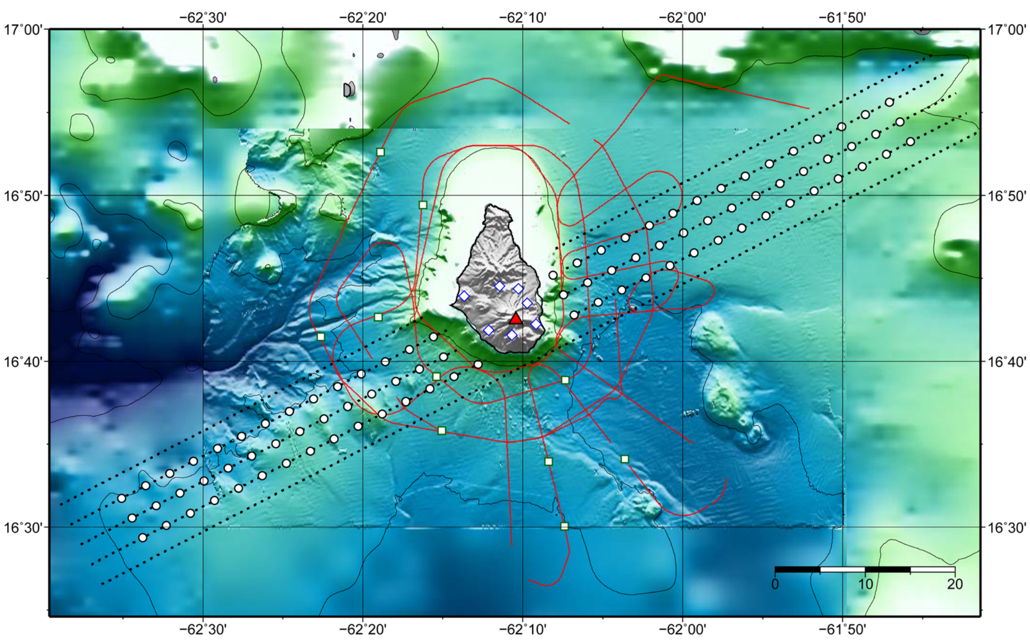

Colour online/ colour hardcopy

Fig. 15.37. Schematic geometry of the proposed 3D controlled source experiment at Montserrat. Red triangle, Soufrière Hills Volcano; white circles, OBS locations; diamonds, permanent land stations of MVO; dotted lines, proposed shooting tracks; squares, SEA-CALIPSO OBS locations; red line, corresponding shooting track.

and volcanologists have, on occasion, led to tensions involving Q9 part of the population (Haynes 2006). Locally, there is a strong desire that the volcano will go back to sleep, volcanologists will go away and tourists will return. Despite these issues, the leaders of the on-land operations of SEA-CALIPSO were met with interest and cooperation from almost all Montserratians. People agreed to locate seismometers on their properties for 3 months, and no stations were vandalized. There was some concern locally about the airgun shooting, which people feared would kill marine life and deafen SCUBA divers. These concerns did not materialize. At our request, the Marine Authority on the island also sent out multiple warnings to local fisherman and local vessels about our cruise to minimize the possibility of vessels impinging on ship tracks and causing interruptions to airgun shooting. The overall cooperation of the Montserrat authorities, civic leaders and population in our endeavour has been greatly appreciated.

Epilogue

Building on the success of SEA-CALIPSO, a proposal was submitted in 2012 to determine the geometry of the entire crustal magmatic system beneath SHV, through the use of conventional 3D travel-time and novel 3D full-waveform tomographical methods. This model will then be used to identify deep crustal structure, constrain numerical simulations of magma chamber growth by episodic sill intrusion, determine magma flux into and through magma chambers in the upper and mid-crust, and explore such fundamental issues as ‘Where does magma differentiation take place?’

Our new experiment takes advantage of technology and insights into the magmatic system that were not available in 2007, and seeks to obtain significantly deeper and higher-resolution images than was possible then. For instance, we expect to recover fine-scale structure within and around the magma chambers using full-wavefield inversion (FWI) seismic tomography. The potential for FWI to improve spatial resolution has been known for some time (Pratt 1999), but the availability of high-performance computing facilities and more efficient algorithms means that realistic-sized problems can now be solved in 3D (Warner *et al.* 2013). A multi-parameter approach will allow us to distinguish regions of partial melt from regions of hot-but-solid rock, and to distinguish mafic and andesitic melt bodies, which will have different melt fractions at a given temperature.

Our proposed experiment geometry (Fig. 15.37) involves two deployments of 45 OBSs and a shooting pattern of five profiles shot twice. In addition to the particular source and receiver geometry, for our FWI to be successful we require a low-frequency source (with signals down to *c.* 0.5 Hz) in order to accurately recover the long-wavelength velocity structure, and our source will need to be sufficiently powerful to give detectable arrivals at the offsets required. An amplitude analysis of the SEA-CALIPSO 2007 dataset (Paulatto *et al.* 2010*b*) shows that with the source used then, airgun shots are distinguishable from noise to source–receiver offsets of around 50 km. From a NERC vessel we can deploy a source comprising up to 14 guns, with a total volume of the order of 7000 cu. in. and a signal strength at least double that obtained in 2007. A profile acquired with a source of this magnitude across the arc to the south of Guadeloupe (Kopp *et al.* 2011) showed that shots could be detected to offsets of at least 150 km in the vicinity of the arc. Our 3D experiment will have maximum source–receiver offsets of the order of 100 km. We will, again, fire the source at 60 s intervals, and will also record these shots on a towed 3 km streamer to image the structure of the sediment column. Streamer data will be incorporated into the FWI scheme and will also be used for conventional deep reflection imaging. Our experiment will require 18 days on site.

Funding was provided by NSF, NERC, Discovery Channel TV, the British Geological Survey, and the Foreign and Commonwealth Office of the UK. R. Reichlin, L. Johnson, R. Kelz, S. Esperanca and S. Shor at NSF provided very strong Q10 support and responded when necessary to special needs. H. Beadman at NERC provided enthusiastic help in scheduling, and essential financial and logistic support for the cruise. Shipboard operations owed a great deal to the skill and dedication of the National Marine Services technical staff under the outstanding leadership of C. Day, the professionalism of the officers and crew of the RV *James Cook* under the command of Master P. Gauld, the efficient work of the GeoPro airgun team under the direction of L. Akentiev, and the skilled assistance of W. Sutherland and others representing Scripps. The excellent contributions of G. Hough, M. Grigor, P. Leary to the shipboard science team was much appreciated. M. Unwin and C. Weir provided skilled service in regard to mitigation of harm to marine animals. The late J. Diebold at Lamont-Doherty provided sound and timely advice on airgun technology at a critical period in our planning, and also donated equipment. The challenging OBS deployment was accomplished thanks to the skill of skipper P. Gervain of the Institut Régional de Pêche Marine, Guadeloupe, and A. Burchell and C. McCoy of OBIC. On-land operations were greatly aided by the PASSCAL group in Socorro, J. Fowler, B. Beaudoin and M. Fort, and expert field teams included in the authorship. Necessary on-land assistance was provided by C. Chen, K. Jeffcoat, R. Malin, L. Malin, D. Smith, J. Walton and J. Winston. Excellent support was provided by the MVO, especially V. Hards, S. De Angelis, and M. Strutt. C. McClintock at PSU greatly assisted various CALIPSO funding efforts. We thank Fusion Petroleum Technologies, Inc., for aid in data processing the offshore seismic lines. N. Ferguson, A. Kiehl, and M. Williams of Darlow Smithson Productions provided media services, leading to the television documentary *Engineering Volcanoes* produced for Discovery Channel by R. Green at Optomen Productions. T. Dawkins of Montserrat contributed our artistic Logo. Finally, our paper benefited from careful reviews by G. Christeson, an anonymous reader and editor G. Wadge.

Appendix 1

Here we present the full list of land seismic stations with location coordinates (see Fig. 15.9) (Tables 15.A1 & 15.A2).

Table 15.A1. *Reftek stations*

Station name	Latitude (°)	Longitude (°)	Elevation (m)
M01	16.81183	−62.19225	384
M02	16.80849	−62.20446	15
M03	16.78856	−62.21336	62
M04	16.79247	−62.19440	174
M05	16.79377	−62.18493	166
M06	16.77659	−62.21387	159
M07	16.77466	−62.20421	298
M08	16.77443	−62.19325	292
M09	16.77962	−62.17775	139
M10	16.76928	−62.21442	227
M11	16.76244	−62.22003	112
M12	16.75660	−62.22633	66
M13	16.75109	−62.23054	50
M14	16.74896	−62.21281	257
M15	16.74125	−62.21508	118
M16	16.73630	−62.23145	60
M17	16.72844	−62.22045	79
M18	16.71909	−62.20630	279
M19	16.72216	−62.19792	218
M20	16.72540	−62.23579	9
M21	16.71760	−62.22098	63
M22	16.69578	−62.21176	9
M23	16.68269	−62.19819	4
M24	16.67694	−62.17917	14
M25	16.67612	−62.16229	14
M26	16.70686	−62.14968	13
M27	16.76716	−62.16986	193
M28	16.76152	−62.15981	9
M30	16.68784	−62.16142	451

Table 15.A2. *Texan stations*

Station name	Latitude (°)	Longitude (°)	Elevation (m)	Station name	Latitude (°)	Longitude (°)	Elevation (m)
B01	16.72218	−62.19792	219	C23	16.75718	−62.18766	621
B02	16.72263	−62.19859	213	C24	16.75615	−62.18802	647
B03	16.72283	−62.19984	219	C25	16.75535	−62.18862	624
B04	16.72356	−62.20003	220	C26	16.75522	−62.18971	653
B05	16.72469	−62.20054	238	C27	16.75557	−62.19109	677
B06	16.72479	−62.20173	279	C28	16.75575	−62.19218	738
B07	16.72528	−62.20250	302	C29	16.75539	−62.19301	747
B08	16.72589	−62.20329	312	C30	16.75503	−62.19387	702
B09	16.72619	−62.20418	307	C31	16.75496	−62.19498	630
B10	16.72673	−62.20479	298	C32	16.75554	−62.19615	684
B11	16.72765	−62.20571	259	C33	16.75740	−62.19824	731
B12	16.72775	−62.20669	251	C34	16.75741	−62.19937	665
B13	16.72755	−62.20755	242	C35	16.75761	−62.20047	641
B14	16.72902	−62.20770	183	C36	16.75832	−62.20185	626
B15	16.72938	−62.20856	173	C37	16.75824	−62.20285	689
B16	16.72983	−62.20937	158	C38	16.75789	−62.20357	681
B17	16.73069	−62.21011	137	C39	16.75686	−62.20407	656
B18	16.73109	−62.21093	129	C40	16.75557	−62.20460	670
B19	16.73154	−62.21161	117	C41	16.75544	−62.20550	634
B20	16.73148	−62.21283	110	C42	16.75484	−62.20628	579
B21	16.73249	−62.21326	96	C43	16.75426	−62.20712	521
B22	16.73306	−62.21412	104	C44	16.75370	−62.20781	494
B23	16.73346	−62.21512	89	C45	16.75295	−62.20853	434
B24	16.73260	−62.21635	83	C46	16.75253	−62.20910	390
B25	16.73288	−62.21730	93	C47	16.75184	−62.21000	357
B26	16.73352	−62.21796	99	C48	16.75125	−62.21074	333
B27	16.73428	−62.21867	87	C49	16.75069	−62.21155	305
B28	16.73573	−62.21875	81	C50	16.75003	−62.21232	263
B29	16.73687	−62.21901	72	C51	16.74894	−62.21284	258
B30	16.73667	−62.22022	49	G01	16.74823	−62.21339	218
B31	16.73892	−62.21977	40	G02	16.74759	−62.21391	198
B32	16.73960	−62.22025	35	G03	16.74783	−62.21552	169
B33	16.74094	−62.22029	33	G04	16.74761	−62.21670	157
B34	16.74143	−62.22117	24	G05	16.74758	−62.21806	157
B35	16.74202	−62.22184	32	G06	16.74696	−62.21850	128
B36	16.74231	−62.22281	29	G07	16.74616	−62.21938	121
B37	16.74258	−62.22381	22	G08	16.74554	−62.21970	104
B38	16.74286	−62.22479	23	G09	16.74453	−62.21997	97
B39	16.74355	−62.22546	27	G10	16.74413	−62.22107	79
B40	16.74369	−62.22650	34	G11	16.74371	−62.22186	50
B41	16.74457	−62.22696	38	G12	16.74301	−62.22266	43
B42	16.74503	−62.22782	43	G13	16.74259	−62.22379	12
B43	16.74523	−62.22889	43	G14	16.74254	−62.22469	15
B44	16.74542	−62.22985	32	G15	16.74161	−62.22521	21
B45	16.74576	−62.23071	33	G16	16.74152	−62.22639	18
B46	16.74579	−62.23197	33	G17	16.74104	−62.22720	27
B94	16.71735	−62.19023	438	G18	16.74069	−62.22823	28
B95	16.71994	−62.19390	304	G19	16.73999	−62.22903	23
B96	16.72030	−62.19473	283	G20	16.73982	−62.23003	28
B97	16.72097	−62.19532	269	G21	16.73909	−62.23049	39
B98	16.72157	−62.19614	243	G22	16.73717	−62.22963	41
B99	16.72207	−62.19681	234	G23	16.73719	−62.23127	53
C01	16.76722	−62.16982	190	G24	16.73632	−62.23141	57
C02	16.76736	−62.17093	217	G25	16.73518	−62.23167	72
C03	16.76706	−62.17172	227	G26	16.73444	−62.23229	97
C04	16.76668	−62.17265	252	G27	16.73394	−62.23267	89
C05	16.76670	−62.17381	249	G28	16.73138	−62.23142	79
C06	16.76631	−62.17460	253	G29	16.73085	−62.23240	104
C07	16.76562	−62.17541	284	G30	16.72992	−62.23266	110
C08	16.76540	−62.17617	297	G31	16.72919	−62.23305	126
C09	16.76504	−62.17707	311	G32	16.72834	−62.23318	105
C10	16.76489	−62.17807	350	G33	16.72736	−62.23382	51
C11	16.76473	−62.17911	421	G34	16.72662	−62.23449	33
C12	16.76480	−62.18006	451	G35	16.72611	−62.23517	20
C13	16.76456	−62.18097	488	G36	16.72541	−62.23577	9
C14	16.76306	−62.18160	502	S01	16.75588	−62.19248	733
C15	16.76305	−62.18242	475	S02	16.75696	−62.19238	735
C16	16.76271	−62.18333	480	S03	16.75769	−62.19244	731
C17	16.76289	−62.18439	497	S04	16.75872	−62.19271	728
C18	16.76235	−62.18504	508	S05	16.75980	−62.19281	726
C19	16.76099	−62.18540	494	S06	16.76054	−62.19317	731
C20	16.76039	−62.18625	548	S07	16.76147	−62.19355	741
C21	16.75874	−62.18643	637	S08	16.76228	−62.19437	721
C22	16.75771	−62.18683	619	S09	16.76320	−62.19501	637

(*Continued*)

Table 15.A2. *Continued*

Station name	Latitude (°)	Longitude (°)	Elevation (m)
S10	16.76412	−62.19507	625
S11	16.76501	−62.19463	574
S12	16.76595	−62.19378	480
S13	16.76685	−62.19330	475
S14	16.76792	−62.19166	434
S15	16.76865	−62.19063	410
S16	16.76947	−62.19069	409
S17	16.77050	−62.19091	389
S18	16.77126	−62.18975	400
S19	16.77214	−62.18986	376
S20	16.77286	−62.18990	369
S21	16.77400	−62.19026	357
S22	16.77484	−62.18962	318
S23	16.77578	−62.18983	313
S24	16.77679	−62.18974	302
S25	16.77757	−62.18965	292
S26	16.77840	−62.18980	282
S27	16.77945	−62.19008	273
S28	16.78040	−62.19128	247
S29	16.78114	−62.19112	239
S30	16.78207	−62.19111	225
S31	16.78311	−62.19227	229
S32	16.78395	−62.19283	229
S33	16.78455	−62.19286	222
S34	16.78579	−62.19261	224
S35	16.78648	−62.19269	221
S36	16.78741	−62.19265	211
S37	16.78841	−62.19320	202
S38	16.78899	−62.19387	192
S39	16.79036	−62.19457	184
S40	16.79099	−62.19561	167
S41	16.79197	−62.19551	159
S42	16.79275	−62.19445	169
S43	16.79382	−62.19433	170
S44	16.79472	−62.19430	172
S45	16.79557	−62.19426	168
S46	16.79658	−62.19459	160
S47	16.79725	−62.19461	147
S48	16.79824	−62.19436	145
S49	16.79915	−62.19466	147
S50	16.80004	−62.19442	166
S51	16.80093	−62.19404	181
S52	16.80197	−62.19460	190
S53	16.80277	−62.19466	216
S54	16.80371	−62.19326	259
S55	16.80466	−62.19312	268
S56	16.80548	−62.19349	264
S57	16.80646	−62.19320	267
S58	16.80728	−62.19269	273
S59	16.80820	−62.19234	288
S60	16.80919	−62.19304	294
S61	16.81001	−62.19189	332
S62	16.81087	−62.19216	374
S63	16.81190	−62.19219	388
M31	16.74178	−62.15800	99
M32	16.73134	−62.15961	186

Q11

Appendix 2

Cruise Operations Diary

Monday 3rd to Saturday 15th December. The GeoPro engineers set up and tested the airgun array and controller on the *James Cook* during the cruise JC18, preceding JC19.

Friday 7th December. The OBS deployment team of C. McCoy, A. Burchell, M. Paulatto and C. Pearce fly to Guadeloupe through Paris Orly. A car is hired. Arrive at Marine de Rivíere Sens, Gourbeyre, Basse Terre and check in at the Hotel La Crosíere.

Saturday 8th December. First meeting with Paul Gervain at IRPM and inspection of the vessel *Beryx* and the workshop. We are informed by the shipping agent that our container with all the OBS instrumentation is still held at the Customs office awaiting clearance. Since the office is closed during the weekend the first possible day for delivery is Monday.

Sunday 9th to Tuesday 11th December. Corrected documentation is supplied through the shipping agent. The container is released on late afternoon Tuesday 11th.

Wednesday 12th December. The container is delivered at 12:00. We set up the lab at IRPM and start the assemblage and initialization of the instruments. At 15:00 the team leaves port on the *Beryx* and performs the acoustic release test in about 1000 m of water off the west coast of Guadeloupe. The test is successful. However, even in the lee of the island, the sea is rough and most of the team soon feels the effects of seasickness. We are back in port at about 18:00.

Thursday 13th December. The OBS team sails at 07:30 on the *Beryx* with four instruments on board. The plan is to deploy them at planning sites 8, 9, 10 and 6. The working conditions on board are very poor. The sea is rough especially when the boat leaves the lee of the island and since the waves come from the east while our course is mainly north–south, the roll of the boat is particularly unpleasant. Soon all the scientific crew is seasick and almost unable to work. The deployment of instruments in these conditions and from such a small boat is a particularly tricky operation, with the risks of injuring the crew or damaging the instruments. The experience of the skipper is essential to the success of the operation. Three out of four instruments are deployed (sites 8, 9 and 10). We are back in port at 19:00.

Friday 14th December. No deployments. Instead all the remaining instruments are assembled and programmed so that they are ready to be deployed, and the operations at sea are simplified and limited to lowering them in the water and log keeping. A new OBS array plan is designed by M. Paulatto and C. Peirce and approved by T. Minshull, with more instruments now to the west, on the lee side of Montserrat, and no instruments to the east. Originally planned sites 1–5 are abandoned and new sites 11–16 are added. (See Fig. 15.2.)

Saturday 15th December. M. Paulatto and C. Peirce fly to Antigua to join the RRS *James Cook*. C. McCoy and A. Burchell leave port onboard the *Beryx* at 06:00 to deploy instruments at sites 11, 12, 15 and 16. Since the weather is slightly improved, the vessel less crowded and the operations better organised, the deployment goes smoothly. Return to port at 19:00. Pre-cruise meeting in Saint John's, Antigua.

Sunday 16th December. C. McCoy and A. Burchell onboard the *Beryx* deploy OBS instruments on sites 6, 7 and 14. Leave port at 06:00, return to port at 19:00. All instruments deployed.

The RRS *James Cook* arrives in port in Saint John's, Antigua, at 09:00 as scheduled. The scientific party boards the ship at 12:00 approximately, after immigration and customs formalities. All equipment is loaded and arranged on deck and in labs. The MCS streamer winch is severely damaged and needs a new hydraulic motor, and a replacement is sought. GPS antennas for data-logger synchronisation are installed. P. Malin and M. Grigor set up a Reftek datalogger in the deck lab to record shot timing. S. Dean, C. Peirce and M. Paulatto set up an OBS datalogger with the same purpose. GeoPro airfreight is delivered at 18:00. The ship leaves port at 19:30, heading to a waypoint south of Antigua.

Monday 17th December. Start of gun deployment at 07:00. At 7:35 deployed Passive Acoustic Monitoring (PAM) equipment and start marine mammal monitoring. At 10:12 beginning of shooting with soft start. Guns are activated sequentially from gun 8 to gun 1 to increase source power gradually. At 10:18 the soft start sequence is interrupted due to a yacht on ship's course. A second soft start commences at 10:24. Soft start completed at 10:46. At 10:43–12:48, streamer deployment. At 14:06, shooting and acquisition system deployment is complete, and MCS acquisition can start. The speed of ship over ground is 4.5 knots. The captain decides that the ship will not sail over the shallow shelf around Montserrat, as had been originally planned. We note that if the ship turns at 5° per minute or more the streamer is pulled too close to the guns. Thus 2° per minute turns are adopted. The shooting track is modified accordingly and a provisional version is passed on to the ship's officers. At 14:11, gun 8 is shut down. At 15:54 the ship's speed is reduced by 1 knot due to overheating of thrusters. At 18:54–23:43, starboard gun array is shut down and brought on deck for repairs. At 19:52–19:59, soft start. The gun controller is rebooted at 20:01, possibly due to power failure. After another soft start is performed, guns are back on full power at 20:59. Guns are shut down at 22:45 due to dolphins in the vicinity. XBT probes keep failing after a few hundred meters and wires get tangled on the guns and streamer.

Tuesday 18th December. Continue shooting. Gun 3 is shut down at 07:13. Speed is increased to 4.5 knots. At 13:02 the portside gun array is shut down and serviced to fix gun 3. Guns are redeployed and soft start begins at 15:30. Starboard gun array is shut down and serviced at 21:08. All guns are shut down at 22:05 due to a yacht near the ship's course. Shooting restarts at 22:44.

Wednesday 19th December. Continue shooting. Shooting track is adjusted to allow maneuvering in proximity of Redonda. From 04:00, gun 8 is repeatedly shut down and turned on again, until 06:24 when it is shut down indefinitely. All guns are shut down at 10:14 for dolphins. Soft start at 10:46. Problems with portside guns at 11:57. Portside array shut down and serviced at 14:41, soft start begins at 18:03, with full array firing at 18:14. Some MCS data plots are produced on board by S. Dean.

Thursday 20th December. Continue shooting. Starboard gun array shut down at 07:24 for service. Soft start begins at 07:43 with full array firing at 07:52. All guns shut down at 09:32 due to marine mammal detection. Soft start at 10:10, with full array firing at 10:30. Some errors on portside guns, possibly caused by an air leak between 10:53 and the end of shooting. A yacht crosses the ship's track at 13:23. The ship is forced to slow down and turn to avoid collision. All guns are shut down at 15:00. Guns and streamer are retrieved.

Friday 21st December. The RRS *James Cook* returns to port in Saint John's, Antigua. OBS instruments recovery accomplished. C. McCoy and A. Burchell leave Guadeloupe on the *Beryx* at 06:00. Instruments 07, 11, 12, 15, 16 are recovered. The team spends the night on the boat anchored in a cove on Montserrat. Arrive at anchorage at 19.00.

Saturday 22nd December. The *Beryx* leaves Montserrat anchorage at 03:00. Instruments 06, 08, 09, 10 are recovered. Return to port at 18:00. M. Paulatto flies back to Guadeloupe from Antigua, to help with instrument recovery and packing.

Sunday 23rd to Monday 24th December. Container packing. C. McCoy flies back to the U.K.

Thursday 27th December. A. Burchell and M. Paulatto fly back to the U.K.

Land Operations Diary

Abbreviated diary. All times are local, 4 h behind GMT time.

Wednesday 3rd to Thursday 4th October. E. Shalev, C. Kenedi, B. Voight meet at SeaDreams villa to discuss number of Texans needed, for example, Centre Hills lines – Jack Boy to MVO to Sea Dreams, 70 instruments; Katy Hill to Silver Hills, 40, etc. Discuss powerpack issues for Texans and related need for reprogramming computers and two PASSCAL people to do this mid-experiment.

Friday 5th October. Meet with Centre Hills Project head, and Director of the Environment, permissions. Permissions from landowners at Reftek sites. Note map issues; published Montserrat map needs correction to be consistent with GPS. Planning Reftek deployment. Planning instrument shipments; contact shipping agents in Miami, customs in Montserrat.

Saturday 6th October. Check Centre Hills trail route via Dick Hill and Katy Hill – B . Voight, V. Miller, A. Lee, A. Custance-Baker. Several others return to car due to difficult steep section. Also test run for a guide who misses 0600 start by 1.5 h, just returning from night out, and demonstrates novel hydration practices. Plan Reftek deployment to several remote areas – hoped for helicopter support, but now helicopter is broken in Antigua.

Sunday 7th October to Sunday 14th October. Instruments arrive! Have been held up in customs. Reftek installation training led by W. Zamora and E. Shalev for all hands. Reftek installations by V. Miller, W. Zamora, A. Lee, K. Kenedi, B. Voight, E. Shalev, R. Stewart. Reftek installations along coast by boat. B. Voight checks out alternate Centre Hills tracks with J. 'Scriber' Dailey. Shalev, Kennedi, Voight work out tentative hiking team assignments for December. Revisit stations for final check and servicing. Plans made for V. Miller to return in November for station maintenance.

Thursday 6th to Sunday 9th December. Arrivals seismometer deployment team personnel from Duke, Penn State, University of Arkansas, IRIS etc. E. Shalev and D. Hidayat review siting plans. We probably could install two exclusion-zone helicopter-access site stations, by hiking because helicopter is not available. However, we need permission from MVO in order to do it. On 7th Shalev and Hidayat go to MVO to explain details about installation plans, both land and sea. MVO objects to the hike-in plan. The PASSCAL (seismic instrument) boxes arrived in the afternoon. About 210 Texans (seismic data recorders), geophones & other supporting instrument are all there. V. Miller and A. Lee go to far north and east to service Refteks and download data, at Bramble (old) airport. Statue Rock, Jack Boy, the new airport at Geralds, etc. On morning of 8th, Miller, Lee and Hidayat attempt to go by boat to service south coast Reftek sites, but trip cancelled due to rough seas and coastal surf. At SeaDreams, Texans are labelled with tape and number codes. On the 9th, weather again too rough to service south coast sites by boat. R. Herd and others check out condition of the trails crossing Centre Hills and check radio communications from there. Silver Hills Reftek site serviced.

Monday 10th to Wednesday 12th December. These were largely days of organizational details and many trips to the airport for people and luggage. SeaDreams villa in Olveston set up as headquarters (HQ) and equipment storage site, overseen by Shalev and C. Kenedi. Made contact with Discovery Channel film team and BV discusses what should be documented in Plymouth and on experiment. Montserrat Department of Environment contacted to inform on experiment. Arrangements and permissions established with MVO. Tappy Syers (MVO) will help with logistics. First meeting as a group. On morning of 10th Miller and Lee managed to service coastal sites by boat at Kinsale and St Patricks, and had a go at O'Garras. At latter, surf very rough and Miller had to swim, injuring shoulder. Power down and team disappointed as fix impossible today. At HQ, training sessions scheduled for Texan installations, on 11th at 1330 h. There are about 200 instruments that need to be installed in 200 different locations. These station sites are already planned and their coordinates are stored in GPS units which are distributed among team. What teams need to do is to find waypoints/station locations using GPS, say, go to waypoint S16. If a better point is needed to locate the Texan, mark a new waypoint name NS16, using average of 25 GPS measurements. Hidayat checks out CALIPSO stations at Air Studios and Geralds, and replaces radios. On 11th Voight/Syers make checkout cruise on local vessel 'Daily Bread' used for coastal seismometer deployments, and land at Kinsale; Miller attempts landing at O'Garras and Shoe Rock, but is prevented by 2-meter surf. Improved alignment of Garibaldi route is discussed with G. Mattioli. Ice breaker in evening at Mango Falls villa. On 12th the Texan routes are scouted out by various teams and instrument sites are flagged. R. Stewart and others service Refteks.

Thursday 13th December. Boat trip for Miller and Hidayat to south coast cancelled because of rough seas.

Met with guides as required by National Trust for entry to national park land, to discuss the final set-up of hiking trails for Texan deployment. We arranged to pick them all up at 0530 h at the petrol station up north and bring them back to SeaDreams to meet the assigned teams. Distributed back packs to guides. Distributed MVO phone number to all hikers and gave all hiking team phone numbers to MVO. Distributed phones to have at least one phone with each hiking group. Confirmed the final hiking/Texan deployment routes, and vehicle transport plans. All teams finish scouting lower elevation routes, checking with property owners, and flagging stations. Group meeting held at HQ with Voight reviewing overall goals and significance, and Shalev discussing hiking team logistic requirements, safety issues, personal gear. Voight reminds full team that public is stressed and very unhappy at present zoning and we need to be sensitive about remarks made in public, including remarks on science issues that unintentionally might reflect on credibility of MVO.

Friday 14th December. Texan installations are underway today for most car-route segments. At 0800 h the northern array team works south from the airport, with Hidayat, L. Brown, K. Byerly, and S. Saldana. Brown and Saldana are the experienced experts for Texans, and the efficient team finishes around noon. The house owners not met previously gave permissions. Miller and L. Carothers had a chance to go out on the boat, and took it. Could not land at Shoe Rock, disappointing, but weather stormy and seas rough. Waited out the storm. A landing then proved possible west of O'Garra's, and Miller had to get in water just after sighting a shark. Hike to the station, carrying replacement battery, and serviced the station. Then got to Rendevous and serviced that station, so two down, two to go. Mechanical problem arises with Montserrat twin-otter aircraft, raising potential problems in getting the New Zealand crew-members to the ship in Antigua. Ultimately the airlines resolved issue. Film team with Mattioli and Miller crews today. Voight has telephone discussion with T. Minshull in UK on OBS problems, with rough seas and big swells, and seasickness affecting the deployments. We can sympathize from our problems with rough seas here. A new deployment plan is devised.

Saturday 15th December. New Zealanders depart to join the ship in Antigua. All Texan crews move to their departure points to deploy the arrays: Mattioli *et al.* at Garibaldi, Lee at Jackboy, Herd at the tough central segment of Centre Hills, Voight at Dick Hill-Katy Hill, Miller in Centre Hills above the MVO trailhead. At that point poor weather much concerns HQ, with heavy rain and Centre Hills enveloped in cloud, but the field crews insist on continuation of deployment. The Dick Hill–Katy Hill team starts at 0745 h, returns via Big River at 1750 h with the film crew exhausted. Other crews finish earlier.

Ship Status: Talk to S. Sparks on the RRS *James Cook*. Got the emergency number onboard ship. The plan is to leave Antigua tomorrow after 1500 h and start shooting late afternoon/evening along the outer ring. The ship location of most concern for volcanic hazard was off Tar River; Sparks agrees to call us to indicate when they were predicted to be off Tar River, in case precautions needed. We will also alert ship if something changes at volcano.

Sunday 16th December. Herd and Voight hike from Trants through Spanish Point to Whites Yard, to install Texans and fill in gap in seismometer array. Later, film crew enters Plymouth for documentary shooting. The Belham River team is sent out to extend their Texan array over St George's Hill and to foot of Gages Mountain.

Ship Status: The *James Cook* left Antigua late, around 1900 h, then anchored to allow ship crew to sleep. A surprise to the land team, as Texan battery issues are a concern. Shooting now supposed to commence at first light of 17 December. HQ called dive companies Green Monkey and Sea Wolf to confirm times of airgun shooting, to alert scuba divers.

Monday 17th December. Shooting began later than anticipated. Guns were deployed early but shooting began around 1000 h, was interrupted by a private yacht crossing the ship's bow, and the airguns were stopped and needed soft restarting. Mattioli and Voight at MVO observing instruments to detect shots. Shot arrivals were detected first on the CALIPSO strainmeters at Geralds and Trants, and then sequentially afterward at MVO seismometers at Windy Hill, then Harris, Flemmings, Garibaldi etc. Called Governor's office to confirm that shooting had begun. Signals noisy at Long Ground, Roches Yard. Overall a good sign as ship is about halfway from Antigua (say ~20 km) and signals should strengthen as ship gets closer. Reason for optimism for our Reftek array data, if our luck holds regarding interruptions. Sparks called at 1620 h: The ship was approaching Montserrat from the NE, then to go clockwise, and take in radials; then guns are near the 'maximum signal' positions. We notice signal strength differs when ship is on radial track, compared to circular track. Sparks is concerned about possible further interference from other ships. Voight will do local video news broadcast with D. Edgecombe to disseminate warning to marine community, for all ships to stay far away from the *James Cook*.

Ship Status: Sperm whales apparently were detected at depth by acoustics but shooting continued. Several interruptions occurred due to mechanical issues and gun array, and nearby dolphin detection. The captain will not sail into water less than 300 feet deep over the shelves, a surprise that requires shift of ship track to ~3 km offshore.

Tuesday 18th December. Three teams work on battery changing for Texans installed near roads. Each Texan line runs on two D-cell batteries, which are convenient but only power a Texan for a few days. With our planned active-seismic experiment the battery power will not be sufficient, so battery changes are required. Due to the logistic situation, batteries for stations on the segments crossing Centre Hills were not changed. The procedure is simple but we have to be very careful not to stop data acquisition while changing the batteries. Crews carry a box containing temporary batteries which are connected to the Texan while existing Texan batteries are replaced with new ones. Fortunately, all goes well and no instrument had interuptions in data acquisition. Voight interview on 'Peoples TV' warns the fishing fleet about interference with the Cook, and local radio and the maritime commision are likewise informed. The Discovery Channel is interviewing team members.

Wednesday 19th December. Sparks and Voight communicate by phone 1730 h. Plans have changed. The ship captain has decided to stop shooting mid-day on Thursday 20 December at 1500, rather than on the 21st, to allow crew to rest prior to voyage to Panama. Later in the day further discussions of the onshore team with Sparks on the configuration of the remaining ship track lead to some track adjustments. Meanwhile S. Dean aboard the Cook has processed streamer data, and reports nice imaging of sediment wedges and growth faults. The hiking groups will collect Texans on Thursday rather than Friday as originally planned. Called all guides and anyone not at SeaDreams to inform of hiking plans the next day. We request to be advised by ship by 0700 h whether shooting will end by noon or 1500 h, in order to facilitate plans for Texan retrievals.

Thursday 20th December. 0705 h, Sparks talks with Voight by telephone. Ship on SW coast, with middle loop completed. Sparks says: 'Mission accomplished!' which means that the basic loops are complete. The rest of continued shooting is more or less gravy. At 0730 h, Carothers, Miller and Lee retrieve coastal Reftek instruments with the 'Daily Bread.' Four stations removed, but landing not possible at Shoe Rock and Tar River due to surf. Around same time guides are picked up for meeting with hike crews at SeaDreams HQ at 0800 h. Ship reports that shooting will continue to 0300 h, so the crews disperse. The guide 'Mapeye' (Philemon Murrain) finds a Guinness and two Caribs for breakfast ... as usual. At 0930 to 1130 h, hiker teams dispersed at trailheads. The Katy Hill team starts at Jackboy Hill, at guide 'Scriber' (James Daley) request; proved an efficient retrieval route. Hidayat goes to MVO to collect MVO seismic data for the period of the shoot.

Friday 21st December. Texan collection from roads. Refteks retrieved from yards, and near coast with the boat. Data downloading from instruments. Packing up instruments is efficient and fast. Many logistics to complete – car payments, people rearranging travel etc. Voight off to Antigua to meet Sparks on the *James Cook*. Both are happy with tracks delivered and data acquired. Meet with the Captain, and Colin Day, 'a genius at putting things together with string and chewing gum', and a key shipboard man for our experiment. Later met with the ship's scientific team. Exchange views of key land data, and streamer profiles; all are pleased with the acquisitions.

Saturday 22nd December – Tuesday 26th December. Arrangements made for shipping equipment back to US. Container pickup by shipping company on 26th. Clean-up villas. Payments to local people. Most of team departs, with a few hanging on through Christmas and the Arrow concert.

References

Annen, C. 2009. From plutons to magma chambers: thermal constraints on the accumulation of eruptible silicic magma in the upper crust. *Earth and Planetary Science Letters*, **284**, 409–416.

Annen, C., Pichavant, M., Bachmann, O. & Burgisser, A. 2008. Conditions for the growth of a long-lived shallow crustal magma chamber below Mount Pelee volcano (Martinique, Lesser Antilles Arc). *Journal of Geophysical Research*, **113**, B07209, http://dx.doi.org/10.1029/2007JB005049

Aspinall, W. P., Miller, A. D., Lynch, L. L., Latchman, J. L., Stewart, R. C., White, R. A. & Power, J. A. 1998. Soufrière Hills eruption, Montserrat, 1995–7: volcanic earthquake locations and fault plane solutions. *Geophysical Research Letters*, **25**, 3397–3400.

Bailey, R. C. & Garces, P. B. 1988. On the theory of air-gun bubble interactions. *Geophysics*, **53**, 192–200.

Barclay, J., Carroll, M. R., Rutherford, M. J., Murphy, M. D., Devine, J. D., Gardner, J. & Sparks, R. S. J. 1998. Experimental phase equilibria: constraints on pre-eruptive storage conditions of the Soufrière Hills magma. *Geophysical Research Letters*, **25**, 3437–3440.

Barclay, J., Herd, R. A., Edwards, B., Kiddle, E. & Donovan, A. 2010. Caught in the act: implications for the increasing abundance of mafic enclaves during the eruption of the Soufrière Hills Volcano, Montserrat. *Geophysical Research Letters*, **37**, L00E09, http://dx.doi.org/10.1029/2010GL042509

Boynton, C. H., Westbrook, G. K., Bott, M. H. P. & Long, R. E. 1979. A seismic refraction investigation of crustal structure beneath the Lesser Antilles island arc. *Royal Astronomical Society Geophysical Journal*, **58**, 371–393.

Byerly, K., Brown, L., Voight, B. & Miller, V. 2010. Reflection imaging of deep structure beneath Montserrat using microearthquake sources. *Geophysical Research Letters*, **37**, L00E20, http://dx.doi.org/10.1029/2009GL041,995

Carlson, R. L. 2001. The effects of temperature, pressure, and alteration on seismic properties of diabase dike rocks from DSDP/ODP Hole 504B. *Geophysical Research Letters*, **28**, 3979–3982, http://dx.doi.org/10.1029/2001GL013426

Chardot, L., Voight, B. *et al.* 2010. Explosion dynamics from strainmeter and microbarometer observations. Soufrière Hills Volcano, Montserrat: 2008–2009. *Geophysical Research Letters*, **37**, L00E24, http://dx.doi.org/10.1029/2010GL044661

Chiodini, G., Cioni, R., Frullani, A., Guidi, M., Marini, L., Prati, F. & Raco, B. 1996. Fluid geochemistry of Montserrat Island, West Indies. *Bulletin Volcanology*, **58**, 380–392, http://dx.doi.org/10.1007/s004450050146

Christensen, N. I. & Mooney, W. D. 1995. Seismic velocity structure and composition of the continental crust: a global view. *Journal of Geophysical Research*, **100**, 9761–9788, http://dx.doi.org/10.1029/95JB00259

Christeson, G. L., Nakamura, Y., McIntosh, K. D. & Stoffa, P. L. 1996. Effect of shot interval on ocean bottom seismograph and hydrophone data. *Geophysical Research Letters*, **23**, 3783–3786.

Christopher, T., Edmonds, M., Humphreys, M. C. S. & Herd, R. A. 2010. Volcanic gas emissions from Soufrière Hills Volcano, Montserrat 1995–2009, with implications for mafic magma supply and degassing. *Geophysical Research Letters*, **37**, LE00E04, http://dx.doi.org/10.1029/2009GL041325

Coffin, M. F., Gahagan, L. M. & Lawyer, L. A. 1998. *Present-day Plate Boundary Digital Data Compilation*. Technical Report, 174. University of Texas.

Costa, A., Melnik, O., Sparks, R. S. J. & Voight, B. 2007. Control of magma flow in dykes on cyclic lava dome extrusion. *Geophysical Research Letters*, **34**, L002303, http://dx.doi.org/10.1029/2006GL027466.

Cruden, A. R. 1998. On the emplacement of tabular granites. *Journal of the Geological Society, London*, **155**, 853–862.

Cunningham, W. D. & Mann, P. (eds) 2007. Tectonics of strike-slip restraining and releasing bends. *Tectonics of Strike-Slip Restraining and Releasing Bend*. Geological Society, London, Special Publications, **290**, 1–12, http://dx.doi.org/10.1144/SP290.1

Deng, Q., Daning, W., Zhang, P. & Chen, S. 1986. Structure and deformational character of strike-slip fault zones. *Pure and Applied Geophysics*, **124**, 203–223, http://dx.doi.org/10.1007/BF00875726

de Saint-Blanquat, M., Habert, G., Horsman, E., Morgan, S. S., Tikoff, B., Launeau, B. & Gleizes, G. 2006. Mechanisms and duration of non-tectonically assisted magma emplacement in the upper crust: the Black Mesa pluton, Henry Mountains, Utah. *Tectonphysics*, **428**, 1–31.

Dewey, J. F., Holdsworth, R. E. & Strachan, R. A. 1998. Transpression and transtension zones. *Journal of the Geological Society, London*, **135**, 1–14.

Druitt, T. H. & Kokelaar, B. P. (eds) 2002. *The Eruption of Soufrière Hills Volcano, Montserrat, Montserrat, from 1995 to 1999*. Geological Society, London, Memoirs, **21**.

Edmonds, M., Aiuppa, A. *et al.* 2011. Excess volatiles supplied by mingling of mafic magma at an andesite arc volcano. *Geochemistry, Geophysics and Geosystems*, **11**, Q04005, http://dx.doi.org/10.1029/2009GC002781

Elsworth, D., Mattioli, G., Taron, J., Voight, B. & Herd, R. 2008. Implications of magma transfer between multiple reservoirs on eruption cycling. *Science*, **322**, 246–248, http://dx.doi.org/10.1126/science.1161297

Evangelidis, C. P., Minshull, T. A. & Henstrock, T. 2004. Three-dimensional crustal structure at Ascension Island from active source tomography. *Geophysical Journal International*, **159**, 311–325.

Feuillet, N., Manighetti, I. & Tapponnier, P. 2001. Active extension perpendicular to subduction in the Lesser Antilles island arc (Guadeloupe, French Antilles). *Comptes Rendus de l'Académie des Sciences, Series IIA, Earth and Planetary Science*, **333**, 583–590.

Feuillet, N., Manighetti, I., Tapponnier, P. & Jacques, E. 2002. Arc parallel extension and localization of volcanic complexes in Guadeloupe, Lesser Antilles. *Journal of Geophysical Research*, **107**, 2331, http://dx.doi.org/10.1029/2001JB000308

Feuillet, N., Leclerc, F. *et al.* 2010. Active faulting induced by slip partitioning in Montserrat and link with volcanic activity: new insights from the 2009 GWADASEIS marine cruise data. *Geophysical Research Letters*, **37**, L00E15, http://dx.doi.org/10.1029/2010GL042556

Foroozan, R., Elsworth, D., Voight, B. & Mattioli, G. 2010. Dual reservoir structure at Soufrière Hills Volcano inferred from continuous GPS observations and heterogeneous elastic modelling. *Geophysical Research Letters*, **37**, L00E12, http://dx.doi.org/10.1029/2010GL042511

Foroozan, R., Elsworth, D., Voight, B. & Mattioli, G. 2011. Magmatic metering controls the stopping and restarting of eruptions. *Geophysical Research Letters*, **38**, L05306, http://dx.doi.org/10.1029/2010GL046591

Girardin, N., Feuillard, M. & Viode, J. P. 1991. Réseau régional sismique de l'arc des Petites Antilles: Sismicité superficielle (1981–1988). sour, **162**, 1003–1015.

Hamilton, E. L. 1980. Geoacoustic modeling of the sea floor. *Journal of the Acoustical Society of America*, **68**, 1313–1340.

Harford, C. L. & Sparks, R. S. J. 2001. Recent remobilisation of shallow-level material on Montserrat revealed by hydrogen isotope composition of amphiboles. *Earth and Planetary Science Letters*, **185**, 285–297.

Harford, C. L., Pringle, M. S., Sparks, R. S. J. & Young, S. R. 2002. The volcanic evolution of Montserrat using $^{40}Ar/^{39}Ar$ geochronology. *In*: Druitt, T. H. & Kokelaar, B. P. (eds) *The Eruption of Soufrière Hills Volcano, Montserrat, Montserrat, from 1995 to 1999*. Geological Society, London, Memoirs, **21**, 93–113.

Haslinger, F., Thurber, C., Mandernach, M. & Okubo, P. 2001. Tomographic image of P-velocity structure beneath Kilauea's East Rift Zone and South Flank: Seismic evidence for a deep magma body. *Geophysical Research Letters*, **28**, 375–378.

Hautmann, S., Gottsmann, J., Sparks, R. S. J., Costa, A., Melnik, O. & Voight, B. 2009. Modelling ground deformation caused by oscillating overpressure in a dyke conduit at Soufrière Hills Volcano, Montserrat. *Tectonophysics*, **471**, 87–95.

Hautmann, S., Gottsman, J., Sparks, R. S. J., Mattioli, G. S., Sacks, I. S. & Strutt, M. H. 2010. Effect of mechanical heterogeneity in arc crust on volcano deformation with application to Soufrière Hills Volcano, Montserrat, West Indies. *Journal of Geophysical Research*, **115**, B09203, http://dx.doi.org/10.1029JB006909

Haynes, K. 2006. Volcanic island in crisis: investigating environmental uncertainty and the complexity it brings. *The Australian Journal of Emergency Management*, **21**, 21–28.

Hobro, J. W. D., Singh, S. C. & Minshull, T. A. 2003. Three-dimensional tomographic inversion of combined reflection and refraction seismic traveltime data. *Geophysical Journal International*, **152**, 79–93.

Humphreys, M. C. S., Edmonds, M., Christopher, T. & Hards, V. 2009. Chlorine variations in the magma of Soufrière Hills Volcano, Montserrat: Insights from Cl in hornblende and melt inclusions. *Geochimica et Cosmochimica Acta*, **73**, 5693–5708, http://dx.doi.org/10.1016/j.gca.2009.06.014

Kenedi, C. L., Sparks, R. S. J. *et al.* 2010. Contrasts in morphology and deformation offshore Montserrat: New insights from the SEA-CALIPSO marine cruise data. *Geophysical Research Letters*, **37**, L00E25, http://dx.doi.org/10.1029/2010GL043925

Kiddle, E., Edwards, B., Loughlin, S., Petterson, M., Sparks, R. S. J. & Voight, B. 2010. Crustal structure beneath Montserrat, Lesser Antilles, constrained by xenoliths, seismic velocity structure and petrology. *Geophysical Research Letters*, **37**, L00E11, http://dx.doi.org/10.1029/2009GL042145

Kopp, H., Weinzierl, W. *et al.* 2011. Deep structure of the central Lesser Antilles Island Arc: Relevance for the formation of contintal crust. *Earth Planetary Science Letters*, **304**, 121–134.

Lahr, J. C. 1999. *HYPOELLIPSE: A Computer Program for Determining Local Earthquake Hypocentral Parameters, Magnitude, and First-Motion Pattern (Y2K compliant version)*. US Geological Survey, Open File Report **99–23**. United States Geological Survey, Denver, CO.

Lees, J. M. 2007. Seismic tomography of magmatic systems. *Journal of Volcanology and Geothermal Research*, **167**, 37–56, http://dx.doi.org/10.1016/j. jvolgeores.2007.06.008

Le Friant, A., Harford, C. L., Deplus, C., Boudon, G., Sparks, R. S. J., Herd, R. A. & Komorowski, J.-C. 2004. Geomorphological evolution of Montserrat, (West Indies): importance of flank collapse and erosional processes. *Journal of the Geological Society, London*, **161**, 171–182, http://dx.doi.org/10.1144/0016-764903-017

Le Friant, A., Lock, E. J. *et al.* 2008. Late Pleistocene tephrochronology of marine sediments adjacent to Montserrat, Lesser Antilles volcanic arc. *Journal of the Geological Society, London*, **165**, 279–289, http://dx.doi.org/10.1144/0016-7692007-019

Le Friant, A., Deplus, C., Boudon, G., Sparks, R. S. J., Trofimovs, J. & Talling, P. 2009. Submarine deposition of volcaniclastic material from the 1995–2005 eruptions of Soufrière Hills volcano, Montserrat. *Journal of the Geological Society, London*, **166**, 171–182, http://dx.doi.org/10.1144/0016-7649 2008-047

Le Friant, A., Deplus, C. *et al.* 2010. Eruption of Soufrière Hills (1995–2009) from an offshore perspective: insights from repeated swath bathymetry surveys. *Geophysical Research Letters*, **37**, L11307, http://dx.doi.org/10.1029/2010GL0435580

Linde, A. T., Sacks, S. *et al.* 2010. Vulcanian explosion at Soufrière Hills Volcano, Montserrat on March 2004 as revealed by strain data. *Geophysical Research Letters*, **37**, L00E07, http://dx.doi.org/10.1029/2009GL041988

Mattioli, G. S., Dixon, T. H., Farina, F., Howell, E. S., Jansma, P. E. & Smith, A. L. 1998. GPS measurement of surface deformation around Soufrière Hills Volcano, Montserrat from October 1995 to July 1996. *Geophysical Research Letters*, **25**, 3417–3420, http://dx.doi.org/10.1029/98GL00931

Mattioli, G. S., Young, S. R. *et al.* 2004. Prototype PBO instrumentation of CALIPSO Project captures world-record lava dome collapse on Montserrat. *Eos, Transactions of the American Geophysical Union*, **85**, 317–325.

Mattioli, G., Herd, R. A., Strutt, M. H., Ryan, G., Widiwijayanti, C. & Voight, B. 2010. Long-term surface deformation of Soufrière Hills Volcano, Montserrat from GPS geodesy: inferences from simple elastic inverse models. *Geophysical Research Letters*, **37**, L00E13, http://dx.doi.org/10.10292009GL042268

Melnik, O. & Costa, A. 2014. Dual-chamber-conduit models of non-linear dynamic behaviour at Soufrière Hills Volcano, Montserrat. *In*: Wadge, G., Robertson, R. E. A. & Voight, B. (eds) *The Eruption of Soufrière Hills Volcano, Montserrat from 2000 to 2010*. Geological Society, London, Memoirs, **39**, 61–69, http://dx.doi.org/10.1144/M39.3

Melnik, O. & Sparks, R. S. J. 2002. Modelling of conduit flow dynamics during explosive activity at Soufrière Hills Volcano, Montserrat. *In*: Druitt, T. H. & Kokelaar, B. P. (eds) *The Eruption of the Soufrière Hills Volcano, Montserrat 1995 to 1999*. Geological Society, London, Memoirs, **21**, 307–318.

Melnik, O. & Sparks, R. S. J. 2005. Controls on conduit magma flow dynamics during lava dome building eruptions. *Journal of Geophysical Research*, **110**, B02209, http://dx.doi.org/10.1029/2004JB003183

Menke, W., West, M. & Tolstoy, M. 2002. Shallow-crustal magma chamber beneath the axial high of the coaxial segment of Juan de Fuca Ridge at the source site of the 1993 eruption. *Geology*, **30**, 359–362.

Michel, J., Baumgartner, J., Putlitz, B., Schaltegger, U. & Ovtcharova, M. 2008. Incremental growth of the Patagonian Torres del Paine laccolith over 90 k.y. *Geology*, **36**, 459–462.

Miller, V., Voight, B., Ammon, C. J., Shalev, E. & Thompson, G. 2010. Seismic expression of magma-induced crustal strains and localized fluid pressures during initial eruptive stages, Soufrière Hills Volcano, Montserrat. *Geophysical Research Letters*, **37**, L00E21, http://dx.doi.org/10.1029/2010GL043997

Minshull, T. A., Pierce, C. & Sinha, M. C. 2005. Multi- disciplinary, sub-seabed geophysical imaging. *Sea Technology*, **46**, 27–31.

Murphy, M. D., Sparks, R. S. J., Barclay, J., Carroll, M. R. & Brewer, T. S. 2000. Remobilization of andesite magma by intrusion of mafic magma at the Soufrière Hills Volcano, Montserrat, West Indies. *Journal of Petrology*, **41**, 21–42.

Nakamura, Y., Donoho, P. L., Roper, P. H. & McPherson, P. M. 1987. Large-offset seismic surveying using ocean-bottom seismographs and air guns: Instrumentation and field technique. *Geophysics*, **52**, 1601–1611.

NOC 2008. *Cruise Report JC19 RRS James Cook and Vessel Beryx*. National Oceanography Centre, Southampton.

Okaya, D., Henrys, S. & Stern, T. 2002. Double-sided onshore-offshore seismic imaging of plate boundary: super-gathers across South Island, New Zealand. *Tectonophysics*, **355**, 243–263.

Paulatto, M., Minshull, T. A. *et al.* 2010*a*. Upper crustal structure of an active volcano from refraction/reflection tomography, Montserrat, Lesser Antilles. *Geophysical Journal International*, **180**, 685–696, http://dx.doi.org/10.1111/j.1365-246X.2009.04445.x

Paulatto, M., Minshull, T. A. & Henstock, T. J. 2010*b*. Constraints on an intrusive system beneath the Soufrière Hills Volcano, Montserrat, from finite difference modelling of a controlled source seismic experiment. *Geophysical Research Letters*, **37**, L00E01, http://dx.doi.org/10.1029/2009GL041805

Paulatto, M., Annen, C., Henstock, T. J., Kiddle, E., Minshull, T. A., Sparks, R. S. J. & Voight, B. 2012. Magma chamber properties from integrated seismic tomography and thermal modelling at Montserrat. *Geochemistry, Geophysics, Geosystems*, **13**, Q01014, http://dx.doi.org/10.1029/2011GC003892

Perret, F. 1939. *The Volcano-Seismic Crisis at Montserrat, 1933–1937*. Carnegie Institution of Washington Publication, **212**.

Powell, C. F. 1938. The Royal Society expedition to Montserrat, B.W.I.: Final Report. *Philosophical Transactions Royal Society London*, **A237**, 1–34.

Power, J. A., Wyss, M. & Latchman, J. L. 1998. Spatial variations in the frequency-magnitude distribution of earthquakes at Soufrière Hills volcano, Montserrat, W.I. *Geophysical Research Letters*, **25**, 3653–3656.

Pratt, R. G. 1999. Seismic waveform inversion in the frequency domain, Part I: Theory and verification in a physical scale model. *Geophysics*, **64**, 888–901.

Rea, W. J. 1974. The volcanic geology and petrology of Montserrat, West Indies. *Journal of the Geological Society, London*, **130**, 341–366.

Reid, R. P., Carey, S. N. & Ross, D. R. 1996. Late Quaternary sedimentation in the Lesser Antilles island arc. *Geological Society of America Bulletin*, **108**, 78–100.

Rowe, C. A., Thurber, C. H. & White, R. A. 2004. Dome growth behavior at Soufrière Hills Volcano, Montserrat, revealed by relocation of volcanic event swarms, 1995–1996. *Journal of Volcanology and Geothermal Research*, **134**, 199–221, http://dx.doi.org/10.1016/j.jvolgeores.2004.01.008

Rutherford, M. J. & Devine, J. D. 2003. Magmatic conditions and magma ascent as indicated by hornblende phase equilibria and reactions in the 1995–2002 Soufrière Hills magma. *Journal of Petrology*, **44**, 1433–1454.

Searle, M. P., Simpson, R. L., Law, R. D., Parrish, R. R. & Waters, D. J. 2003. The structural geometry, metamorphic and magmatic evolution of the Everest massif, High Himalaya of Nepal-South Tibet. *Journal of the Geological Society, London*, **160**, 345–366.

Seher, T., Singh, S. C., Crawford, W. C. & Escartin, J. 2010. Upper crustal velocity structure beneath the central Lucky Strike Segment from seismic refraction measurements. *Geochemistry, Geophysics, Geosystems*, **11**, Q05001, http://dx.doi.org/10.1029/2009GC002894

Sevilla, W. I., Ammon, C. J., Voight, B. & De Angelis, S. 2010. Crustal structure beneath the Montserrat region of the Lesser Antilles island arc. *Geochemistry, Geophysics, Geosystems*, **11**, Q06013, http://dx.doi.org/10.1029/2010GV003048

Shalev, E. & Lees, J. M. 1998. Cubic b-splines tomography at Loma Prieta. *Bulletin of the Seismological Society of America*, **88**, 256–269.

Shalev, E., Kenedi, C. L. *et al.* 2010. Three-dimensional seismic velocity tomography of Montserrat from SEA-CALIPSO offshore/onshore experiment. *Geophysical Research Letters*, **37**, L00E17, http://dx.doi.org/10.1029/2010GL042498

Shepherd, J. B., Tomblin, J. F. & Woo, D. A. 1971. Volcano-seismic crisis in Montserrat, West Indies 1966–67. *Bulletin of Volcanology*, **35**, 143–163.

Sparks, R. S. J. & Young, S. R. 2002. The eruption of Soufrière Hills Volcano, Montserrat (1995 to 1999): overview of scientific results. *In*: Druitt, T. H. & Kokelaar, B. P. (eds) *The Eruption of Soufrière Hills Volcano, Montserrat, from 1995 to 1999*. Geological Society, London, Memoirs, **21**, 45–69.

Strandenes, S., Vaage, S., Zallberg-Meteselaar, G. & Sodal, A. 1991. Comparison of airgun clusters. *Society of Exploration Geophysicists, Abstracts*, **61**, 792–795.

Trofimovs, J., Amy, L. *et al.* 2006. Submarine pyroclastic deposits formed at the Soufrière Hills Volcano, Montserrat (1995–2003); what happens when pyroclastic flows enter the ocean? *Geology*, **34**, 549–552.

Trofimovs, J., Sparks, R. S. J. & Talling, P. J. 2008. Anatomy of a submarine pyroclastic flow and associated turbidity current: July 2003 dome collapse, Soufrière Hills volcano, Montserrat, West Indies. *Sedimentology*, **55**, 617–634.

Trofimovs, J., Fisher, J. K. *et al.* 2010. Evidence for carbonate platform failure during rapid sea-level rise; ca 14000 year old bioclastic flow deposits in the Lesser Antilles. *Sedimentology*, **57**, 735–759, http://dx.doi.org/10.1111/j.1365-3091.2009.01117.x

Trofimovs, J., Foster, C. *et al.* 2011. Submarine pyroclastic flow deposits formed during the 20th May 2006 dome collapse of the Soufrière Hills Volcano, Montserrat. *Bulletin of Volcanology*, **73**, http://dx.doi.org/10.1007/s00445-011-0533-5

Voight, B. & Sparks, R. S. J. 2010. Introduction to special section on the eruption of Soufrière Hills Volcano, Montserrat, the CALIPSO Project, and the SEA-CALIPSO arc-crust imaging experiment. *Geophysical Research Letters*, **37**, L00E23, http://dx.doi.org/10.1029/2010GL044254

Voight, B., Sparks, R. S. J. *et al.* 1999. Magma flow instability and cyclic activity at Soufrière Hills Volcano, Montserrat, B.W.I. *Science*, **283**, 1138–1142.

Voight, B., Linde, A. T. *et al.* 2006. Unprecedented pressure increase in deep magma reservoir triggered by lava-dome collapse. *Geophysical Research Letters*, **33**, L03312, http://dx.doi.org/10.1029/2005GL024870

Voight, B., Hidayat, D. *et al.* 2010*a*. Unique strainmeter observations of Vulcanian explosions, Soufrière Hills Volcano, Montserrat, July 2003. *Geophysical Research Letters*, **37**, L00E18, http://dx.doi.org/10.1029/2010GL042551

Voight, B., Sparks, R. S. J. *et al.* 2010*b*. Active source seismic experiment peers under Soufriére Hills Volcano. *Eos, Transactions of the American Geophysical Union*, **91**, 245, http://dx.doi.org/10.1029/2010EO280002

Voight, B., Widiwijayanti, C., Mattioli, G., Elsworth, D., Hidayat, D. & Strutt, M. 2010*c*. Magma-sponge hypothesis and stratovolcanoes: Case for a compressible reservoir and quasi-steady deep influx at Soufrière Hills Vocano, Montserrat. *Geophysical Research Letters*, **37**, L00E05, http://dx.doi.org/10.1029/2009GL041732

Wadge, G., Herd, R., Ryan, G., Calder, E. S. & Komorowski, J.-C. 2010. Lava production at Soufrière Hills Volcano, Montserrat: 1995–2009. *Geophysical Research Letters*, **37**, L00E03, http://dx.doi.org/10.1029/2009GL041466

Warner, M. T., Nangoo, T. *et al.* 2013. Anisotropic 3D full-waveform inversion. *Geophysics*, **78**, R59–R80.

Widiwijayanti, C., Clarke, A., Elsworth, D. & Voight, B. 2005. Geodetic constraints on the shallow magma system at Soufrière Hills Volcano, Montserrat. *Geophysical Research Letters*, **32**, L11309, http://dx.doi.org/10.1029/2005GL022846

Wiebe, R. & Collins, W. J. 1998. Depositional features and stratigraphic sections in granitic plutons: implications for the emplacement and crystallization of granitic magma chambers. *Journal of Structural Geology*, **20**, 1273–1289.

Zandomeneghi, D., Barclay, A., Almendros, J., Ibanez Godoy, J. M., Wilcock, W. S. D. & Ben Zvi, T. 2009. Crustal structure of Deception Island volcano from P wave seismic tomography: Tectonic and volcanic implications. *Journal of Geophysical Research*, **114**, B06310, http://dx.doi.org/10.1029/2008JB006119

Zellmer, G. F., Hawkesworth, C. J., Sparks, R. S. J., Thomas, L. E., Harford, C., Brewer, T. S. & Loughlin, S. 2003*a*. Geochemical evolution of the Soufrière Hills volcano, Montserrat, West Indies. *Journal of Petrology*, **44**, 1349–1374.

Zellmer, G. F., Sparks, R. S. J., Hawkesworth, C. J. & Wiedenbeck, M. 2003*b*. Magma emplacement and remobilization timescales beneath Montserrat: insights from Sr and Ba profiles across plagioclase phenocrysts. *Journal of Petrology*, **44**, 1413–1432.

Zelt, A. C. 1998. Lateral velocity resolution from 3-d seismic refraction data. *Geophysical Journal International*, **135**, 1101–1112.